**UNIVERSITY OF SOUTHAMPTON**

FACULTY OF PHYSICAL SCIENCES AND ENGINEERING

Electronics and Computer Science

# Why is Life? An Assessment of the Thermodynamic Properties of Dissipative, Pattern-forming Systems

by

**Stuart J. Bartlett**

Thesis for the degree of Doctor of Philosophy

July 2014

UNIVERSITY OF SOUTHAMPTON

ABSTRACT

FACULTY OF PHYSICAL SCIENCES AND ENGINEERING

Electronics and Computer Science

Doctor of Philosophy

# WHY IS LIFE? AN ASSESSMENT OF THE THERMODYNAMIC PROPERTIES OF DISSIPATIVE, PATTERN-FORMING SYSTEMS

by Stuart J. Bartlett

This document charts a series of investigations into some basic questions concerning the relationship between life and the physical theories of thermodynamics. While equilibrium thermodynamics represents a foundational component of modern physics, methods for non-equilibrium systems have yet to reach the same level of maturity. The first part of this thesis aims to establish the validity of a burgeoning theory of non-equilibrium thermodynamics known as the Maximum Entropy Production Principle (MEPP), in the context of heat transfer by convective fluid motion between heated boundaries. Applying the MEPP to systems with both fixed and negative feedback boundary conditions revealed that in fact, the steady state of convective fluids cannot be accurately predicted from an assumption of maximum entropy production alone. Rather the subtleties of the boundary conditions and the physical properties of the fluid must be properly accounted for. It is thus proposed that the MEPP should not, as has sometimes been suggested, be treated as a universally applicable law of nature.

The second part of this thesis investigates the pattern-forming and transport properties of reactive fluid systems. It is found that under thermal driving forces, closed systems utilise the physical processes of reaction and advection to augment their heat transport abilities. Furthermore, the addition of thermal kinetics and fluid flow to the Gray-Scott reaction diffusion system, reveals a new range of phenomena including positive feedback, self-inhibition, competition and symbiosis. Such behaviour can readily be viewed from an ecological, rather than purely physico-chemical, perspective.

# Contents

**Declaration of Authorship** xvii

**Acknowledgements** xix

**Nomenclature** xxi

**1 Introduction** 1
- 1.1 Thermodynamics: Its Role and Current State . . . 2
- 1.2 Life's Difficult Relationship with Thermodynamics . . . 8
- 1.3 The Many Faces of Disequilibrium . . . 12
- 1.4 The Structure of the Thesis . . . 14
  - 1.4.1 Maximum Entropy Production and Fluid Convection . . . 14
  - 1.4.2 Reactive Systems and Ecological Dynamics . . . 15
- 1.5 Contributions . . . 16

**2 Lattice Boltzmann Model with BGK Collision, Single-phase** 17
- 2.1 The Physical Basis of the Lattice Boltzmann Model . . . 18
- 2.2 Theoretical Derivation . . . 20
- 2.3 Definition of Boundary Conditions . . . 24
- 2.4 Isothermal Benchmark Tests . . . 29
  - 2.4.1 Poiseuille Flow . . . 29
  - 2.4.2 Flow Past a Cyclinder . . . 31
- 2.5 Conclusions . . . 32

**3 Lattice Boltzmann Model with Internal Energy as a Passive Scalar** 35
- 3.1 Equations of Motion . . . 36
- 3.2 Theoretical Derivation . . . 37
- 3.3 Definition of Boundary Conditions . . . 43
- 3.4 Thermal Benchmark Tests . . . 45
  - 3.4.1 Constant Internal Energy . . . 45
  - 3.4.2 Constant Boundary Temperatures . . . 48
    - 3.4.2.1 Horizontal Gradient . . . 48
    - 3.4.2.2 Vertical Gradient . . . 51
  - 3.4.3 Constant Boundary Fluxes . . . 57
- 3.5 Conclusions . . . 60

**4 What Can Maximum Entropy teach us about Convection?** 63
- 4.1 Ozawa's Scaling Law . . . 65

4.2 How does the Maximum Entropy Production Principle Measure up? . . . 68
4.3 Conclusions . . . 73

**5 Negative Feedback Boundary Conditions 75**
5.1 The Model System and its Macroscopic Variables . . . 77
5.2 Definition of Boundary Conditions . . . 80
5.3 New Results . . . 82
5.4 Can the Maximum Entropy Production Principle be Trusted? . . . 88
5.5 Conclusions . . . 91

**6 Doing Chemistry with an Isothermal Lattice Boltzmann Model 93**
6.1 Theoretical Considerations . . . 95
6.2 Benchmark Tests . . . 96
6.2.1 Two-species Linear Reaction in a Closed System . . . 96
6.2.1.1 Analytical Solution . . . 96
6.2.1.2 Reactive Lattice Boltzmann Model Implementation . . . 98
6.2.1.3 Test Results . . . 99
6.2.2 Two-species Non-linear Reaction in an Open System . . . 100
6.2.2.1 Reaction-Diffusion Dynamics . . . 100
6.2.2.2 Reactive Lattice Boltzmann Model Implementation . . . 103
6.2.2.3 Test Results . . . 103
6.3 Conclusions . . . 106

**7 Turning up the Heat: Enthalpy Changes and Convection 109**
7.1 Theoretical Considerations . . . 110
7.2 Two-Species Diffusive . . . 113
7.2.1 Linear Closed System . . . 113
7.2.2 Non-linear Open System . . . 118
7.3 Two-Species Convective . . . 126
7.3.1 Linear Closed System . . . 126
7.3.2 Non-linear Open System . . . 131
7.3.2.1 Thermally Neutral Reaction . . . 131
7.3.2.2 Exothermic Reaction . . . 133
7.3.2.3 Endothermic Reaction . . . 135
7.3.2.4 Precariousness . . . 140
7.4 Thermal Symbiosis: Four-Species Convective . . . 147
7.5 Conclusions . . . 151

**8 Conclusions and Further Work 153**
8.1 Theories of Maximum Entropy Production . . . 154
8.2 New Avenues for Heat Transfer . . . 155
8.3 The Ecology of Spots . . . 156
8.4 Further Work . . . 158
8.4.1 Transport Properties of Closed Systems . . . 158
8.4.2 Open Reaction Diffusion Systems . . . 158
8.4.3 N-Species Systems . . . 159
8.5 Where are we now? . . . 160

**References** **163**

# List of Figures


2.1 Discrete velocity vector set for the D2Q9 Lattice Boltzmann Model. . . . 23

2.2 Streaming step for boundary nodes using the bounce-back method. a) Pre-streaming velocity distributions, $f_i^-$. b) Post-streaming velocity distributions, $f_i$. Note that distributions streaming into the wall have had their directions completely reversed. Other distributions have propagated along their respective velocity vectors $\mathbf{e}_i$. . . . . 25

2.3 Poiseuille flow diagram. The pressure gradient $\nabla p = (P_{in} - P_{out})/L$ drives a purely horizontal flow through the 2D channel, $\mathbf{U} = U(y)\hat{i}$. Note the origin of the y-axis is in the central plane of the channel. $H$ is the half-width of the channel. . . . . 30

2.4 RMS error as a function of lattice size for LBM simulations of 2D Poiseuille flow. . . . . 30

2.5 Vortex shedding caused by wind flowing past the Juan Fernández Islands off the Chilean coast. Image by Bob Cahalan, NASA GSFC. . . . . 31

2.6 Horizontal momentum density fields for channel flow past a circular obstacle. Colours correspond to momentum magnitude with red being strongest and blue weakest. a) Laminar wake formation at $Re = 80$, below the critical value of $Re_c \sim 90$. b) Non-laminar vortex shedding at $Re = 100$, above the critical value of $Re_c \sim 90$. c) Non-laminar vortex shedding at $Re = 1000$. . . . . 32

3.1 Equilibration of an isolated fluid cavity with two halves initially at temperatures $T_{a_0} = 1$ and $T_{b_0} = 0$. There is no net fluid motion and heat moves purely by diffusion. . . . . 47

3.2 Isotherms for convection flows in a square cavity with a horizontal temperature gradient at different Rayleigh numbers. a) $Ra = 10^3$, b) $Ra = 10^4$, c) $Ra = 10^5$, d) $Ra = 10^6$. . . . . 49

3.3 Mean horizontal temperature as a function of vertical coordinate, and temperature fields for fixed boundary temperature convection systems of different Rayleigh numbers. Flow streamlines are also displayed showing the characteristic boundary layers and convection rolls. a) $Ra = 10^3$, below the critical Rayleigh number ($Ra_c \approx 1706$) there is no convective motion and heat transport occurs purely by diffusion, b) $Ra = 10^4$, c) $Ra = 10^5$, d) $Ra = 10^6$. Note that the boundary layers become increasingly well defined with increasing Rayleigh number. . . . . 54

3.4 Nusselt number as a function of Rayleigh number for a fixed temperature convective fluid system with an aspect ratio of 2. Red asterisks correspond to values from TLBM simulations and black triangles to the benchmark solution of Clever and Busse (1974). . . . . 55

3.5 Nusselt number as a function of Rayleigh number for a fixed temperature convective fluid system with an aspect ratio of 2. Black triangles correspond to the benchmark solution of Clever and Busse (1974), red asterisks correspond to values from TLBM simulations, the black line is the scaling law observed in the direct numerical simulations of Johnston and Doering (2009) and the blue dashed line is the MEPP prediction of Ozawa et al. (2001). . . . . 56
3.6 Temperature field of a fixed temperature NC system with $Ra = 10^8$. The snapshot shows the system during the early transient phase, during which the first set of convective plumes are growing towards the cold upper boundary. . . . . 56
3.7 Nusselt number as a function of Rayleigh number for a fixed heat flux convective fluid system with an aspect ratio of 2. Blue circles correspond to values from TLBM simulations, and the black line corresponds to the scaling law observed in the direct numerical simulations of Johnston and Doering (2009). . . . . 59
3.8 Temperature field for a fixed flux NC flow with $Ra = 1.2 \times 10^5$. Note the apparent lack of distinctive boundary layers compared to the fixed temperature systems (see Figure 3.3). This flow structure allows fixed flux systems of low $Ra$ to achieve higher magnitudes of convective transport than equivalent fixed temperature systems. . . . . 60
3.9 Nusselt number as a function of Rayleigh number for fixed temperature and fixed heat flux convective fluid systems with an aspect ratio of 2. Red asterisks correspond to fixed temperature BCs and blue circles to fixed flux BCs. The black line is the scaling law observed in the direct numerical simulations of Johnston and Doering (2009). . . . . 61

4.1 An illustration of the changes in transport properties of NC systems with two different types of fixed BCs. Note that going from the upper configurations to the lower set, the fluid viscosity is reduced while keeping the thermal diffusivity constant. This takes the Rayleigh number from $Ra < Ra_c$ to $Ra > Ra_c$, causing the onset of convection. Thus on the left, the temperature difference $\Delta T$ remains constant while the boundary temperature gradient (heat flux) changes, and on the right, the boundary temperature gradient remains constant while the temperature difference changes. . . . . 71

5.1 Schematic of a negative feedback BC system showing the various steady state fluxes, which comprise the boundary energy balances. Boundaries are periodic in the horizontal direction and upper and lower walls enforce the no-slip velocity condition. . . . . 77
5.2 Macroscopic transport properties of the model system. External flux parameters are fixed at $Q_{in,a} = 0.1, Q_{in,b} = 0.01, \beta = 0.1$. The numerical value of the boundary heat flux $Q_{ab}$ is varied between its lower and upper extremes, 0 and $(Q_{in,a} - Q_{in,b})/2$. The resulting boundary temperatures $T_a$ and $T_b$ can then be calculated. . . . . 79

5.3 Dimensionless heat flux ratio $Nu$ as a function of dimensionless thermal driving force $Ra$ for NC systems with negative feedback BCs. Red circles correspond to systems with uniform boundary temperature profiles and blue triangles correspond to systems with a variable boundary temperature profile. The solid line shows the empirical scaling law $Nu \approx 0.138 Ra^{0.285}$ due to Johnston and Doering (2009). . . . . 83
5.4 Normalised steady state temperature difference as a function of heat flux for TLBM simulations with negative feedback BCs. Red circles and blue triangles show results from the *uni* and *vari* simulations respectively. The black dotted line shows the heat flux value corresponding to a state of MEP and the black asterisk shows the corresponding value of the temperature difference. As predicted from the energy balance equations (and displayed in Figure 5.2), higher heat fluxes result in a lower temperature difference. . . . . 85
5.5 Normalised steady state temperature difference as a function of normalised heat flux for TLBM simulations with negative feedback BCs. Red circles and blue triangles show results from the *uni* and *vari* simulations respectively. The black dotted line shows the heat flux value corresponding to a state of MEP. As predicted from the energy balance equations (and displayed in Figure 5.2), higher heat fluxes result in a lower temperature differential. On this figure there are three separate data sets, each corresponding to a different value of the parameter $\beta$, but all had common values for the other BC parameters, $Q_{in,a} = 0.1, Q_{in,b} = 0.01$. The leftmost cluster of points represent simulations with $\beta = 4$, the central cluster $\beta = 1.3$, and the rightmost cluster $\beta = 0.1$. . . . . 88

6.1 Numerical error of RD simulations as a function of relaxation parameter $\tau_A$ for several reaction rates $k$. For each simulation the dimensionless parameters $\phi^2$ and $t$ were kept constant allowing an objective comparison between $[\tau_A, k]$ combinations. . . . . 100
6.2 RLBM simulation of a GS RD system. The feed rate $F$ and depletion rate $R$ were varied continuously across the domain, allowing all the characteristic structures to emerge in a single simulation. The relaxation parameter is fixed at $\tau_A = 0.9$. The colourmap shows the order parameter $\phi(\mathbf{x}, t) = \psi_A(\mathbf{x}, t) - \psi_B(\mathbf{x}, t)$, with red corresponding to values of $\phi = 1$ and the deepest blue corresponding to $\phi \approx -0.5$. . . . . 105
6.3 RLBM simulations of a GS RD system with different relaxation parameters $\tau_A$. The feed rate $F$ and depletion rate $R$ were varied continuously across the domain. The colourmap shows the order parameter $\phi(\mathbf{x}, t) = \psi_A(\mathbf{x}, t) - \psi_B(\mathbf{x}, t)$, with red corresponding to values of $\phi = 1$ and the deepest blue corresponding to $\phi \approx -0.5$. . . . . 106
6.4 RLBM simulation of a GS RD system. The feed rate $F$ and depletion rate $R$ were varied continuously across the domain. The relaxation parameter is fixed at $\tau_A = 3$. The colourmap shows the order parameter $\phi(\mathbf{x}, t) = \psi_A(\mathbf{x}, t) - \psi_B(\mathbf{x}, t)$, with red corresponding to values of $\phi = 1$ and the deepest blue corresponding to $\phi \approx -0.5$. . . . . 107

7.1 Schematic of a typical exothermic chemical reaction. The reactant state is represented by the initial portion of the curve and the product state by the final portion. The reaction coordinate approximately represents how far through the microscopic reaction process the reaction has proceeded. . 110
7.2 Temperature and concentration profiles for TRD systems. Simulations were initiated with $\psi_A = 1$ and $\psi_B = 0$, and $T(x, z) = T_b + \Delta T(H - z)/H$, with a small degree of noise. The parameters were varied as follows: a) $A_f = 1, A_r = 0, \Delta H = 0$, b) $A_f = 1, A_r = 1, \Delta H = 0$. Profiles are plotted for several different times through the simulation. The time intervals are logarithmically spaced due to the exponential decay inherent to these systems. Red indicates early times in the simulation, turning to blue as the simulation progresses. . . . . 114
7.3 Temperature and concentration profiles for TRD simulations with varying kinetic parameters. Simulations were initiated with $\psi_A = 1$ and $\psi_B = 0$, and $T(x, z) = T_b + \Delta T(H - z)/H$, with a small degree of noise. The parameters were varied as follows: a) $A_f = 1, A_r = 0, \Delta H = -0.5$, b) $A_f = 1, A_r = 1, \Delta H = -0.5$, c) $A_f = 1, A_r = 0, \Delta H = 0.5$, d) $A_f = 1, A_r = 1, \Delta H = 0.5$. Profiles are plotted for several different times through the simulation. The time intervals are logarithmically spaced due to the exponential decay inherent to these systems. Red indicates early times in the simulation, turning to blue as the simulation progresses. . . . 116
7.4 Changes in reaction rate as a function of temperature for different activation energies $E_f$. The frequency factor is calculated using $A_f = e^{E_f/T_0}$ where $T_0 = 1.5$ is the mean temperature. The range of activation energies plotted extends from $E_f = 0$ in red to $E_f = 2$ in blue. . . . . 119
7.5 Temperature profiles and chemical order parameter $(\psi_A - \psi_B)$ fields for a thermal GS RD simulation at several different times through the simulation. There is no enthalpy change $\Delta H = 0$, and the time intervals are logarithmically spaced. . . . . 123
7.6 Temperature profiles and chemical order parameter $(\psi_A - \psi_B)$ fields for an exothermic GS RD simulation at several different times through the simulation. The enthalpy of reaction is $\Delta H = -5 \times 10^{-3}$. The time intervals are logarithmically spaced. See an animation of this simulation in additional digital material. . . . . 124
7.7 Temperature profiles and chemical order parameter $(\psi_A - \psi_B)$ fields for an endothermic GS RD simulation at several different times through the simulation. The enthalpy of reaction is $\Delta H = 5 \times 10^{-3}$. The time intervals are logarithmically spaced. See an animation of this simulation in additional digital material. . . . . 125
7.8 Steady state of a RTLBM simulation in which a passive scalar species $A$ can undergo a reversible decay reaction $A \rightleftharpoons B$ to a lower energy product $B$. The top image shows the temperature field with fluid velocity streamlines, the middle image the concentration field for the first component $\psi_A$, and in the lower image the concentration field for the second component $\psi_B$. The simulation was initialised with $\overline{\psi_{A0}} = \overline{\psi_{B0}} = 2$. . . . . 127

7.9 Component heat fluxes as a function of average chemical species concentration for RTLBM simulations at two different Rayleigh numbers. The heat flux values (corresponding to diffusion in blue, convection in red and advection by passive scalar chemical species in green) are normalised by the total heat flux. . . . . 130
7.10 Temperature and chemical order parameter ($\psi_A - \psi_B$) fields for a thermally neutral ($\Delta H = 0$), convective GS TRD simulation at several different times through the simulation. The time intervals are logarithmically spaced. See an animation of this simulation in additional digital material. 132
7.11 Temperature and chemical order parameter ($\psi_A - \psi_B$) fields for an exothermic, convective GS TRD simulation with $\Delta H = -1 \times 10^{-3}$ at several different times through the simulation. The time intervals are logarithmically spaced. See an animation of this simulation in additional digital material. . . . . 134
7.12 Temperature and chemical order parameter ($\psi_A - \psi_B$) fields for an endothermic, convective GS TRD simulation with $\Delta H = 2 \times 10^{-3}$ at several different times through the simulation. The time intervals are logarithmically spaced. See an animation of this simulation in additional digital material. . . . . 135
7.13 Temperature and chemical order parameter ($\psi_A - \psi_B$) fields for an endothermic, convective GS TRD simulation with $\Delta H = 5 \times 10^{-3}$ at several different times through the simulation. The time intervals are logarithmically spaced. See an animation of this simulation in additional digital material. . . . . 136
7.14 Temperature and chemical order parameter ($\psi_A - \psi_B$) fields for an endothermic, convective GS TRD simulation with $\Delta H = 10 \times 10^{-3}$ at several different times through the simulation. The time intervals are logarithmically spaced. See an animation of this simulation in additional digital material. . . . . 137
7.15 Temperature and chemical order parameter ($\psi_A - \psi_B$) fields for an endothermic, convective GS TRD simulation with $\Delta H = 25 \times 10^{-3}$ at several different times through the simulation. The time intervals are logarithmically spaced. See an animation of this simulation in additional digital material. . . . . 139
7.16 Temperature and chemical order parameter ($\psi_A - \psi_B$) fields for an exothermic, convective GS TRD simulation with $\Delta H = -1 \times 10^{-3}$ at several different times through the simulation. The time intervals are logarithmically spaced. See an animation of this simulation in additional digital material. . . . . 142
7.17 Temperature and chemical order parameter ($\psi_A - \psi_B$) fields for an exothermic, convective GS TRD simulation with $\Delta H = -2 \times 10^{-3}$ at several different times through the simulation. The time intervals are logarithmically spaced. See an animation of this simulation in additional digital material. . . . . 143
7.18 Temperature and chemical order parameter ($\psi_A - \psi_B$) fields for an exothermic, convective GS TRD simulation with $\Delta H = -3 \times 10^{-3}$ at several different times through the simulation. The time intervals are logarithmically spaced. See an animation of this simulation in additional digital material. . . . . 144

7.19 Temperature and chemical order parameter ($\psi_A - \psi_B$) fields for an exothermic, convective GS TRD simulation with $\Delta H = -4 \times 10^{-3}$ at several different times through the simulation. The time intervals are logarithmically spaced. See an animation of this simulation in additional digital material. . . . . 145
7.20 Temperature and chemical order parameter ($\psi_A - \psi_B$) fields for an exothermic, convective GS TRD simulation with $\Delta H = -3 \times 10^{-3}$ at several different times through the simulation. The time intervals are linearly spaced and the temperature of the right half of the lower boundary is linearly reduced from $T_{a_r} = 2$ to $T_{a_r} = 1$ between times $t = 50000$ and $t = 70000$. See an animation of this simulation in additional digital material. 146
7.21 Temperature and chemical order parameter fields ($\psi_{A_1} - \psi_{B_1}$) and ($\psi_{A_2} - \psi_{B_2}$) for a dual spot species, convective GS TRD simulation with $\Delta H_1 = -4 \times 10^{-3}$ and $\Delta H_2 = 4 \times 10^{-3}$ at several different times through the simulation. The time intervals are logarithmically spaced. See an animation of this simulation in additional digital material. . . . . 148
7.22 Temperature and chemical order parameter fields ($\psi_{A_1} - \psi_{B_1}$) and ($\psi_{A_2} - \psi_{B_2}$) for a dual spot species, convective GS TRD simulation with $\Delta H_1 = -4 \times 10^{-3}$ and $\Delta H_2 = 2 \times 10^{-3}$ at several different times through the simulation. The time intervals are linearly spaced. See an animation of this simulation in additional digital material. . . . . 149
7.23 Temperature and chemical order parameter fields ($\psi_{A_1} - \psi_{B_1}$) and ($\psi_{A_2} - \psi_{B_2}$) for a dual spot species, convective GS TRD simulation with $\Delta H_1 = -4 \times 10^{-3}$ and $\Delta H_2 = 2 \times 10^{-3}$ at several different times through the simulation. The time intervals are linearly spaced and the temperature of the right half of the lower boundary is linearly reduced from $T_{a_r} = 2$ to $T_{a_r} = 1$ between times $t = 50000$ and $t = 70000$. See an animation of this simulation in additional digital material. . . . . 151
7.24 Temperature and chemical order parameter fields ($\psi_{A_1} - \psi_{B_1}$) and ($\psi_{A_2} - \psi_{B_2}$) for a dual spot species, convective GS TRD simulation with $\Delta H_1 = -20 \times 10^{-3}$ and $\Delta H_2 = 25 \times 10^{-3}$ at several different times through the simulation. The time intervals are linearly spaced. See an animation of this simulation in additional digital material. . . . . 152

# List of Tables

3.1 Convective flow properties for a 2D cavity with a horizontal temperature gradient. Results are shown for the benchmark calculations of De Vahl Davis (1983) (BM) and for TLBM simulations. . . . . 51

# Declaration of Authorship

I, Stuart J. Bartlett, declare that the thesis entitled *Why is Life? An Assessment of the Thermodynamic Properties of Dissipative, Pattern-forming Systems* and the work presented in the thesis are both my own, and have been generated by me as the result of my own original research. I confirm that:

- this work was done wholly or mainly while in candidature for a research degree at this University;
- where any part of this thesis has previously been submitted for a degree or any other qualification at this University or any other institution, this has been clearly stated;
- where I have consulted the published work of others, this is always clearly attributed;
- where I have quoted from the work of others, the source is always given. With the exception of such quotations, this thesis is entirely my own work;
- I have acknowledged all main sources of help;
- where the thesis is based on work done by myself jointly with others, I have made clear exactly what was done by others and what I have contributed myself;
- parts of this work have been published as: Bartlett and Bullock (2014)

Signed:.....

Date:.....

# Acknowledgements

There are many people who were instrumental in helping me achieve the finished thesis that you're now holding with excitement. My supervisor Seth Bullock took rather a dubious bet on a loose cannon giving me free reign to investigate whatever scientific problem I chose. I'll always appreciate his sticking by my aspirations through thick and thin. A PhD is a difficult course to steer and I would have for sure ended up in sea monster infested waters if it wasn't for his help.

To my parents I owe an infinite debt of gratitude. Their guidance and example throughout my life have given me the confidence to take on any challenge I saw fit, including this one. I can only hope to provide such an outstanding start in life to my own children.

Thanks also to my second supervisor James Dyke for providing ideas, criticism, offence and the opportunity to speak at a TEDx event, which I was very very grateful for. Thanks to my third supervisor George Attard, whose incredible knowledge, insight, help, endless supply of ideas and support proved invaluable to me during my PhD. Thanks to the other members of staff in Building 16 of ECS: Jason Noble, Markus Brede and Brendan Neville for providing help, guidance, bundles of laughs and opportunities. Thanks especially to our DTC secretary Nicki Lewin, a shining light in the administrative abyss. But also the source of social cohesion and emotional support that groups of eccentric students and academics cannot survive without. I also want to thank other students of the DTC especially Alexandra Diem for her tireless support, Elisabeth zu-Erbach Schoenberg, Jordi Arranz, Adam Davies, Millie Zedan, Andreas Loengarov, Sonya Ridden, Maximillian Albert, Gabriel Amine-Eddine, Miguel Gonzalez and Simon Tudge. What a great place to do a PhD thanks to you guys.

Thanks finally to Bains (2004) for introducing me to the Carl Sagan quote with which this thesis commences.

# Nomenclature

| | |
|---|---|
| $f_i$ | Velocity distribution function |
| $f_i^{eq}$ | Equilibrium velocity distribution function |
| $g_i$ | Internal energy distribution function |
| $g_i^{eq}$ | Equilibrium internal energy distribution function |
| $h_i^{\sigma}$ | Chemical species distribution function |
| $h_i^{eq,\sigma}$ | Equilibrium chemical species distribution function |
| $i$ | Discrete velocity index |
| $\omega_i$ | Velocity weight factor |
| $\sigma$ | Chemical species index |
| $\rho$ | Mass density |
| $\epsilon$ | Internal energy density |
| $T$ | Temperature |
| $\psi_\sigma$ | Chemical species concentration |
| $\tau_\nu$ | Fluid relaxation parameter |
| $\tau_c$ | Internal energy relaxation parameter |
| $\tau_\sigma$ | Chemical species relaxation parameter |
| $\nu$ | Kinematic viscosity |
| $\chi$ | Thermal diffusivity |
| $D_\sigma$ | Chemical species diffusivity |
| $\mathbf{x}$ | Spatial coordinate |
| $t$ | Time |
| $Ra$ | Rayleigh number |
| $Nu$ | Nusselt number |
| $Pr$ | Prandtl number |
| $Q$ | Heat flux |

# Chapter 1

# Introduction

> "There is a famous book published about 1912 by Lawrence J. Henderson . . . in which Henderson concludes that life necessarily must be based on carbon and water, and have its higher forms metabolizing free oxygen. I personally find this conclusion suspect, if only because Lawrence Henderson was made of carbon and water and metabolized free oxygen. Henderson had a vested interest."
> Sagan (1973)

I am not the first person to quote this poignant passage from the great science communicator and arguably the founder of Astrobiology. It beautifully captures a sentiment that re-surfaces in my mind every time I read a paper or book from that fascinating new field. Although there is now a concerted effort to explore the concept of life as it could be, the majority of research in the fields of the origin of life and astrobiology basically assumes that life in the universe will be similar to life on Earth. Why?

There are obvious reasons of course ranging from purely pragmatic ones (how can we compare an unobservable biology to our own, and how does one go about inventing alternative biologies) to pure expectation bias (at present we have only one example of life to study). We still face the problem of forging the tools necessary to recognise life, now that we are increasingly equipped with the tools to look for it. The problem of defining life is nothing short of a philosophical minefield decorated with pitfalls,

paradoxes and dead ends. I will discuss my own position on this subject in the following sections.

The search for life as it could be was the primary motivation for this thesis. It has led me down a myriad of roads, many of which turned out to be *cul de sacs*. The origin of life on Earth is an exciting field with pioneering developments emerging at a terrific pace. But I did not wish to explore the detailed, exact chemical process which led to the formation of our last universal common ancestor (LUCA). I see this partly as a process of historical re-tracing. Through phylogenetic analysis, researchers now have a reasonably good estimate for the genetic make up of the LUCA. Although further back in time there is neither genetic or a fossil record of earlier forms of life. Therefore this phase of life's history remains shrouded in mystery. Despite this, some researchers believe they have a relatively accurate picture for biogenesis (Martin and Russell, 2003; Martin et al., 2008).

Rather than contribute to this effort I instead tried to consider life from a more abstract perspective. What is its physical role in its universal context? What might drive it into existence in other locales? This line of thinking led me to consider deeply whether life might be definable through its thermodynamic properties. Therefore the starting point for this thesis will be to contemplate the position of thermodynamics as it stands today.

## 1.1 Thermodynamics: Its Role and Current State

The famous French engineer Sadi Carnot (1796-1832) was far ahead of his time intellectually, being the first to recognise some of the basic laws of nature, which now underpin thermal physics (Carnot, 1824). But like many of the pioneers of thermodynamics he had a sad life. He died at a terribly young age from a Cholera epidemic, and before that he had been sent to an asylum due to mental illness. We can only imagine the enhanced state of science and technology we would enjoy now, had he lived a full life or had his entire collection of work survived.

Let us consider for a moment the translated title of his book: Reflections on the Motive Power of Fire. Carnot had recognised that fire, a hot state of gas, had *motive* power, i.e., it could be turned into mechanical work. He had taken the first steps towards the recognition that heat and work were two manifestations of the same physical property.

Although in that period steam engines had been around for some time, it is unlikely that many other people had properly understood the basis of their function. In the present day the equivalence of heat and work is understood before a child leaves school. But in Carnot's era, before it was common knowledge, it would not have been obvious that there was a direct correspondence between the two.

In the end it was the work of James Prescott Joule which established the quantitive relation between energies of different forms. However Carnot had not only noticed that heat and work are both forms of energy, he had realised that the transformation of one type to the other is not symmetric. This was the first recognition of the second law of thermodynamics, one of the most powerful, relevant and enigmatic theories ever to have been discovered. There are many ways to summarise it but I prefer to use the following statement: There are astronomically more ways for an isolated system with a large number of constituents to be disordered, than ordered.

We now understand heat engines very well, and the absolute limits upon their performance that Carnot discovered, can almost be reached by modern gas turbines. The contemporary form of the second law is due to the work of many pioneering figures including Clausius, Thomson, Boltzmann and Gibbs. It was Boltzmann who first noticed that if the basic constituents of matter were discrete particles (atoms), then the second law is essentially a statistical statement. In this sense it is slightly misleading that it is described as a law. It has the power and influence of a law, but it is nonetheless just a statistical effect. It is not a force, in the same way that electromagnetism is.

Another way of stating the second law is this: An isolated system, when left for a sufficient amount of time, will reach a state of equilibrium, in which the system's state variables no longer change with time, and which contains negligible gradients of intensive variables. Intensive variables are those which do not scale with the size of the system, such as temperature and pressure. For simple systems such as ideal gases in isolated containers, the equilibrium state is completely understood, and characterised by a uniform distribution of particles across the volume in which they are enclosed. If we viewed such a system from a dynamics perspective, we might describe it as having a set of states, defined by the positions and momenta of all $N$ particles in the box. Let us assume those positions and momenta are discrete. This would be true for real quantum

particles and the discussion which now follows can be translated to the continuous case with suitable modifications.

Each unique state of the system can be specified by the $6N$ numbers indexing all the particle coordinates and momenta. When the system changes state according to its microscopic equations of motion, it starts to trace out a trajectory in a $6N$-dimensional phase space. The constraints upon the system, such as the finite range of particle velocities and the finite size of the container, mean that all the possible phase space trajectories occupy a finite volume. We could pick any point in this enclosed space (since it is divided up discretely this is usually referred to as a cell) and imagine the trajectory emerging from it if that system were allowed to evolve. Let us go further and imagine all the trajectories allowed by the constraints placed on the system. We assume that the microscopic equations of motion are deterministic and time reversible. This means that the trajectories do not intersect because if they did then there could be a non-unique history for a given path, which would contradict the assumption of time reversibility.

Let us take a step back and look at the tangled web of phase space paths winding their way from state to state, each path corresponding to a unique set of states through which the system can pass, if initialised somewhere along that path. Now consider the properties of a typical state in the phase space region. With a little thought (or experimentation) we would soon conclude that most of the states are completely disordered. A common pedagogical approach here is to calculate the relative probabilities of coin-throwing between all heads and half heads and half tails, as the number of coin throws becomes very large.

Most of the system states are disordered, whether we look at an individual trajectory or the whole volume in which the compatible states are enclosed. We can of course pick out ordered states by imagining the box with all particles concentrated in one corner for example. But if we were to trace the time evolution of such a system, it would soon transition to a more disordered state. If we looked at the time reverse path we might notice something odd: the disordered state reverts to an ordered one. In fact for every state that evolves from order to disorder, there is an associated reverse path in which a disordered state becomes ordered. How can we reconcile this apparent spontaneous ordering with the second law of thermodynamics?

In fact we have not taken a fair sample of system state changes. Imagine we are focussing on state changes occurring over a length of time $\delta t$. We can find trajectories of this length where the system goes from an ordered to disordered state. And for each of those we can take the time reversed version. So we have as many disorder-order transitions as order-disorder transitions. However we have only looked at transitions in the vicinity of ordered states. We have not taken a representative sample of trajectory segments of length $\delta t$. If we instead take all segments of that length, what we will find is that the vast majority of them correspond to systems going from disordered states to other disordered states.

So ordered states are actually rather anomalous, temporary deviations from the normal state of affairs: one of complete disorderliness. Many discussions of the second law of thermodynamics get dragged into conceptual difficulties because of inherent observer biases, which make us focus a disproportionate amount of time on ordered states. In the end the second law is simple: there are vastly more ways to be disordered than ordered. Therefore the normal state that you are likely to find an isolated system with many degrees of freedom in, is one of complete disorder.

So now we can see that the second law really is just a statistical statement borne out of the combinatorics of systems containing large numbers of components. The validity of it is therefore not contingent on any one set of physical laws. For example, it applies to a Newtonian system as well as a quantum one. It would also apply equally well to other, perhaps imaginary, sets of physical laws. The main constraint is that the dynamics be time reversible and deterministic (considering systems with stochastic and variable dynamics is a difficult endeavour).

The consequences of the second law for systems such as non-interacting ideal gases and simple chemical mixtures have been rigorously worked out and stand as a seemingly unshakeable cornerstone of physics. We have a thorough understanding of the equilibrium state, and we know that isolated systems march inexorably towards it. Note that there is nothing to stop an isolated system in equilibrium becoming ordered, it is just so unlikely as to be effectively unobservable. If the system is relatively small or if we observe it for short time scales, apparent violations of the second law can occur (Wang et al., 2002). In these small systems or over short time scales, fluctuations can be sufficient to move a system spontaneously to a more ordered state. There is however a quantitative

expression - known as the fluctuation theorem - capable of describing the distribution of such deviations (Crooks, 1999; Wang et al., 2002).

Ludwig Boltzmann was an early proponent of the atomic theory of matter and we owe much of modern thermodynamic theory to his achievements. Arguably his greatest contribution was a formal definition of the quantity known as entropy. He argued that there is a physically meaningful quantity related to the number of microscopic states a system can exhibit for a given set of macroscopic constraints (a macrostate). For example consider two boxes, each filled with gas at the same pressure. If one box has twice the volume of the other it will have access to a significantly larger number of microstates, hence its entropy will be greater. The exact expression, which was engraved on Boltzmann's tombstone reads,

$$S = k_b \ln W \tag{1.1}$$

where $S$ is the entropy, $k_b$ is a constant and $W$ is the number of states a system can be found in under a given set of conditions. The presence of the logarithm is actually just for mathematical convenience. If we want to calculate the entropy of two systems, for each state of system 1, system 2 could be in any of its accessible states. Therefore the number of states for the composite system is the product of the numbers of states for the two separate systems. The entropy of the composite system can thus be calculated as the sum of the separate system entropies thanks to the form of the above expression.

Despite the formal definition, entropy has many physical interpretations. Without wanting to go into exhaustive detail, entropy can be roughly thought of as a measure of the extent to which a system has come to equilibrium. An equilibrium system has uniform distributions of intensive variables. There are thus many microstates that could satisfy these constraints. In fact the equilibrium state is exactly that state with the maximum possible number of microstates.

If we think back to the discussion of phase spaces, the entropy is proportional to the volume of phase space corresponding to states that are compatible with the system's external constraints. The entropy of a system can change when external alterations give the system access to a different number of microstates. Heating a box of gas for example increases the range of possible molecular speeds and this expands the accessible phase space volume for that system.

In summary, I have described some of the basic facets of modern thermodynamics, specifically the second law and the concept of equilibrium. We know that systems come to equilibrium, and we can calculate various properties of equilibrium systems.

However there is still no general theory for systems not in equilibrium. There has been progress with regard to systems that respond linearly to driving forces and systems close to equilibrium (Kondepudi and Prigogine, 1998). But it has not yet been possible to rigorously extend the framework of dynamical systems to systems with large numbers of constituents i.e., those described by thermodynamics.

In recent years one theory has emerged that has caused both excitement and discord. It is called the Maximum Entropy Production Principle (MEPP) and it will constitute a significant focus of this thesis. The principle's basic premise is that a non-equilibrium system will adjust itself into a steady state such that its rate of entropy production is maximised (Dewar, 2009; Dyke and Kleidon, 2010; Kleidon, 2009; Martyushev and Seleznev, 2006). The nature and consequences of this idea will be discussed in detail in chapter 4 and chapter 5, where I will carry out a set of simulations to test the validity of the principle for an interesting class of non-equilibrium system: heated fluids.

My interest in the MEPP stems from the need for a theory of non-equilibrium systems that can make predictions about their steady states no matter what they are composed of, or how far they are from equilibrium. In the next section I will discuss the relationship between biological systems and thermodynamics. Biological systems are never isolated, nor are they even close to being in equilibrium (an equilibrium system is the epitome of a dead state). If we had a general theory for non-equilibrium systems we could apply it also to biological systems and there might be profound consequences for evolutionary theory and ecology. Indeed the MEPP has been applied to ecological systems, but with mixed success (Dewar, 2010; Meysman and Bruers, 2010; Vallino, 2010).

If the MEPP fails for a characteristic, non-equilibrium system such as a heated fluid, it might imply that its validity is limited. Therefore my testing of its predictive power in chapter 4 and chapter 5 will provide evidence for whether it can provide useful results for the more complex systems investigated in chapter 6 and chapter 7.

## 1.2 Life's Difficult Relationship with Thermodynamics

The laws of thermodynamics place fundamental constraints on how physical systems behave. The first law of thermodynamics states that energy is conserved, and that it can be transformed from one type to another. Not all transformations are equally efficient. Heat especially is difficult to transform into other forms of energy without large losses. Any system in isolation will eventually come to a homogeneous, time-independent state of equilibrium.

The 'arrow of time' effect of the second law of thermodynamics has led to the belief that organisms are capable of defying it. Such erroneous ideas can be immediately dispensed with if the system is properly considered. Isolated systems come to equilibrium. Organisms are not isolated, they are constituents of a much larger system that is isolated (though we probably should avoid discussing the 'entropy of the universe'). The fact that organisms exchange matter and energy with the wider environment means they are not constrained to simply come to equilibrium like isolated systems.

Naturally, the second law still applies, but in a slightly different way. It helps us distinguish spontaneous processes from impossible processes. So while organisms are not isolated, they still have irreversible processes occurring within and around them. By irreversible processes, I am referring to phenomena such as the diffusion of solutes from a high to low concentration, the movement of heat from hot to cold bodies. Organisms *need* these processes to occur. An example is the exchange of gases in the alveoli of the human lung. If molecular diffusion did not act to equalise concentration gradients, the removal of carbon dioxide and the incorporation of oxygen into the blood would not occur sufficiently fast to keep the body alive through aerobic respiration.

In contrast, many biochemical phenomena occur against the natural tendencies of the second law. One example is the active transport of protons across lipid bilayer membranes. This creates an electrochemical potential gradient which would not arise spontaneously. So the picture that emerges when we evaluate life and thermodynamics together, is one of both conflict and harmony.

Organisms have to fight against the randomising tendencies of equilibration to maintain their structural and chemical organisation. But organisms also make use of energy gradients. For instance heterotrophs use the chemical potential gradient between their

food and waste to power all their activities. Plants and other phototrophic organisms use the energy of high frequency UV photons to build complex molecules from simpler building blocks. The energy contained in those photons will eventually be re-radiated to space as infrared photons. The entropy difference between the incident radiation and the outgoing radiation is manifested in the fact that the energy of a single incident UV photon will leave the Earth system in the form of 20 infrared photons.

That organisms produce entropy is not disputed. Boltzmann once said:

> "The general struggle for existence of animate beings is not a struggle for raw materials – these, for organisms, are air, water and soil, all abundantly available – nor for energy which exists in plenty in any body in the form of heat, but a struggle for entropy, which becomes available through the transition of energy from the hot sun to the cold earth."
> Boltzmann (1974)

We can be sure that he meant negative entropy (associated with useful or free energy) rather than entropy itself, but he nevertheless had noticed that organisms are quite effective dissipators. I'll take dissipation to mean the conversion of energy from more useful to less useful forms (electricity to heat for example). Chronologically, the next widely known consideration of the thermodynamics of life came when Erwin Schrödinger delivered a series of lectures in 1943 at Trinity College, Dublin (Schrödinger, 1944). Schrödinger affirmed that despite some belief to the contrary, organisms obey exactly the same physical laws as non-living systems. He also had the incredible insight to essentially predict the existence of a genome, which he described as an "aperiodic crystal". The basic idea being that crystals have a repeating, unchanging microscopic structure. Therefore if a crystal was free of this symmetry condition, it would have the ability to encode information, the same way that digital information is stored on a magnetic disk.

The ideas presented by Schrödinger (1944) have served as the primary inspiration for much of the modern work concerning biological thermodynamics. The literature base of this field is now rather large, but quite a fraction of it is, by some measures, undeserving of credibility. Even the respectable works often do not go far beyond re-confirming that life does obey the second law of thermodynamics. Given the intellectual talent and time

that has been spent pondering this problem, the lack of any ground-breaking theoretical understanding attests to its difficulty.

At its heart, this is a problem of non-equilibrium thermodynamics, which itself does not yet have a broad theoretical base. We know that the Earth is a strongly driven, non-equilibrium system. We know that organisms store information about their environments genetically. We also know that organisms play a major role in the energy and matter exchanges of the planet. But is that role mathematically definable?

Schneider and Sagan (2005) expressed the idea that life is a manifestation of the second law of thermodynamics. The concept is intriguing and hard to deny but also somewhat empty when it comes to predictive power. We know that organisms contend with and use the second law of thermodynamics. And life may have started because of the strong disequilibrium found at off-axis hydrothermal vents (Branscomb and Russell, 2013). But the ideas of Schneider and Sagan (2005) do not seem to offer a lot more insight.

Chaisson (2011a,b) has proposed his own physical metric for complexity (and by extrapolation, life): energy rate density. This variable corresponds to the intensity with which energy is passing through a unit volume of space. He states that early in the lifetime of the universe, it was virtually devoid of shape or form, but with time has developed organised structures which experience progressively stronger flows of energy, and a higher degree of complexity. Life is the epitome of this sequence of self-organisation and exhibits the highest energy rate density of any structure in the known universe, he argues. Of all the contemporary works on biological thermodynamics, his stands out as having a quantitative basis and being subject to testing and analysis. The data that he presents naturally suggests his hypothesis is correct but further independent study will be required to prove its absolute validity. If it did prove accurate it could reshape our thinking of the role of energy within evolutionary theory. This leads us to question: Can natural selection be defined in thermodynamic terms?

The theory of evolution by natural selection can seem to be somewhat subjective. Although it may explain the fitness of organisms in a given environment, for persistence over greater time scales, the ability to adapt to changes is as crucial as fitness to the present surroundings. After all, the Earth is not a constant, homogeneous, stable place. Quite the opposite. In fact in any environment (Earthly or otherwise), change is the rule, rather than the exception.

Thus the concept of natural selection might benefit from a more rigorous theoretical basis and the ability to apply over a range of length and time scales, i.e., to chemical structures, single-celled organisms, larger more complex organisms, even groups of organisms and structures within economic or social systems. Such a theory ought to encompass both stability and robustness to perturbations.

Kauffman (1996) has argued that the process of evolution consists of both natural selection and self-organisation. He proposed that self-organisation (also rather ill-defined as a concept) provides the building blocks and evolution filters out which combinations of those building blocks make robust organisms. But it could be argued that natural selection and self-organisation are just two facets of the same underlying effect.

Natural selection favours organisms which can make a living in a particular niche. Self-organisation (in my interpretation) is a process in which objects interacting in simple ways form non-trivial aggregate structures (for example large molecules such as proteins or groups of organisms such as coral reefs). Self-organisation could be seen as a selection mechanism for stable complex structures. After all, the specific tertiary structure of a macromolecule such as a protein, forms due to the energetic interactions of its constituents. There is an immense range of *possible* tertiary structures, but those structures that one actually observes is a tiny subset of what is possible, due to the physical constraints upon the molecule. So in this case, the physical interactions of the components of the system have caused the selection of the resultant structure.

Natural selection could also be viewed as an ordering pressure for stable complex structures. In their current forms, there is no need for both the concepts of self-organisation *and* natural selection. But ideally, there should be a single unified formulation of evolution based on the idea of robustness to perturbations, which applies equally to all length scales.

Even before Schrödinger's pioneering lecture series, Lotka (1922) considered the energetics of the evolutionary process. This short but insightful work expressed the fact that organisms are in some ways analogous to heat engines (plants were referred to as *accumulators*). The author also succinctly wrote that while the first and second laws of thermodynamics are obeyed by biological systems, they are not *sufficient* to define how a given biological system will change over time. In essence, the first and second laws are

constraints, but they are not a set of dynamical rules. Though even as constraints they are powerful (imagine a world where perpetual motion machines were possible).

The idea of organisms as heat engines was further elaborated by Cottrell (1979), whose work helped inspire the idea of free energy converters (Branscomb and Russell, 2013). All organisms facilitate energy transformations. Indeed I have previously put forth a tentative definition for life as: A set of linked energy transformations whose action aims to allow the continuation or augmentation of those transformations (Bartlett, 2012). Energy transformations occur in living and non-living systems. But in living systems there is a reflexive, goal-directed element. The set of transformations which comprise an organism are both the means for building and maintaining the organism but they also *are* the organism. It is simultaneously the means and the end for its own activities.

## 1.3 The Many Faces of Disequilibrium

I have discussed what life does from a thermodynamic perspective but not why it carries out those actions. It is difficult to argue against the idea that the very first organism to emerge, did so as a result of large energy gradients (Branscomb and Russell, 2013). Contemporary life is driven by gradients and without them, there would have been no need for a set of organised, dissipative processes to be thrust into being. It was the nobel laureate Ilya Prigogine who first coined the term "Dissipative Structure" (Kondepudi and Prigogine, 1998). He was a pioneer of non-equilibrium thermodynamics who first recognised that systems driven out of equilibrium sometimes form organised patterns as a result of the gradients imposed upon them. Two of the most characteristic classes of dissipative structures, convection cells and reaction diffusion spots, will be explored in depth in this thesis.

There is compelling evidence that organisms are dissipative structures, taking part in the equilibration process of the universe, as the Sun gradually burns through its nuclear fuel, heading inevitably towards a higher entropy state. But what is the thermodynamic role played by organisms? Does natural selection imply a pressure for greater entropy production? Or perhaps lower entropy production? Producing lots of entropy implies that a large amount of useful energy is being transformed into (less useful) heat. So

perhaps having a higher efficiency and producing less entropy, is the more successful strategy.

The opposite could also be argued. If a particular functional process can be achieved with lower entropy production, an organism might be able to utilise the remaining free energy content in a different process. Squeezing every last Joule from a given free energy gradient would imply a pressure for a greater entropy production overall since a larger entropy production would imply a larger fraction of the useful energy of a particular source has been utilised.

There is currently no modelling framework that is capable of providing concrete answers to these lines of enquiry. However numerical simulations can help us make progress on some basic questions of non-equilibrium thermodynamics, in particular with regard to pattern forming systems. Simulations can allow us to carry out highly controlled "digital experiments" where every degree of freedom can be observed.

Many of the most interesting non-equilibrium systems involve fluids and fluid flows. The chemical processes of life occur in aqueous solution and one could very loosely summarise the physics of life as: fluid dynamics and chemistry.

What happens when a system with many degrees of freedom, such as a reacting fluid, is driven out of equilibrium? Generally speaking, we observe fluxes of matter and energy. These are flows of heat, changes in chemical potential, and the movement of mass due to fluid motion. They serve to transport energy from regions where it is concentrated, to regions where it is more diffuse, playing their part in the effects captured by the second law. What limits the rates of these fluxes? Can they be arbitrarily strong?

Systems driven by extremely strong gradients often experience turbulence, a chaotic, disordered state of flow where only the statistical properties are predictable. In contrast, at low driving rates we observe weak, linear flows of matter and energy, usually by the process of diffusion only. It seems that life operates at neither of these extremes. It is an organised set of structures and processes, not completely chaotic. At the same time it is not so ordered that it is completely static and predictable, like the periodic crystals which Schrödinger pointed out life is not. That life exists on the middle-ground between order and chaos has been proposed before (e.g., Kauffman, 1996).

If we simulate such systems, how do they respond to increases in their number of degrees of freedom? Do they produce more entropy, or less? In extant ecosystems we see an entangled network of interactions where the autotrophs use an inanimate source of free energy to locally decrease the entropy of organic compounds. The heterotrophs then allow those more complex compounds to fall back into higher entropy states and harvest the useful energy given off in the process, for their growth and reproduction. The material of the system is simply propelled around the cycle (Bartlett, 2013). The motive force for this material processing is an external source of free energy (normally solar radiation, but could also be inorganic chemical energy). Is it possible to observe anything remotely similar in a complex, but non-living system? How complex a system do we need for such phenomena to occur?

I will attempt to answer some of these questions in this thesis, through a series of numerical simulations of fluid systems of varying degrees of complexity. I intend to analyse the entropy production rate of systems that are materially closed and see how it changes in response to changes in driving forces and boundary conditions. I will also examine chemically reacting flow systems which are open to matter fluxes, and observe whether any life-like phenomena can be identified as the number of constituents and reactions is increased. Exploring such systems will facilitate the testing of the MEPP. It will allow hypotheses to be assessed. It may also stimulate the creation of new ideas or theories concerning the role of dissipative structures in their non-equilibrium environment.

## 1.4 The Structure of the Thesis

This work is approximately divided into two separate, albeit related, parts.

### 1.4.1 Maximum Entropy Production and Fluid Convection

The first part has several objectives. Initially it introduces, derives and tests a numerical scheme known as the Thermal Lattice Boltzmann Model. The performance of this model is validated through a series of benchmark tests consisting first of isothermal systems in chapter 2 and then thermal systems in chapter 3. Having established that the model is capable of simulating simple flows accurately, I move on to consider the role of entropy

production in heated fluid systems in chapter 4. I will critically evaluate the MEPP and previous results (Ozawa et al., 2001) that claim it can reliably predict the steady states of systems undergoing natural convection (NC), defined as buoyancy driven fluid flow caused by temperature gradients.

The results presented in chapter 3 are consistent with previously published works, since they describe the transport properties of NC systems that have been thoroughly studied, both theoretically and experimentally (Doering and Constantin, 1996; Grossmann and Lohse, 2000; Howard, 1963; Johnston and Doering, 2009; Kraichnan, 1962; Malkus, 1954a; Malkus and Veronis, 1958; Malkus, 1954b). Nevertheless using these well-known results, I will demonstrate that the MEPP is not capable of consistently predicting NC steady states.

To add further evidence to my argument, in chapter 5 I will simulate another convective fluid system but with a less constrained set of boundary conditions. The boundary conditions will permit a greater freedom in the steady state variables that the fluid can exhibit. Amongst these possible configurations there will be a unique state of maximum entropy production (MEP). Despite having the ability to adopt this MEP state, the results will show that the system never actually does. Instead it shows a range of states, each dependent on the exact physical parameters describing the fluid.

### 1.4.2 Reactive Systems and Ecological Dynamics

In the second part of the thesis I will extend the modelling framework presented in chapter 2 and chapter 3 to include chemical reactions. In chapter 6 an isothermal Reactive Lattice Boltzmann Model (RLBM) is introduced and two sets of assessments of the abilities of this model are described. We then move on in chapter 7 to the full form of the model representing a key objective of all the previous work of the thesis: non isothermal reacting systems capable of fluid flow. This numerical model is capable of simulating a variety of physical processes in a consistent and coherent manner including diffusive heat transfer, diffusive mass transfer, thermally induced fluid convection, advection of passive scalar chemical species and reactions between those species. This represents a powerful modelling framework with which a plethora of complex systems can be simulated. In this thesis I will only scratch the surface of the model's capabilities. The investigations I present in chapter 7 aimed to elucidate the influence of thermal and convective effects on

the dynamics of the Gray-Scott (GS) reaction diffusion (RD) system (Gray and Scott, 1985; Pearson, 1993). It will be shown that competition can emerge, not just between different RD structures, but also between RD structures and fluid convection patterns.

## 1.5 Contributions

There are several novel aspects to the work presented here. Firstly, it is generally assumed in the literature that NC heat transfer is an example of a MEP system (Ozawa et al., 2001; Meysman and Bruers, 2010). But this assumption is unfounded when one considers all the subtle details of such systems. With the careful analysis of chapter 4 and chapter 5, I present compelling evidence that MEP is not a valid selection rule for NC systems. This work has been submitted for publication and is currently under review (Bartlett and Bullock, 2014).

The second set of contributions are the version of the Lattice Boltzmann Model (LBM) that I develop, allowing it to simulate the combined processes of diffusion, convection and chemical reaction. I am not the first person to extend the LBM to incorporate these effects (Amaya-Ventura and Rodriguez-Romo, 2011; Ayodele et al., 2011; Di Rienzo et al., 2012; Zhang and Yan, 2012), but the version that I present is the simplest and most general way to simulate all of these phenomena simultaneously.

The majority of research on abstract non-linear reaction systems has been constrained either by well mixed reactor assumptions (e.g., Gray and Scott, 1985), or has focussed on purely diffusive (non-convective) mass transport (Mahara et al., 2004; Pearson, 1993). It seems that introducing thermal effects to the GS RD system has not been done before. I appear to be the first researcher to employ thermal kinetic schemes for the 2D GS RD model. Consequently chapter 7 represents the first study of how the combined processes of enthalpy changes and fluid convection affect the patterns formed in the GS RD system. The competitive interactions between different types of dissipative structure in section 7.3 are also novel.

In the next chapter, the core of the thesis begins, by introducing the modelling framework that serves as the foundation of all the simulations presented herein.

# Chapter 2

# Lattice Boltzmann Model with BGK Collision, Single-phase

In this chapter I present the basic workings of the numerical method that will be used to investigate the questions and hypotheses posed in chapter 1. I have several important criteria for the simulation technique to be adopted. Firstly, it must be physically realistic. Abstract models based on a very small number of constraints have a crucial role to play in the scientific endeavour, as do those highly complicated models with significant predictive power (General Circulation Models of the climate system for example). Any theoretical model exists upon a continuum between these extremes. The user must decide upon the trade-off between physical realism and simplicity, between heavy computational demands and rapid production of results, between a model almost as complicated as the real system and one for which the dynamics can be readily understood.

For the purposes of this thesis, physical accuracy is important for I hope to uncover phenomena which are representative of real systems. On the other hand, a model that simulated every physical detail would be hopelessly complicated and prohibitively demanding of computational resources. Therefore the method used will be physically accurate for the simpler systems analysed, and for the more complex scenarios, simplifying assumptions and benchmark tests will be employed where necessary to keep track of the accuracy/simplicity balance.

The method should be as simple and flexible as possible. Many simulation techniques are simple in principle but end up being extremely complicated when applied to more

complex situations. It should be possible for the method to be naturally extended without an exponential explosion of complicatedness. It must be straightforward to extract thermodynamic variables and measurements from the model, and it should be transparent so that all of its inner workings can be easily understood and controlled. Finally, it must be as fast and efficient as possible. The objective of this thesis is to simulate relatively complex systems, and many standard simulation techniques would require an impractical amount of computer power and/or memory for the scenarios to be modelled.

The method that satisfies these demands in the most optimal way is the Lattice Boltzmann Model (LBM). It has emerged relatively recently as a simple, fast and efficient numerical scheme for a wide range of physical systems, primarily those involving fluid flows. In contrast to a commercial package, I can construct LBM codes myself and have complete knowledge of their inner workings. The only assumptions and interactions occurring in the simulations will be those that I wish to be present. For a wide range of problems in computational fluid dynamics (CFD), the LBM has been shown to be just as accurate as competing simulation techniques (Chen et al., 1992).

Moreover, it is thermodynamically consistent, obeying Boltzmann's H-theorem (isolated systems tend to an equilibrium state). It is easily parallelisable since all its interactions are local. Coupled with its simple construction, this makes it a relatively fast method. I will also be able to straightforwardly add additional components and interactions to the model. The algorithm itself does not require significant modification for this, rather it just requires additional memory and processing power. Having explained why I have chosen the LBM, I will now describe the physics behind it, which will clarify further why it is a natural choice for the problems explored in this thesis.

## 2.1 The Physical Basis of the Lattice Boltzmann Model

The LBM represents a relatively novel method in CFD. Rather than calculating an approximate, numerical solution of the continuum Navier-Stokes equations, which describe the fluxes of mass and momentum in a fluid, the LBM begins at a finer, kinetic length scale. As per Boltzmann's 19th century assumption, the fluid is represented by a collection of many hard particles moving and colliding with one another.

The LBM drew significant inspiration from the Lattice Gas Automata (LGA) of Frisch et al. (1986). This is another CFD technique that models the fluid as a collection of discrete particles, occupying the links of a discrete lattice. Each time step they propagate along their current lattice link. They then undergo elastic collisions with the other particles that share the lattice node they have just arrived upon. The collisions conserve mass and momentum and such a simple model of a fluid on a triangular lattice can actually be used to simulate real systems. In fact, the Navier-Stokes equations can be derived from the microscopic evolution equations of the LGA (Frisch et al., 1986).

While the LGA has the advantage of being unconditionally stable, it has been shown that it does not satisfy Galilean invariance and the pressure of a LGA fluid contains a dependence upon velocity. An ideal gas equation of state has no such velocity dependence. Furthermore, it exhibits a considerable degree of statistical noise due to its particulate nature. It is thus necessary to conduct some process of ensemble or time-averaging to extract macroscopic data from LGA simulations.

From one perspective, the LBM represents a method for circumventing this problem since it is essentially a coarse-grained, meso-level scheme for the lattice gas (Chen et al., 1992; McNamara and Zanetti, 1988). Rather than modelling the translation and collision of individual particles, the LBM describes the evolution of *collections* of particles. The mass of the fluid is represented by sets of velocity distribution functions. At any given time and location in the numerical domain, the model stores the density of particles moving in each of a discrete set of directions. It proceeds by solving the equations governing the time evolution of these velocity distributions. There is no explicit representation or solution of the Navier-Stokes equations. Instead, through a re-scaling technique known as the Chapman-Enskog expansion, it is possible to *derive* the Navier-Stokes equations *from* the equations of the LBM (Chen et al., 1992).

This feature is quite remarkable. The LBM is founded upon a completely fictitious model for the microscopic behaviour of fluids (as we know from quantum mechanics, atoms and molecules are *not* hard spheres undergoing elastic collisions), and yet in the macroscopic limit, it leads to physically correct behaviour. It is perhaps less of a surprise when we bear in mind that the majority of physical models are not derived from first principles (certainly not from the quantum level) but rather constructed from higher level, known phenomena.

This begs some interesting metaphysical questions such as: why is it that there seems to exist a family of fictitious molecular dynamics which all map to the correct fluid behaviour at the macroscopic level? Or more generally, what is required for completely robust emergence of higher level laws from another set of laws at a smaller length scale? The emergence of Newton's laws from quantum mechanics or of chemistry from quantum mechanics for example. In our case with lattice-based CFD models, it seems that conservation of mass and momentum are the most fundamental characteristics of a fluid dynamical system and other details are much less relevant to the large-scale behaviour. While interesting, these questions unfortunately are somewhat beyond the scope of this thesis and we must return to the task at hand.

As well as a coarse-grained average of the LGA, the LBM can be thought of as a discretised numerical scheme for the Boltzmann equation (He and Luo, 1997a,b). The Boltzmann equation is a continuity equation for distribution functions of fluid properties such as momentum and internal energy. It essentially states that the rate of change of the distribution function at a point in space is equal to changes caused by advection (net fluid flow) and from collisions between the particles.

Now that we have an approximate understanding of the physical basis of the LBM, we can proceed to construct the equations to be solved in a LBM code.

## 2.2 Theoretical Derivation

The form of the model that I present here is a single-phase isothermal model. In later chapters I will extend it to include additional components including the internal energy in chapter 3, and passive scalar species in chapter 6.

We begin with a foundational component of kinetic theory, the continuous Boltzmann equation:

$$\frac{\partial f}{\partial t} + \mathbf{v}\nabla f = \Omega(f), \tag{2.1}$$

which describes the evolution of the velocity distribution function $f(\mathbf{x}, \mathbf{v}, t)$. This function represents the mass of particles per unit volume moving at velocity $\mathbf{v}$ measured over some small volume centred on position $\mathbf{x}$ at time $t$. Changes in $f$ within this volume element occur through advection by the particle motion (at velocity $\mathbf{v}$), and through

collisions between particles within the element, encapsulated in the collision term $\Omega(f)$. Note that $\mathbf{v}$ is the microscopic velocity of the volume element. Macro-level properties of the fluid can be derived from the appropriate moments of the velocity distribution,

$$\rho = \int f d\mathbf{v} \tag{2.2}$$

$$\rho\mathbf{u} = \int \mathbf{v} f d\mathbf{v} \tag{2.3}$$

where $\rho$ is the fluid density, $\mathbf{u}$ is the velocity, and the integrals are evaluated over the entire velocity space. The full form for the collision operator $\Omega$ contains some rather complicated integrals which led Bhatnagar et al. (1954) to devise a greatly simplified form for this term. The so-called BGK LBM approximates the collision process with a single-time relaxation:

$$\frac{\partial f}{\partial t} + \mathbf{v}\nabla f = -\frac{f - f^{eq}}{\tau_\nu} \tag{2.4}$$

where $\tau_\nu$ is the characteristic time scale for equilibration and $f_{eq}$ is the velocity distribution of the equilibrium state. For this state, the Maxwell-Boltzmann distribution is assumed:

$$f^{eq} = \frac{\rho}{(2\pi RT)^{D/2}} \exp\left[-\frac{(\mathbf{v}-\mathbf{u})^2}{2RT}\right] \tag{2.5}$$

where $R$ is the molar gas constant and $D$ is the dimensionality of space. In order to construct a solvable numerical scheme, Equation 2.4 must be discretised in terms of space, time and particle velocity. The appropriate equilibrium distributions (discrete forms of Equation 2.5) must also be found for such a velocity set. Let us choose velocities $\mathbf{v}_i$ where $i = 0, 1, ..., N-1$ and corresponding distributions $f_i$. The evolution equation becomes

$$\frac{\partial f_i}{\partial t} + \mathbf{v}_i\nabla f_i = -\frac{f_i - f_i^{eq}}{\tau_\nu}. \tag{2.6}$$

This is known as the discrete Boltzmann equation since it describes a discrete velocity space. In contrast, the discretised Boltzmann equation, which we shall now derive, describes the evolution of a discrete set of velocities over a discretised space and time domain.

First the above equation must be de-dimensionalised by introducing a characteristic speed $U$, length scale $L$, density $n_r$, and time between collisions $t_\nu$. This allows the dimensionless velocities $\mathbf{e}_i = \mathbf{v}_i/U$, normalised gradient operator $\hat{\nabla} = L\nabla$, dimensionless time $\hat{t} = tU/L$, relaxation time $\hat{\tau}_\nu = \tau_\nu/t_\nu$ and distribution function $F_i = f_i/n_r$ to be

defined. Finally the dimensionless parameter $\epsilon_\nu = t_\nu U/L$ must be introduced, that is the ratio of two time scales: collision time to characteristic flow time. When $\epsilon_\nu \ll 1$, collisions occur sufficiently fast that they do not sense the net fluid advection. The non-dimensional discrete Boltzmann equation now reads

$$\begin{aligned} \frac{U}{L}\frac{\partial}{\partial \hat{t}}(n_r F_i) + \frac{U\mathbf{e}_i}{L}\hat{\nabla}(n_r F_i) &= -\frac{n_r}{\hat{\tau}_\nu t_\nu}(F_i - F_i^{eq}) \\ \frac{\partial F_i}{\partial \hat{t}} + \mathbf{e}_i \hat{\nabla} F_i &= -\frac{1}{\hat{\tau}_\nu \epsilon_\nu}(F_i - F_i^{eq}). \end{aligned} \tag{2.7}$$

Discretising this equation in space and time using a uniform grid spacing $\Delta\hat{\mathbf{x}}$ and time scale $\Delta\hat{t} = \delta t U/L$ such that $\mathbf{e}_i = \Delta\hat{\mathbf{x}}/\Delta\hat{t}$ leads, after some algebra to

$$F_i\left(\hat{\mathbf{x}} + \mathbf{e}_i\Delta\hat{t}, \hat{t} + \Delta\hat{t}\right) - F_i(\hat{\mathbf{x}}, \hat{t}) = -\frac{\Delta\hat{t}}{\hat{\tau}_\nu \epsilon_\nu}(F_i - F_i^{eq}) \tag{2.8}$$

If the time between collisions and time step are set equal: $\delta t = t_\nu$, this yields $\Delta\hat{t} = t_\nu U/L = \epsilon_\nu$. Equation 2.8 now becomes:

$$f_i\left(\mathbf{x} + \mathbf{e}_i\Delta t, t + \Delta t\right) - f_i(\mathbf{x}, t) = -\frac{1}{\tau_\nu}(f_i - f_i^{eq}) \tag{2.9}$$

where carets have been omitted and the distribution function has been returned to lower case. The dimensionless version of our evolution equation is essentially identical to the dimensional version and only the parameter $\tau_\nu$ is required to alter the viscosity of the simulated fluid (the desired flow characteristics can then be obtained with a suitable selection of domain size and characteristic fluid velocity).

It can be shown that the equilibrium distribution functions that have identical moments (up to fourth order) to the Maxwell Boltzmann distribution (Equation 2.5) are the following (Wolf-Gladrow, 2000),

$$f_i^{eq} = \omega_i \rho \left[1 + 3\frac{\mathbf{e}_i \cdot \mathbf{u}}{c^2} + \frac{9}{2}\frac{(\mathbf{e}_i \cdot \mathbf{u})^2}{c^4} - \frac{3}{2}\frac{\mathbf{u}^2}{c^2}\right]. \tag{2.10}$$

Throughout this thesis, the 2-dimensional D2Q9 model will be used, which utilises a square lattice with 8 velocities and rest particles (see Figure 2.1). For this velocity set the weights $\omega_i$ are $\omega_0 = 4/9$, $\omega_i = 1/9$ for $i = 1, 2, 3, 4$ and $\omega_i = 1/36$ for $i = 5, 6, 7, 8$.

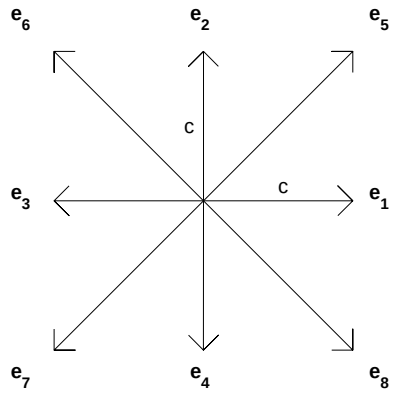


Figure 2.1: Discrete velocity vector set for the D2Q9 Lattice Boltzmann Model.

The velocity vectors are thus defined,

$$\begin{aligned} \mathbf{e}_0 &= (0,0) \\ \mathbf{e}_{1,3}, \mathbf{e}_{2,4} &= (\pm c, 0), (0, \pm c) \\ \mathbf{e}_{5,6,7,8} &= (\pm c, \pm c) \end{aligned} \tag{2.11}$$

To calculate macroscopic fluid variables, the appropriate moments of the distribution functions must be taken (now discrete):

$$\begin{aligned} \rho(\mathbf{x}, t) &= \sum_i f_i(\mathbf{x}, t) \\ \rho(\mathbf{x}, t)\mathbf{u}(\mathbf{x}, t) &= \sum_i \mathbf{e}_i f_i(\mathbf{x}, t) \end{aligned} \tag{2.12}$$

Using the Chapman-Enskog expansion, it can be shown that at the macro-level, a fluid obeying the above equations satisfies the Navier-Stokes equations with a kinematic viscosity given by:

$$\nu = \frac{1}{3}\left(\tau_\nu - \frac{1}{2}\right) c^2 \delta t. \tag{2.13}$$

The integration step $\delta t$ plays no physical role so it will be set to 1 and omitted from all equations henceforth. All that remains at this stage is to define the dimensionless relaxation time $\tau_\nu$. Unit lattice spacing $c$ can be used since there is no requirement to adjust its value. However in later chapters, the non-isothermal LBM will require a value for $c$ that depends on the average temperature (see section 3.2).

As expressed by dynamical similarity, flow conditions for a given fluid system often

depend only upon a small number of dimensionless parameters. The most important of these is the Reynolds number:

$$Re = \frac{UL}{\nu}, \tag{2.14}$$

which is a ratio of inertial forces to viscous forces. The Reynolds number seems to correlate experimentally with the degree of turbulence (although definitions of turbulence and the transition to turbulent conditions are still an area of active research and are by no means fully understood). In this expression, $U$ is a characteristic velocity (such as the free stream velocity of a flow past an obstacle), $L$ is a characteristic length scale (such as the size of a flow obstacle) and $\nu$ is the fluid viscosity. Almost everything required to construct a LBM-based CFD code is now present. All that remains is to define the boundary conditions (BCs).

## 2.3 Definition of Boundary Conditions

The most commonly used BCs of the LBM will now be introduced. At a plane boundary, there will be three distributions that are unspecified after the streaming step. At a corner node, there will be five unknown distributions. Here I describe in detail, two different approaches from the literature for calculating values for these unknown distributions at the streaming step of the algorithm. I will also discuss some other BCs featuring in the literature and describe their relationship to these two methods.

It is not immediately obvious how BCs should be defined for the LBM, since there is no clear intuitive picture for how probability distribution functions should behave when encountering a solid boundary. However, inspiration can be taken from the LGA, since the LBM is in some sense a coarse-grained version of it. In the LGA a very simple approach is taken to particles encountering a wall. The boundary acts to completely reverse the velocity of the incoming particles (their velocity vectors are rotated by 180°). This is known as the bounce-back method and it is the most common technique for specifying the unknown distributions after the streaming step in the LBM. As the name implies, distributions that stream out of the domain are simply reversed in direction by the solid wall, that is assumed to lie half a grid spacing away from the boundary nodes (see Figure 2.2).

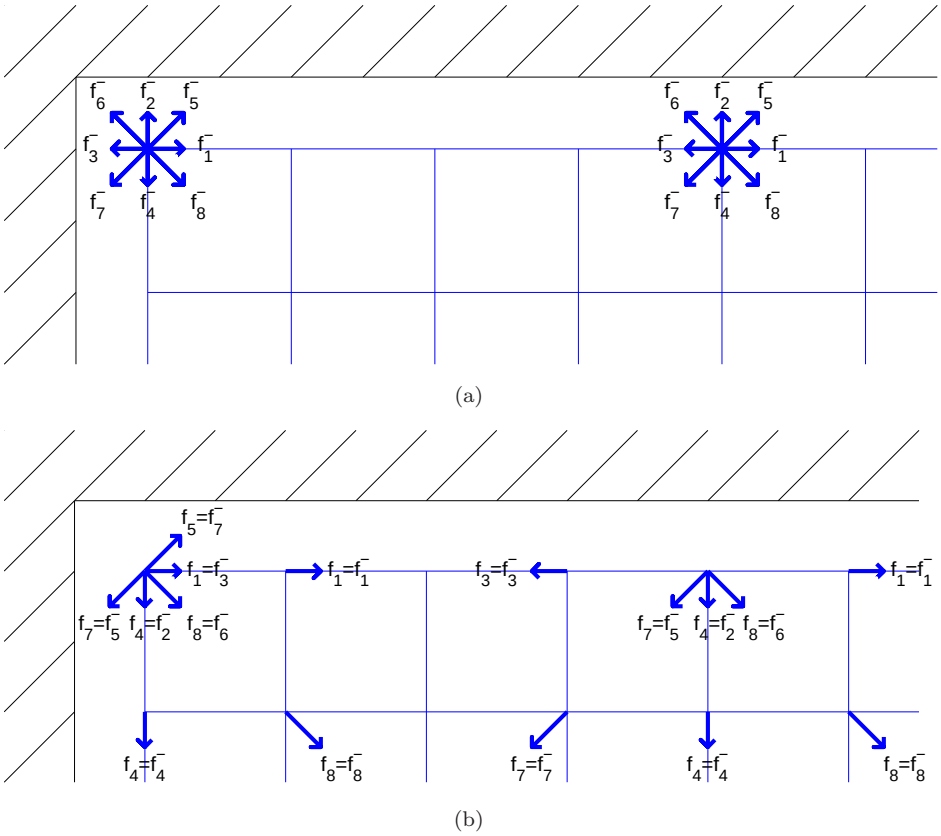


Figure 2.2: Streaming step for boundary nodes using the bounce-back method. a) Pre-streaming velocity distributions, $f_i^-$. b) Post-streaming velocity distributions, $f_i$. Note that distributions streaming into the wall have had their directions completely reversed. Other distributions have propagated along their respective velocity vectors $\mathbf{e}_i$.

The fact that the distributions have their directions completely reversed rather than undergoing specular reflection, ensures that the wall imposes a viscous shear stress on the fluid and enforces a no-slip condition at the solid boundary. A detailed analysis of several variations of the bounce-back method have shown that the halfway wall version, which is the version I have described and made use of, is second order accurate (He et al., 1997).

Note that upon first inspection, it appears that at corner nodes, there will always be two distributions which perpetually bounce-back at the corner, and never stream into the bulk of the fluid. There are several resolutions of this issue. Firstly it should be noted that they do interact with the rest of the domain because of the collision step (Equation 2.9), wherein they may lose or gain mass to or from other distributions. They are not completely isolated. Secondly some authors choose to simply set those

distributions to their equilibrium values with some characteristic density value (Peng et al., 2003). And finally, in this thesis the majority of the simulations will have periodic BCs in the horizontal direction. Therefore such corner BCs will not be used except in one set of simulations in subsubsection 3.4.2.1.

As an alternative to the bounce-back method, a no-slip condition could be enforced by placing the wall very close to the boundary nodes or by forcing the extrapolated velocity at the wall to zero. Since the LBM came to light about 20 years ago, there have been many BCs put forward in addition to the bounce-back method, which arguably remains the most popular due to its ease of application for complex boundaries such as porous media. The aim is to ensure that the BCs do not reduce the accuracy of the numerical scheme. In the bulk of the domain the LBM is second order accurate (Chen and Doolen, 1998).

Taking inspiration from finite difference methods, Chen et al. (1996) proposed an extrapolation scheme for calculating unknown distributions at boundaries. Other extrapolation schemes have also been proposed more recently (Guo et al., 2002; Tang et al., 2005). The principle of diffuse reflection from kinetic theory has also been used to derive the 'counter-slip' approach (D'Orazio et al., 2004; Inamuro et al., 1995; Sofonea and Sekerka, 2005). With this BC, the particles reflected from the wall are assumed to have velocities distributed according to a Maxwell-Boltzmann distribution with mean velocity equal to that of the wall. Zou and He (1997) deduced a modified bounce-back method where the non-equilibrium part of the distribution perpendicular to the wall is reflected and the remaining two unknown distributions are calculated using the constraints of specified wall velocity and/or pressure. This method is similar to that of Maier et al. (1996). Assuming equal and opposite non-equilibrium distributions at a solid wall stems from a fortunate symmetry property of the non-equilibrium part of the velocity distributions (He et al., 1998). The last three methods have a similar conceptual foundation of specifying provisional values for the unknown distributions (usually using some form of bounce-back) and then enforcing a correction procedure to ensure that the wall velocity and/or density conditions are adhered to.

The authors of each of these variations of LBM wall BCs have shown that their method is accurate to second order, in line with the LBM itself. Therefore it seems clear that the LBM is somewhat indifferent to the specific method used to calculate the values of the

unknown distributions. The crucial factor is that there is some implementation of the no-slip condition, either by using bounce-back to provide a shear stress from a halfway wall, or by explicitly forcing the velocity at the boundary nodes to zero. It would be instructive to see whether there is any advantage to be had with a non-bounce-back method. Therefore the BC of Zou and He (1997) will now be defined in complete detail, and in the next section the accuracy of this method will be compared to that of the bounce-back method for a simple flow.

Consider an upper horizontal wall. After the streaming step all new distributions are known except for $f_4$, $f_7$ and $f_8$ (these shall henceforth be written as $f_4^*$, $f_7^*$ and $f_8^*$ since they are as yet unknown). The new values for these distributions must be calculated by considering the mass and momentum constraints at the wall. In this thesis, there will be no requirement for moving walls, only a no-slip velocity BC will be needed ($u_w = v_w = 0$). Equation 2.12 gives expressions for the density, horizontal momentum and vertical momentum at the boundary:

$$\begin{aligned} \rho_w &= f_0 + f_1 + f_2 + f_3 + f_4^* + f_5 + f_6 + f_7^* + f_8^* \\ \frac{\rho_w u_w}{c} &= f_1 - f_3 + f_5 - f_6 - f_7^* + f_8^* = 0 \\ \frac{\rho_w v_w}{c} &= f_2 - f_4^* + f_5 + f_6 - f_7^* - f_8^* = 0. \end{aligned} \tag{2.15}$$

Adding the first and last equations yields

$$\rho_w = f_0 + f_1 + f_3 + 2\left(f_2 + f_5 + f_6\right), \tag{2.16}$$

giving a value for the density at the wall node, $\rho_w$. With these equations alone there are too few constraints to close the system. Therefore, following the method of Zou and He (1997), it can be assumed that the non-equilibrium part of the distribution normal to the wall and pointing inward is equal to the non-equilibrium part of the distribution pointing in the opposite distribution. So in this case, $f_4^* - f_4^{eq} = f_2 - f_2^{eq}$. Since there is a velocity of 0 at the wall, the equilibrium distributions for opposite directions are equal, $f_4^{eq} = f_2^{eq}$ (see Equation 2.10). This in turn means that $f_4^* = f_2$. With this in hand, $f_7^*$ can now be calculated by adding the two momentum equations (Equation 2.15)

together:

$$\begin{aligned} f_1 - f_3 + 2f_5 - 2f_7^* &= 0 \\ f_7^* &= \frac{1}{2}\left[f_1 - f_3 + 2f_5\right] \end{aligned} \tag{2.17}$$

and $f_8^*$ can be calculated by subtracting the vertical momentum from the horizontal:

$$\begin{aligned} f_1 - f_3 - 2f_6 + 2f_8^* &= 0 \\ f_8^* &= \frac{1}{2}\left[-f_1 + f_3 + 2f_6\right] \end{aligned} \tag{2.18}$$

Corner nodes can now also be considered. At the upper left corner the following distributions are unknown after the streaming step, $f_1$, $f_4$, $f_5$, $f_7$, $f_8$. It is assumed that the non-equilibrium parts of the distributions that are normal to both the upper and the left walls are set equal to their opposing counterparts, i.e., $f_4^* - f_4^{eq} = f_2 - f_2^{eq}$ and $f_1^* - f_1^{eq} = f_3 - f_3^{eq}$ (Zou and He, 1997). Again, with the case of zero velocity, oppositely directed equilibrium distributions are equal in magnitude, therefore the expression for the wall density becomes

$$\begin{aligned} \rho_w &= f_0 + f_1^* + f_2 + f_3 + f_4^* + f_5^* + f_6 + f_7^* + f_8^* \\ &= f_0 + 2f_2 + 2f_3 + f_5^* + f_6 + f_7^* + f_8^*, \end{aligned} \tag{2.19}$$

while the two momentum equations are

$$\begin{aligned} \frac{\rho_w u_w}{c} &= f_1^* - f_3 + f_5^* - f_6 - f_7^* + f_8^* = 0 \\ &= f_5^* - f_6 - f_7^* + f_8^* \end{aligned} \tag{2.20}$$

$$\begin{aligned} \frac{\rho_w v_w}{c} &= f_2 - f_4^* + f_5^* + f_6 - f_7^* - f_8^* = 0 \\ &= f_5^* + f_6 - f_7^* - f_8^*. \end{aligned} \tag{2.21}$$

Subtracting the vertical momentum from the horizontal gives

$$\begin{aligned} -2f_6 + 2f_8^* &= 0 \\ f_8^* &= f_6. \end{aligned} \tag{2.22}$$

At this point there is once more an insufficient number of equations to specify the final

two distributions $f_5^*$ and $f_7^*$. To solve this issue, Zou and He (1997) simply specify the density at the corner node. Other authors have taken alternative approaches but in practice, the choice makes very little difference to the simulation results. The most important requirement is that the prescribed constraints are satisfied. So the expressions for density and horizontal momentum can once again be used,

$$\rho_w = f_0 + 2(f_2 + f_3 + f_6) + f_5^* + f_7^* \tag{2.23}$$

$$\frac{\rho_w u_w}{c} = f_5^* - f_6 - f_7^* + f_6 = 0, \tag{2.24}$$

giving the final unknown distributions:

$$f_5^* = f_7^* = \frac{\rho_w - (f_0 + 2(f_2 + f_3 + f_6))}{2}. \tag{2.25}$$

Analogous procedures can be used for other boundaries and corners. This concludes the derivation of the BCs due to Zou and He (1997). Their performance on a simple test problem will be compared to the performance of the bounce-back method in the following section.

## 2.4 Isothermal Benchmark Tests

### 2.4.1 Poiseuille Flow

With the description of the isothermal LBM in hand, it is now possible to begin testing the algorithm on characteristic flows for which there are either analytic or benchmark solutions. The model will be used to simulate a simple flow system: 2D laminar channel flow, or Poiseuille flow. A horizontal pressure gradient will be imposed and this will drive the fluid through the channel (see Figure 2.3). The pressure gradient will be imposed using a body force method, since imposing a density gradient between inlet and outlet leads to high frequency instabilities due to compressibility effects (Maier et al., 1996). Since only laminar flows will be considered (low Reynolds number), the following analytical solution for a channel flow can be used:

$$U(y) = U_0 \left(1 - \frac{y^2}{H^2}\right), \tag{2.26}$$

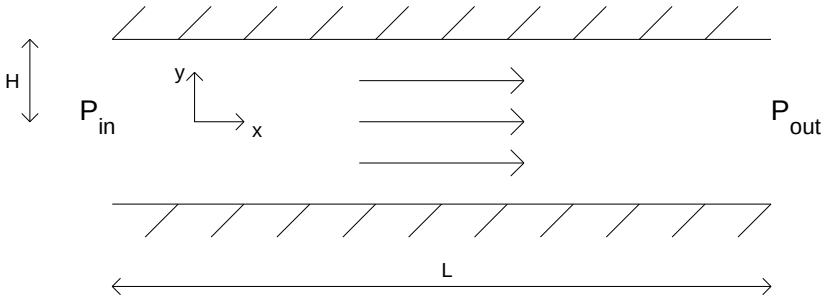


Figure 2.3: Poiseuille flow diagram. The pressure gradient $\nabla p = (P_{in} - P_{out})/L$ drives a purely horizontal flow through the 2D channel, $\mathbf{U} = U(y)\hat{i}$. Note the origin of the y-axis is in the central plane of the channel. $H$ is the half-width of the channel.

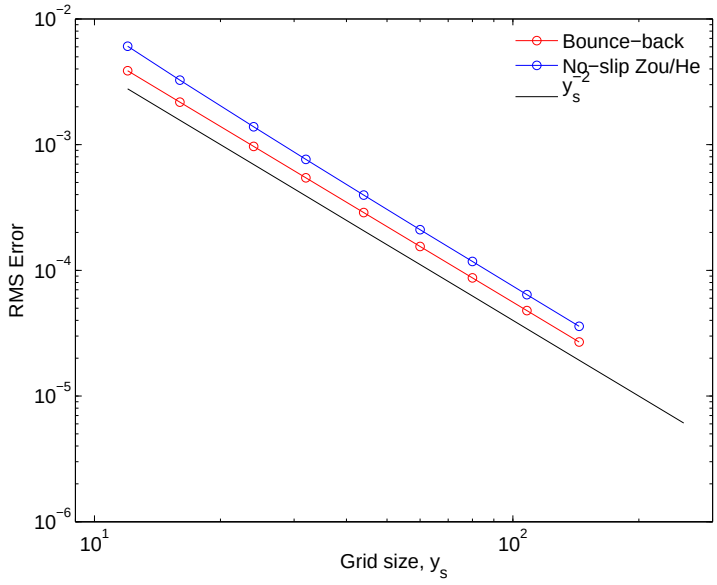


Figure 2.4: RMS error as a function of lattice size for LBM simulations of 2D Poiseuille flow.

which gives a parabolic velocity profile. The accuracy of the following two BCs will be compared: halfway wall bounce-back and the non-slip method of Zou and He (1997). Figure 2.4 shows the root mean square error (normalised by the centreline velocity $U_0$) of the two methods as a function of grid resolution. Also shown is a straight line proportional to the inverse square of the grid spacing. It is clear that both methods retain the second order accuracy of the LBM itself.

The method of Zou and He (1997) does exhibit a slight problem compared with the bounce-back method: if the simulation is initialised with very small random perturbations in the velocity field, it become unstable. In contrast, the bounce-back method

remains stable in the presence of small initial perturbations. Furthermore, it is faster than most other methods since it involves only memory manipulation, and thus no calculations are required for its implementation. Coupled with its superior versatility (it applies equally easily to corners or irregular boundaries), simplicity and accuracy, it makes sense to use this method in all simulations henceforth. Its accuracy will be put to the test further in the next chapter where more comparisons of LBM results with literature benchmarks will be carried out.

### 2.4.2 Flow Past a Cyclinder

To conclude this chapter, a qualitative demonstration of the performance of the isothermal LBM will be presented. One of the most characteristic flow patterns observed in nature and the laboratory is known as the von Kármán vortex street (see Figure 2.5). This occurs when a steady flow encounters an obstacle such as a plate or cylinder. At low Reynolds number under laminar conditions, flow past an obstacle is completely smooth and steady, and exhibits a symmetric wake caused by the drag of the obstacle. However once the Reynolds number is raised above $\sim 90$, that laminar flow becomes unstable to perturbations and vortices begin to be produced alternately from either side of the obstacle.

The hydrodynamic details of this fascinating behaviour are still the subject of research and beyond the scope of this thesis. However for the purposes of this section, the flow pattern will simply be used as an example to demonstrate that the LBM can successfully

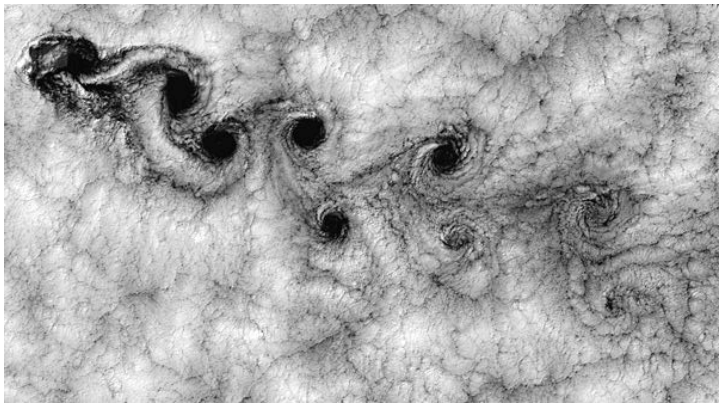

Figure 2.5: Vortex shedding caused by wind flowing past the Juan Fernández Islands off the Chilean coast. Image by Bob Cahalan, NASA GSFC.

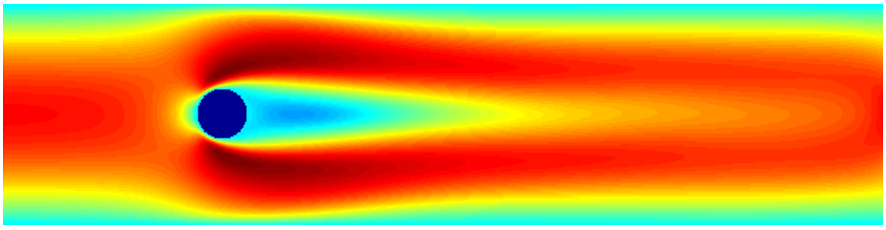

(a)

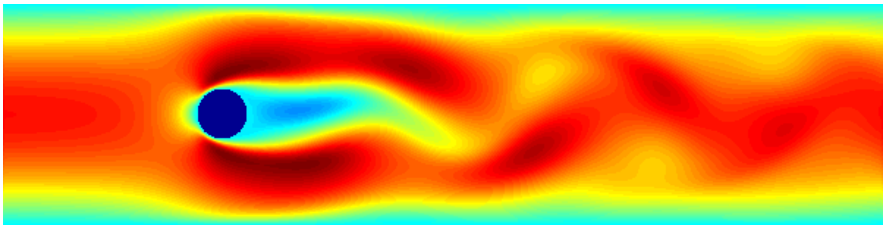

(b)

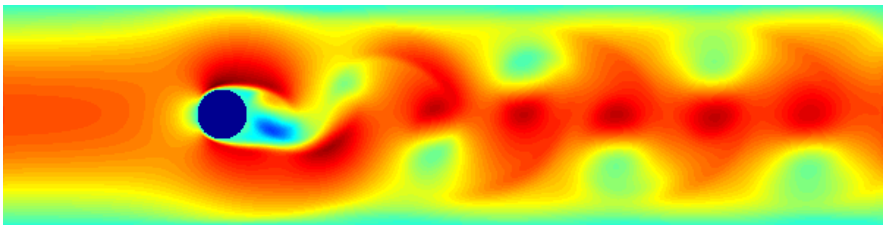

(c)

Figure 2.6: Horizontal momentum density fields for channel flow past a circular obstacle. Colours correspond to momentum magnitude with red being strongest and blue weakest. a) Laminar wake formation at $Re = 80$, below the critical value of $Re_c \sim 90$. b) Non-laminar vortex shedding at $Re = 100$, above the critical value of $Re_c \sim 90$. c) Non-laminar vortex shedding at $Re = 1000$.

simulate such phenomena. Figure 2.6(a) shows the simulated flow field at a Reynolds number of 80. There is a stationary, symmetric wake formed downstream of the obstacle, as expected for a laminar flow. In contrast, figure 2.6(b) shows a vortex street, since the Reynolds number has now been raised to 100. For comparison, figure 2.6(c) also shows the same flow at $Re = 1000$. Note how much more pronounced the vortices have become.

## 2.5 Conclusions

In this chapter the physical and algorithmic basis of the LBM has been presented, such that isothermal simulation codes could be constructed. The specification of BCs was discussed and two of the most commonly used methods were compared with a benchmark

flow for which an analytical solution exists. It was found that the simple bounce-back method is not only simple, versatile and fast, but also has the same accuracy as the slightly more complicated BCs of Zou and He (1997). This led to the conclusion that the bounce-back method is the most logical choice for further simulations. Finally, additional qualitative evidence of the LBM's efficacy was given. The vortex shedding phenomena characteristic of obstacle flows was successfully re-created by the LBM.

Having established the validity of the method for isothermal flows, it can now be extended to fluids that do not have a constant, uniform temperature. This will allow significantly more freedom in terms of the formation of patterns and will also pave the way for making assessments of the non-equilibrium thermodynamic properties of heated fluids. It will then be possible to carry out an interesting and completely novel test of the Maximum Entropy Production Principle in chapter 5.

# Chapter 3

# Lattice Boltzmann Model with Internal Energy as a Passive Scalar

This chapter will describe how the isothermal assumption of the Lattice Boltzmann Model (LBM) can be relaxed by adding an extra level of description to the model. Being able to model a system with variable temperature is crucial since the aims of this thesis are centred upon the ways in which non-equilibrium systems respond to driving forces. A temperature gradient is a prime example of such a driving force, that can provoke a system to exhibit a vast array of interesting behaviours including convection cells and turbulence. There is more than one way in which the LBM can be extended to include thermal variations. The internal energy can actually be calculated through an appropriate moment of the velocity distribution function, so it is possible to simply calculate the temperature of the standard LBM. However it turns out that such an approach requires additional particle velocities or additional relaxation times to prevent numerical instabilities (McNamara et al., 1995).

Instead the temperature field can be modelled as an additional distribution function undergoing streaming and collision processes as the velocity distributions do. This method, which is arguably the most popular modern thermal LBM (TLBM), models the internal energy as a passive scalar, which is advected by the fluid flow and has no influence upon it unless extra interactions are incorporated into the collision term.

In the following section, the governing equations controlling changes in fluid velocity and temperature as a function of space and time will be defined. By de-dimensionalising these equations, it can be shown that there are only two dimensionless parameters that dictate the properties of a given thermal fluid flow. The derivation of the model equations for the TLBM will then be presented. Finally, a series of benchmark tests will be carried out to establish the model's validity.

## 3.1 Equations of Motion

A non-isothermal fluid can be described using the Navier-Stokes equations for the conservation of momentum, the continuity equation for the conservation of mass, and the advection-diffusion equation for the conservation of internal energy. In order to make the equations more tractable, it can also be assumed that the physical properties of the fluid are constant with respect to time, space and temperature. This is known as the Boussinesq approximation and has been successfully applied to a variety of thermal flow problems for many years. One crucial property of a Boussinesq fluid is that it is assumed to be incompressible except with regards to buoyancy forces. The assumption of incompressibility allows a simple continuity equation to be written:

$$\nabla \cdot \mathbf{v}' = 0 \tag{3.1}$$

where $\mathbf{v}' = u'\hat{i} + w'\hat{k}$ is the dimensional fluid velocity. This equation simply states that the mass of the fluid is conserved. The incompressibility assumption means that for any given control volume, the mass of fluid leaving is balanced by fluid entering. This leads to the vanishing velocity divergence shown above. Applying Newton's second law to a fluid parcel yields the momentum equation:

$$\frac{\partial \mathbf{v}'}{\partial t} + \mathbf{v}' \cdot \nabla \mathbf{v}' + \frac{1}{\rho}\nabla P' = \nu \nabla^2 \mathbf{v}' + \beta g_0 (T' - T_0)\hat{k} \tag{3.2}$$

where $P'$ is the pressure, $\beta$ is the coefficient of thermal expansion, $g_0$ is the strength of gravitational acceleration and $T'$ is the temperature. This equation simply states that changes in the fluid velocity occur through driving forces such as pressure gradients (third term) and thermal expansion leading to gravitational buoyancy forces (last term). Flows can also be attenuated through viscous dissipation (fourth term). Finally, the equation

describing flows of heat in the fluid reads:

$$\frac{\partial T'}{\partial t} + \mathbf{v}' \cdot \nabla T' = \chi \nabla^2 T'. \tag{3.3}$$

This equation embodies the fact that heat flows occur either through advection by the fluid velocity or diffusion. Defining a set of characteristic scales will make it possible to de-dimensionalise this equation. A characteristic length scale $\delta$, and time scale $\delta^2/\chi$ will be used (Otero et al., 2002). As a temperature scale the total temperature difference across the system $\Delta T'$ can be adopted. Returning to the momentum equation, it can be seen that each term has units of $Lt^{-2}$. Therefore the equation must be multiplied by $(\delta^2/\chi)^2/\delta = \delta^3/\chi^2$ to express it in dimensionless form,

$$\frac{\delta^3}{\chi^2}\frac{\partial \mathbf{v}'}{\partial t} + \frac{\delta^3}{\chi^2}\mathbf{v}' \cdot \nabla \mathbf{v}' + \frac{\delta^3}{\chi^2}\frac{1}{\rho}\nabla P' = \frac{\delta^3}{\chi^2}\nu \nabla^2 \mathbf{v}' + \frac{\delta^3}{\chi^2}\frac{\Delta T'}{\Delta T'}\beta g_0 (T' - T_0)\hat{k} \tag{3.4}$$

$$\frac{\partial \mathbf{v}}{\partial t} + \mathbf{v} \cdot \nabla \mathbf{v} + \nabla P = \frac{\nu}{\chi}\nabla^2 \mathbf{v} + \frac{\nu}{\chi}\frac{\beta g_0 \Delta T' \delta^3}{\nu \chi} T \hat{k}, \tag{3.5}$$

where $\mathbf{v}$, $T$ and $P$ are the new dimensionless variables. Note that this leaves two coefficients, which are also dimensionless. The first, the Prandtl number $Pr = \nu/\chi$ measures the ratio of momentum to thermal diffusivity. The second, the Rayleigh number $Ra = \beta g_0 \Delta T \delta^3/\nu\chi$ measures the strength of thermal driving forces. The Rayleigh number is of key importance, and will be very relevant to the discussions in following chapters. The purpose of this section and the derivation just given, was simply to show that these two parameters naturally emerge from the equations of motion of a thermal fluid.

## 3.2 Theoretical Derivation

The LBM framework is ideal for adding extra components to a system. With suitable definitions of relaxation parameters, equilibrium distributions and collision terms, extra constituents can be added, whether they are extra fluid phases, dissolved solutes or internal energy. The reason for this generality stems from the fact that (as the name implies) the LBM is based upon the Boltzmann equation, which applies equally to almost any well-defined statistical property of a system (one which can be expressed in terms of a distribution function). In this chapter, the objective is to model the diffusion

and advection of heat and this extra physical component will be represented using its own distribution function. The current model is therefore a two-phase version where a coupling between the phases must be defined to ensure the correct large-scale behaviour. It was presented originally by He et al. (1998) and then re-formulated into a simplified version by Peng et al. (2003), which is the version to be adopted here.

Modelling temperature through a second distribution function assumes that heat is a passive scalar that does not affect the net fluid flow (apart from inducing buoyancy-driven convection when a body force is added). This assumption is valid in the limit of low Mach number flows (this assumption is discussed in more detail below) where viscous heat dissipation and compression work are negligible. All simulations in this thesis will reside within this limit. The internal energy distribution function must first be defined,

$$g = \frac{(\mathbf{v}-\mathbf{u})^2}{2} f. \tag{3.6}$$

Note that $\int g d\mathbf{v} = \rho\epsilon$ where $\epsilon = DRT/2$ is the internal energy density. The function $g$ corresponds to the kinetic energy (per unit volume) present in any given discrete velocity direction with the mean flow $\mathbf{u}$ subtracted from it. Now Equation 3.6 must be inserted into Equation 2.1, the Boltzmann equation:

$$\frac{\partial}{\partial t}\left(\frac{2g}{(\mathbf{v}-\mathbf{u})^2}\right) + \mathbf{v}\nabla\left(\frac{2g}{(\mathbf{v}-\mathbf{u})^2}\right) = \Omega(f). \tag{3.7}$$

Some stages of manipulation are now required to come to the final expression:

$$\begin{aligned}
2g\frac{\partial}{\partial t}(\mathbf{v}-\mathbf{u})^{-2} + \frac{2}{(\mathbf{v}-\mathbf{u})^2}\frac{\partial g}{\partial t} + \mathbf{v}\left(2g\nabla(\mathbf{v}-\mathbf{u})^{-2} + 2(\mathbf{v}-\mathbf{u})^{-2}\nabla g\right) &= \Omega(f) \\
4g(\mathbf{v}-\mathbf{u})^{-3}\frac{\partial \mathbf{u}}{\partial t} + \frac{2}{(\mathbf{v}-\mathbf{u})^2}\frac{\partial g}{\partial t} + 2\mathbf{v}\left(2g(\mathbf{v}-\mathbf{u})^{-3}\nabla\mathbf{u} + (\mathbf{v}-\mathbf{u})^{-2}\nabla g\right) &= \Omega(f) \\
2g(\mathbf{v}-\mathbf{u})^{-1}\frac{\partial \mathbf{u}}{\partial t} + \frac{\partial g}{\partial t} + \mathbf{v}\left(2g(\mathbf{v}-\mathbf{u})^{-1}\nabla\mathbf{u} + \nabla g\right) &= \frac{(\mathbf{v}-\mathbf{u})^2}{2}\Omega(f) \\
\frac{\partial g}{\partial t} + \mathbf{v}\nabla g = \frac{(\mathbf{v}-\mathbf{u})^2}{2}\Omega(f) - 2g(\mathbf{v}-\mathbf{u})^{-1}\frac{\partial \mathbf{u}}{\partial t} - 2g\mathbf{v}(\mathbf{v}-\mathbf{u})^{-1}\nabla\mathbf{u} & \\
\frac{\partial g}{\partial t} + \mathbf{v}\nabla g = \frac{(\mathbf{v}-\mathbf{u})^2}{2}\Omega(f) - 2g(\mathbf{v}-\mathbf{u})^{-1}\left(\frac{\partial \mathbf{u}}{\partial t} + \mathbf{v}\nabla\mathbf{u}\right) & \\
\frac{\partial g}{\partial t} + \mathbf{v}\nabla g = \frac{(\mathbf{v}-\mathbf{u})^2}{2}\Omega(f) - f(\mathbf{v}-\mathbf{u})\left(\frac{\partial \mathbf{u}}{\partial t} + \mathbf{v}\nabla\mathbf{u}\right) & \\
\frac{\partial g}{\partial t} + \mathbf{v}\nabla g = \frac{(\mathbf{v}-\mathbf{u})^2}{2}\Omega(f) - fq, &
\end{aligned} \tag{3.8}$$

where the last term on the right-hand side represents viscous heat dissipation:

$$q = (\mathbf{v} - \mathbf{u}) \cdot \left[ \frac{\partial \mathbf{u}}{\partial t} + \mathbf{v} \cdot \nabla \mathbf{u} \right]. \tag{3.9}$$

For low mach number, incompressible flows, this term can be neglected (Peng et al., 2003). Now we will again use the BGK approximation for the collision term in the evolution equation for the internal energy,

$$\frac{(\mathbf{v} - \mathbf{u})^2}{2} \Omega(f) = -\frac{g - g^{eq}}{\tau_c}. \tag{3.10}$$

A Maxwellian equilibrium distribution is also assumed,

$$g^{eq} = \frac{\rho (\mathbf{v} - \mathbf{u})^2}{2(2\pi RT)^{D/2}} \exp\left[ -\frac{(\mathbf{v} - \mathbf{u})^2}{2RT} \right]. \tag{3.11}$$

The evolution equation for the internal energy distribution is thus:

$$\frac{\partial g}{\partial t} + \mathbf{v} \nabla g = -\frac{g - g^{eq}}{\tau_c}. \tag{3.12}$$

The discretisation steps presented in section 2.2 can be applied analogously to this equation yielding:

$$g_i \left( \mathbf{x} + \mathbf{e}_i \Delta t, t + \Delta t \right) - g_i(\mathbf{x}, t) = -\frac{1}{\tau_c} (g_i - g_i^{eq}) \tag{3.13}$$

The equilibrium distributions for the internal energy are, like those for the velocity distributions, truncated polynomials of the fluid velocity (Peng et al., 2003),

$$\begin{aligned} g^{eq}_{i=0} &= -\frac{2}{3} \rho \epsilon \frac{\mathbf{u}^2}{c^2} \\ g^{eq}_{i=1,2,3,4} &= \frac{1}{9} \rho \epsilon \left[ \frac{3}{2} + \frac{3}{2} \frac{\mathbf{e}_i \cdot \mathbf{u}}{c^2} + \frac{9}{2} \frac{(\mathbf{e}_i \cdot \mathbf{u})^2}{c^4} - \frac{3}{2} \frac{\mathbf{u}^2}{c^2} \right] \\ g^{eq}_{i=5,6,7,8} &= \frac{1}{36} \rho \epsilon \left[ 3 + 6 \frac{\mathbf{e}_i \cdot \mathbf{u}}{c^2} + \frac{9}{2} \frac{(\mathbf{e}_i \cdot \mathbf{u})^2}{c^4} - \frac{3}{2} \frac{\mathbf{u}^2}{c^2} \right]. \end{aligned} \tag{3.14}$$

It is now possible to calculate an additional macroscopic variable from the new distribution function, namely the internal energy density (proportional to the temperature):

$$\begin{aligned} \rho(\mathbf{x}, t) \epsilon(\mathbf{x}, t) &= \rho(\mathbf{x}, t) RT(\mathbf{x}, t) \\ &= \sum_i g_i(\mathbf{x}, t). \end{aligned} \tag{3.15}$$

The diffusivity of this extra component (the thermal diffusivity) is given by

$$\chi = \frac{2}{3}\left(\tau_c - \frac{1}{2}\right)c^2, \tag{3.16}$$

and the lattice spacing by

$$c = \sqrt{3RT_0}, \tag{3.17}$$

where $T_0$ is the average temperature of the system and $C_s = \sqrt{RT_0} = c/\sqrt{3}$ is the speed of sound (He et al., 1998). The relationship between pressure and density is: $p = C_s^2\rho$.

At this point the flow field influences the internal energy through the presence of the fluid velocity $\mathbf{u}$ in the equilibrium distributions for the internal energy. However, the internal energy still has no effect on the fluid flow since there is no 'reverse' coupling between them in the system of equations. To model natural convection (NC) processes, a means for temperature gradients to induce a buoyancy force must be introduced. This force can be represented through an additional term in the evolution equation for the velocity distribution function (He et al., 1998; Peng et al., 2003):

$$f_i\left(\mathbf{x} + \mathbf{e}_i\Delta t, t + \Delta t\right) - f_i(\mathbf{x}, t) = -\frac{1}{\tau_\nu}(f_i - f_i^{eq}) + F_i, \tag{3.18}$$

where

$$F_i = \frac{\mathbf{G}\cdot(\mathbf{e}_i - \mathbf{u})}{RT_0} f_i^{eq}. \tag{3.19}$$

Introduction of this additional term does not violate mass conservation,

$$\begin{aligned}
\sum_i F_i &= \sum_i \frac{\mathbf{G}\cdot(\mathbf{e}_i - \mathbf{u})}{RT_0} f_i^{eq} \\
&= \frac{1}{RT_0}\mathbf{G}\cdot\left[\sum_i \mathbf{e}_i f_i^{eq} - \mathbf{u}\sum_i f_i^{eq}\right] \\
&= \frac{1}{RT_0}\mathbf{G}\cdot[\rho\mathbf{u} - \rho\mathbf{u}] \\
&= 0.
\end{aligned} \tag{3.20}$$

The external force term is given by (Peng et al., 2003):

$$\mathbf{G} = \beta g_0(T - T_0)\hat{j}. \tag{3.21}$$

This force term makes use of the Boussinesq approximation, mentioned in the previous

section, wherein it is assumed that thermally induced density variations are small enough that they do not cause compression work (the fluid is effectively still incompressible), but they are strong enough to induce a gravitational forcing effect. It is also assumed that fluid properties such as the thermal expansion coefficient and viscosity remain constant with changes in temperature. This approximation is standard practice for the simulation of NC problems (Johnston and Doering, 2009; Otero et al., 2002) and it allows the above simple form for the buoyancy force to be employed.

To complete the numerical scheme the set of equations must be closed. So far, the following equations have been defined: the evolution equations (Equation 3.18 and Equation 3.13), equilibrium distributions (Equation 2.10 and Equation 3.14), macroscopic variables (Equation 2.12 and Equation 3.15), and lattice spacing (Equation 3.17). However, values for the relaxation times $\tau_\nu$ and $\tau_c$ and the thermal expansion coefficient $\beta$ are still required.

Here the principal of dynamical similarity and dimensionless groups can be used as a guide. The Reynolds number, that measures the ratio of inertial to viscous forces, was defined previously. For convective flows, there are two key parameters, as shown in section 3.1. The Prandtl number is the ratio of momentum diffusivity to thermal diffusivity, and the Rayleigh number is a measure of the relative strength of buoyancy forces to viscous and thermal diffusive forces:

$$Ra = \frac{\beta g_0 \Delta T H^3}{\chi \nu} \tag{3.22}$$

where $\Delta T$ is the temperature difference existing across the characteristic length scale $H$. Large temperature gradients, gravitational fields, and coefficients of thermal expansion make convection more likely, whereas high viscosity fluids which are also effective thermal conductors will be more likely to transport heat via diffusion than convection.

When dealing with a convection problem, the Rayleigh number can be used to define the unknown lattice parameters since it is known that all flows with the same Rayleigh and Prandtl numbers will be dynamically similar (this was shown in section 3.1 through the de-dimensionalisation of the equations of motion for a convecting fluid). The Prandtl

number is given by:

$$\begin{aligned} Pr &= \frac{\nu}{\chi} \\ &= \frac{(\tau_\nu - \frac{1}{2})}{2(\tau_c - \frac{1}{2})} \end{aligned} \tag{3.23}$$

Before the relaxation times $\tau_\nu$ and $\tau_c$ can be calculated, a value for the thermal expansion coefficient $\beta$ must be found, since it was not yet defined for the lattice fluid. Here, the Mach number can be utilised,

$$\begin{aligned} Ma &= \frac{|\mathbf{u}|}{C_s} \\ &= \frac{[\beta g_0 \Delta T H]^{\frac{1}{2}}}{C_s}, \end{aligned} \tag{3.24}$$

where $|\mathbf{u}| = [\beta g_0 \Delta T H]^{1/2}$ is the characteristic convective velocity (Dixit and Babu, 2006). Simulations with this model must be restricted to flows of low Mach number. This is because the equilibrium distributions are truncated (to second order) polynomials of the fluid velocity and flows of high Mach number (in which the velocity is of similar magnitude to the speed of sound) would require the retention of higher order terms of those series expansions.

Note that the low Mach number assumption is not fundamentally restrictive. Imagine that a relatively turbulent flow must be simulated. It might be found that the low Mach number assumption breaks down for a particular simulation setup. However the flow can still be simulated simply by increasing the grid resolution and then altering the viscosity to retain the same Reynolds number. The LBM relies on local deviations from equilibrium being small (large changes in intensive variables cannot occur on very short length scales). Even though this sounds limiting, it is always possible to simply increase the resolution of a given simulation to the extent that local gradients are sufficiently small, so as to not violate the founding assumptions of the model.

Returning to the problem of calculating the thermal parameters, the Mach number can be set at $Ma = 0.1$ to ensure that the basic assumptions of the model are not violated. The temperature scales for the lattice system can be set arbitrarily (e.g., $\Delta T = 1, T_0 = 0.5$) since variations in temperature are relevant but numerical magnitudes are not. Assuming a size for the simulation domain has been chosen, $\beta$ can then be

calculated,

$$\begin{aligned}\beta &= \frac{[MaC_s]^2}{g_0 \Delta T H} \\ &= \frac{Ma^2 R T_0}{g_0 \Delta T H}.\end{aligned} \tag{3.25}$$

Note that parameters such as the molar gas constant $R$ and the acceleration of gravity $g_0$ can be set to unity in the model. Since they are just linear scaling factors, there is no real requirement to ever adjust them, and so their influence can be removed without loss of generality. If $Ra$ and $Pr$ are now combined,

$$\begin{aligned}Ra &= \frac{\beta g_0 \Delta T H^3 Pr}{\nu^2} \\ &= \frac{\beta g_0 \Delta T H^3 Pr}{\left[RT_0(\tau_\nu - \frac{1}{2})\right]^2}\end{aligned} \tag{3.26}$$

It is now possible to solve for the first of the relaxation times $\tau_\nu$ making use of Equation 3.26, and assuming values for $Ra$ and $Pr$ have been chosen,

$$\tau_\nu = \left[\frac{\beta g_0 \Delta T H^3 Pr}{Ra(RT_0)^2}\right]^{1/2} + \frac{1}{2} \tag{3.27}$$

This also allows the calculation of the second relaxation time using Equation 3.23,

$$\tau_c = \frac{1}{2}\left[\frac{\tau_\nu - \frac{1}{2}}{Pr} + 1\right] \tag{3.28}$$

At this stage almost all the tools necessary to write a LBM code have been presented. The physical properties of the fluid are encompassed within the relaxation times $\tau_\nu$, $\tau_c$ and the thermal expansion coefficient $\beta$.

## 3.3 Definition of Boundary Conditions

Before performing numerical tests, the model requires a suitable set of boundary conditions (BCs) for the internal energy distributions. A common procedure for insulated walls is to simply use the bounce-back rule as was used for the velocity distributions. The fact that internal energy distributions are bounced back ensures a zero-flux condition. Even though the temperature gradient at the boundary may not be exactly zero,

it is at least guaranteed that no heat has been lost from the numerical domain at such a boundary. But it must still be possible to add or remove heat from the system at non-insulated walls. At a boundary that is held at a constant temperature, the bounced-back distributions can be adjusted to ensure the correct temperature is maintained. Taking the case of the upper wall and making use of Equation 3.15, the boundary temperature can be calculated from the post-streaming distributions:

$$\rho_w \epsilon_w = g_0 + g_1 + g_2 + g_3 + g_4^* + g_5 + g_6 + g_7^* + g_8^*. \tag{3.29}$$

Note that in contrast to the velocity distributions, there is only one equation like the one above because the internal energy is a single scalar quantity, as opposed to a scalar (the mass density) and a vector quantity (the fluid velocity). An additional component can be added to the bounced-back distributions such that the boundary temperature is correctly enforced. The contribution from each unknown distribution is set proportional to its velocity vector weight factor $\omega_i$:

$$g_i^* = g_{-i}^- + \frac{\omega_i^*}{\sum \omega_i^*}\phi \tag{3.30}$$

where $g_{-i}^-$ is the pre-streaming value for the distribution in the opposite direction of $\mathbf{e}_i$. So for example the new value for $g_4$ would be

$$g_4^* = g_2^- + \frac{\omega_4}{\omega_4 + \omega_7 + \omega_8}\phi \tag{3.31}$$

(see Figure 2.1 for discrete velocity directions). Re-writing the equation for the wall temperature gives an expression for the energy deficit $\phi$,

$$\rho_w \epsilon_w = g_0 + g_1 + g_2 + g_3 + g_2^- + g_5 + g_6 + g_5^- + g_6^- + \phi \tag{3.32}$$

$$\phi = \rho_w \epsilon_w - (g_0 + g_1 + g_2 + g_3 + g_2^- + g_5 + g_6 + g_5^- + g_6^-) \tag{3.33}$$

Note that the wall internal energy density $\epsilon_w$ is defined by the prescribed conditions, and the wall density $\rho_w$ can be calculated from the velocity distributions. Corner nodes can be resolved using an analogous process to that described above.

This is the simplest way to specify internal energy BCs for our TLBM. Some authors make use of the counter-slip approach for TLBMs (D'Orazio et al., 2004), and one can

also use a finite difference method to extrapolate the boundary temperature for zero-flux walls (He et al., 1998). For all the benchmark tests presented in the next section, the differences in accuracy between the bounce-back and counter-slip/zero flux methods were found to be negligible, so the bounce-back method was adopted for all further simulations.

## 3.4 Thermal Benchmark Tests

In this section a set of numerical tests will be performed using the TLBM where the internal energy is represented by a separate distribution function. As described previously, this distribution function also undergoes collision and streaming stages but since heat is a passive scalar, there is only a scalar field associated with it (in contrast to the vector field of the fluid velocity). Fluid motion is modelled using the velocity distributions, and the diffusion and advection of heat is modelled using the internal energy distributions. It is assumed that the flows are sufficiently slow that viscous dissipation can be neglected (valid in the limit of low Mach numbers) and so the only effect of the temperature field on the fluid velocity is through the buoyancy term. This imposes a vertical body force due to density gradients, which causes warm fluid to rise and colder fluid to sink.

Thermal flows in 2-dimensional cavities will be modelled, starting with isolated systems that will be left to simply come to equilibrium, moving on to driven systems with various BCs. Such systems have been invoked previously as a useful demonstration of certain concepts of thermodynamics (Kleidon, 2009, 2010a,b). The tests to follow are performed using well established flow scenarios that have been simulated repeatedly in the past with a variety of numerical methods including the TLBM.

### 3.4.1 Constant Internal Energy

The simplest conceivable system is one in which all the walls are insulated such that the total internal energy of the system remains constant. Whatever configuration the system is initialised in, it is expected that after sufficient time, it will settle into a homogeneous steady state containing no gradients of energy density. This principle is formalised by the second law of thermodynamics, which was discussed in chapter 1. The second law directly applies to the system modelled in this section since it is thermally isolated from

its surroundings. Any simulation of such a system should obey the second law (or an H theorem) so it will be used as an elementary test. If a square cavity is divide into two imaginary halves, it can be initialised such that each half has a different temperature, $T'_{a_0}$ and $T'_{b_0}$. This then reduces to an elementary one-dimensional diffusion problem, governed by the following partial differential equation,

$$\frac{\partial T'}{\partial t'} = \chi \frac{\partial^2 T'}{\partial x'^2} \tag{3.34}$$

with initial condition

$$T'_0(x') = \begin{cases} T'_{a_0} & 0 \leq x' < W/2 \\ T'_{b_0} & W/2 \leq x' \leq W \end{cases} \tag{3.35}$$

and boundary conditions

$$\left.\frac{\partial T'}{\partial x'}\right|_{x'=0,W} = 0, \tag{3.36}$$

since the walls of the cavity are non-conductive. The governing equation can be de-dimensionalised using a characteristic temperature scale $T^*$, length scale $W$ and time scale $t_d = W^2/\chi$, which essentially represents the time required for a diffusion front to traverse the entire domain horizontally. The dimensionless version of the problem now reads:

$$\begin{aligned} \frac{t_d}{T^*}\frac{\partial T'}{\partial t'} &= \frac{t_d}{T^*}\chi\frac{\partial^2 T'}{\partial x'^2} \\ \frac{\partial T}{\partial t} &= \frac{W^2}{\chi T^*}\chi\frac{\partial^2 T'}{\partial x'^2} \\ \frac{\partial T}{\partial t} &= \frac{\partial^2 T}{\partial x^2} \end{aligned} \tag{3.37}$$

with initial condition

$$T_0(x) = \begin{cases} 1 & 0 \leq x < 1/2 \\ 0 & 1/2 \leq x \leq 1 \end{cases} \tag{3.38}$$

and boundary conditions

$$\left.\frac{\partial T}{\partial x}\right|_{x=0,1} = 0 \tag{3.39}$$

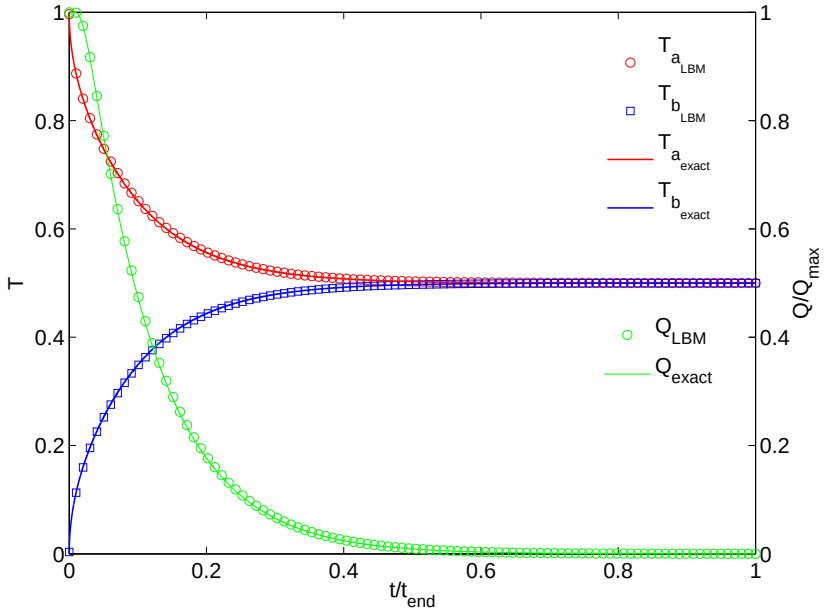


Figure 3.1: Equilibration of an isolated fluid cavity with two halves initially at temperatures $T_{a_0} = 1$ and $T_{b_0} = 0$. There is no net fluid motion and heat moves purely by diffusion.

where $T'_{b_0} = 0$ and $T^* = T'_{a_0} - T'_{b_0} = T'_{a_0}$. This initial-boundary-value problem can be solved by separation of variables to give a Fourier series solution:

$$T(x,t) = \sum_{n=1}^{\infty} C_n \exp\left(-n^2\pi^2 t\right) \cos\left(n\pi x\right) \tag{3.40}$$

where the coefficients are given by

$$\begin{aligned} C_n &= 2\int_0^1 T_0(x) \cos\left(n\pi x\right) dx \\ &= \frac{2}{n\pi} sin\left(\frac{n\pi}{2}\right). \end{aligned} \tag{3.41}$$

It is thus possible to directly compare the evolution of the temperature profile $T(x,t)$ from the TLBM to the analytic solution above.

The TLBM does seem to model the diffusion of heat correctly and this can be seen in Figure 3.1, where the mean temperatures for the two halves of the cavity, $T_a$ and $T_b$, are plotted as a function of time. Also plotted is the mean horizontal heat flux $Q$. As dictated by the second law, the cavity comes to a uniform temperature profile and the flux of heat decays to zero. As seen in the figure, there is very little difference between the exact solution, and that of the TLBM. This accuracy is invariant to the

value of the relaxation parameter $\tau_c$. In some ways it makes sense that the LBM is effective at numerically solving the diffusion equation. Any isotropic cellular automata or regular grid based method would work in a similar manner, i.e., recursive spreading and averaging of a scalar variable (assuming a sufficient number of discrete lattice vectors).

It is now permissible to allow heat to move by convection as well as diffusion.

### 3.4.2 Constant Boundary Temperatures

The assumption of a thermally isolated system will now be relaxed and energy fluxes can be applied to the cavity so that it exhibits non-equilibrium steady states. At this stage it is not expected that highly complex, organised patterns will emerge since a single-phase fluid is limited in its ability to express such patterns. The system can only show variations in density, velocity and temperature and it therefore lacks the freedom required for elaborate structure formation. At present the objective is purely to validate the accuracy of the TLBM.

#### 3.4.2.1 Horizontal Gradient

In this section the two vertical walls of the cavity will be maintained at different temperatures to induce convective fluid motion (now the temperature field is coupled to the velocity field through the buoyancy force term, shown in Equation 3.19). The upper and lower walls will be insulated. This constant boundary temperature system is frequently used as a benchmark test for thermal computational fluid dynamics (CFD) models. The standard numerical solution of De Vahl Davis (1983) will be compared to the results from the TLBM. The Prandtl number is fixed at $Pr = 0.71$ to allow comparison with the benchmark solutions.

Figure 3.2 shows the temperature fields for the four different Rayleigh numbers analysed. These are in excellent agreement with the literature (Liu et al., 2010; Peng et al., 2003). Also, Table 3.1 lists various measurements of the convection flows performed in the numerical tests alongside benchmark values. The results shown are the maximum horizontal velocity on the vertical midplane $u_{max}$, the vertical location of that maximum $y$, the maximum vertical velocity on the horizontal midplane $v_{max}$, the horizontal location of that maximum $x$, and finally the Nusselt number $Nu$, which is a dimensionless

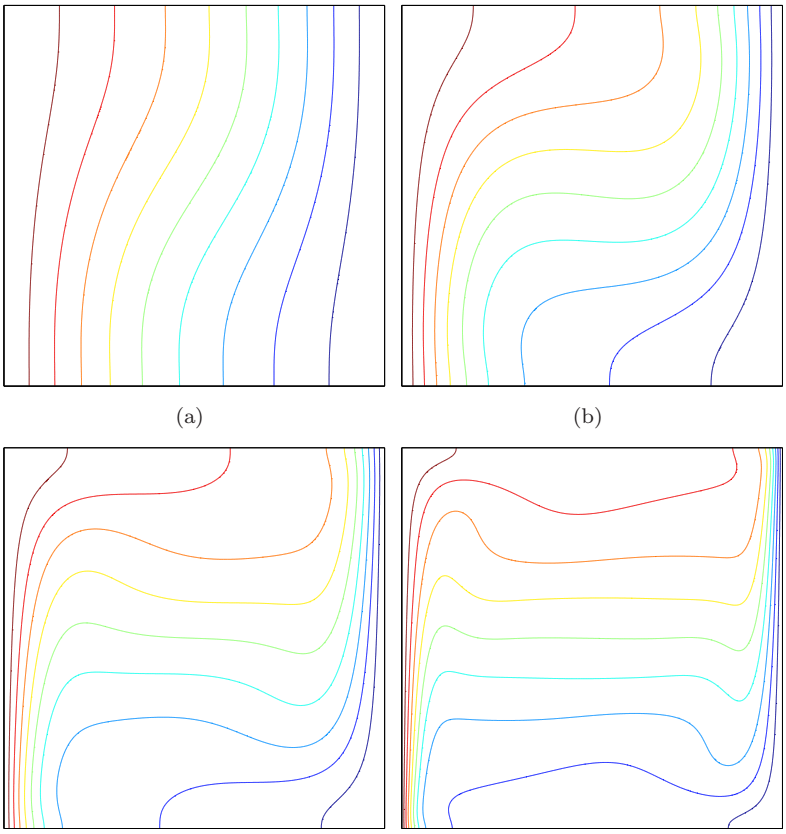


Figure 3.2: Isotherms for convection flows in a square cavity with a horizontal temperature gradient at different Rayleigh numbers. a) $Ra = 10^3$, b) $Ra = 10^4$, c) $Ra = 10^5$, d) $Ra = 10^6$.

ratio of total heat transport to conductive heat transport. It is defined as

$$Nu = \frac{\langle Q_{tot} \rangle / A}{\langle Q_{diff} \rangle / A} \tag{3.42}$$

where $Q_{tot}$ is the total heat flux, $Q_{diff}$ is the diffusive heat flux and $\langle \cdot \rangle$ denotes a time average. The instantaneous local heat flux (per unit area) in the horizontal direction is:

$$q_x = u_x T - \chi \frac{\partial T}{\partial x} \tag{3.43}$$

the first term being due to advection, and the second to diffusion. Here Fourier's Law for heat conduction has been assumed. Inserting this into the definition for the Nusselt

number,

$$\begin{aligned} Nu &= \frac{\left\langle \int q_x dV \right\rangle}{\left\langle \int q_{x_{diff}} dV \right\rangle} \\ &= \frac{\left\langle \int u_x T - \chi \frac{\partial T}{\partial x} dV \right\rangle}{\left\langle - \int \chi \frac{\partial T}{\partial x} dV \right\rangle} \\ &= 1 + \frac{\left\langle \int u_x T dV \right\rangle}{\left\langle -\chi \int \frac{\partial T}{\partial x} dV \right\rangle} \\ &= 1 + \frac{\left\langle \overline{u_x T} HLW \right\rangle}{\langle \chi \Delta T HL \rangle} \\ &= 1 + \frac{W}{\chi} \frac{\left\langle \overline{u_x T} \right\rangle}{\langle \Delta T \rangle} \end{aligned} \tag{3.44}$$

This equation can be modified for temperature gradients in other directions by replacing the characteristic length and velocity component (e.g., replacing $W$ and $u_x$ with $H$ and $u_z$ for vertical heat flows). Note that this expression has been left in a slightly more general form than normal, by leaving the averaging operation on the temperature difference $\Delta T$. This allows the expression to apply equally to configurations where the two boundary temperatures are not fixed by the BCs. Also note that the averaging process $\overline{\cdot}$ is a spatial average (the boundary temperatures will also be spatially averaged in later simulations in which they are not horizontally uniform).

The Nusselt number is often referred to as a dimensionless measure of heat flux. However this can lead to confusion since it is a ratio of two fluxes and therefore does not express the magnitude of a dimensional flux. This point will be discussed in detail in section 4.2.

There are several different (dimensional) heat fluxes involved with the system. There are the two boundary flux values, one for each of the two vertically-oriented boundaries, an average bulk heat flux for the body of heated fluid, and the diffusive flux that would occur through the system if there were no convection. In steady state (no net change in the system's total internal energy with time), the heat flux within the fluid, when averaged over the entire volume, and also averaged over a sufficient window of time (to eliminate the effect of transient fluctuations) must equal the boundary flux. This is basically an expression of a steady state continuity condition (the system cannot have a sustained heat transport bottleneck when in a stationary state).

Having derived the Nusselt number, it can now be used to assess the performance of the TLBM when simulating the horizontal convecting fluid problem. Table 3.1 shows the

Table 3.1: Convective flow properties for a 2D cavity with a horizontal temperature gradient. Results are shown for the benchmark calculations of De Vahl Davis (1983) (BM) and for TLBM simulations.

| Ra | | $10^3$ | $10^4$ | $10^5$ | $10^6$ |
|---|---|---|---|---|---|
| $u_{max}$ | BM | 3.649 | 16.18 | 34.73 | 64.63 |
| | TLBM | 3.642 | 16.22 | 35.01 | 65.66 |
| $y$ | BM | 0.813 | 0.823 | 0.855 | 0.850 |
| | TLBM | 0.812 | 0.823 | 0.854 | 0.849 |
| $v_{max}$ | BM | 3.697 | 19.62 | 68.59 | 219.4 |
| | TLBM | 3.689 | 19.68 | 69.09 | 223.5 |
| $x$ | BM | 0.178 | 0.119 | 0.066 | 0.0379 |
| | TLBM | 0.179 | 0.120 | 0.066 | 0.0382 |
| $Nu$ | BM | 1.118 | 2.243 | 4.519 | 8.800 |
| | TLBM | 1.118 | 2.251 | 4.558 | 8.976 |

results of these tests. Comparison of the TLBM results with those of the benchmark imply that the TLBM does indeed simulate NC accurately. Note that making use of counter-slip (D'Orazio et al., 2004) and zero-flux BCs (Shu et al., 2002) instead of the halfway wall bounce-back method had no effect on the results shown in Table 3.1.

#### 3.4.2.2 Vertical Gradient

In this section another system with constant temperature boundaries will be simulated, but this time the fluid will be heated from below and cooled from above. The cavity will be rectangular with an aspect ratio of 2. The horizontal boundaries will be periodic so topologically this system is equivalent to the surface of a cylinder. Such a configuration has been used many times as a benchmark for convection experiments (Clever and Busse, 1974). The Nusselt number will be measured as a function of Rayleigh number for the following values: $Ra = 10^3, 10^4, 10^5, 10^6$. The total temperature difference $\Delta T$ will be kept constant and the viscosity and thermal diffusivity will be reduced (while keeping the ratio of the two, $Pr = \nu/\chi$, fixed).

Figure 3.3 shows the mean temperature profiles (as a function of vertical coordinate) for the four different steady state flow fields. Also shown are the corresponding temperature fields and flow streamlines. The first simulation at $Ra = 10^3$ is below the critical Rayleigh number ($Ra_c \approx 1706$), at which the static diffusive state becomes unstable to

perturbations. Therefore the temperature profile is linear and heat is moving purely by diffusion. Above the critical value, the diffusive state is unstable to perturbations, which can grow and cause the system to settle into a steady state of sustained fluid motion (NC). As the convective driving force increases, the system responds by partitioning itself into two boundary layers, which become progressively more pronounced with increasing $Ra$. Note that the net effect of this partitioning is that the temperature gradient at the boundaries increases.

Heat can only move into and out of the system by diffusion since there is no fluid motion at the boundaries due to the no-slip velocity BC. An increase in boundary temperature gradient would suggest a concomitant increase in heat flux. However heat flux is proportional to both temperature gradient *and* thermal diffusivity $\chi$. Since both the viscosity $\nu$ and the diffusivity $\chi$ were reduced, it is not clear whether the increased temperature gradient is sufficient to offset the loss in thermal diffusivity. In fact, measurements of the boundary heat flux reveal that it does actually decrease as $Ra$ increases. This relation of decreasing heat flux with increasing $Ra$ is not universally applicable since there are many ways to increase $Ra$. For example the system size $H$ or the thermal expansion coefficient $\beta$ could have been increased. Both of these changes would have augmented the heat flux because they would have made the system more amenable to convective transport, that can deliver more heat through the system than diffusion alone (assuming the thermal diffusivity is left constant).

Alternatively the viscosity could have been reduced while keeping the thermal diffusivity constant. Again, this would have made the body of fluid more liable to convect (due to reduced friction) and without a change in the thermal diffusivity the boundary (and hence the average total) heat flux would have increased. Again, increasing the thermal driving force $Ra$ can be achieved by several different means. They all lead to an increase in the ratio of total to diffusive heat flux $Nu$. However they do not universally cause an increase in heat flux, some of them cause the heat flux to decrease. Therefore even though in the literature and textbooks the Nusselt number is often referred to as the dimensionless heat flux, it can increase without an increase in the *dimensional* heat flux. So just because the Rayleigh number increases, it does not always follow that the heat flux and the entropy production should also increase. Entropy production is the product of heat flux and the difference of inverse temperatures, and will be dealt with in depth in chapter 4 and chapter 5.

Returning to the task of assessing the performance of the TLBM, Figure 3.4 shows the scaling of $Nu$ against $Ra$ for the system with an imposed vertical temperature gradient. Also shown for comparison is the numerical solution of Clever and Busse (1974). The simulation results are once more in excellent agreement with the benchmark solutions. While these results are encouraging, it is also desirable to see whether the TLBM can handle larger driving forces since the flows at moderate $Ra$ are somewhat sedentary.

Thus simulations with higher grid resolutions and $Ra \leq 10^8$ were also carried out. For $Ra > 10^8$, the computational cost becomes prohibitive and the use of non-uniform grid meshes was not explored. Values for the mean Nusselt number will be compared to the benchmark direct numerical simulation results of Johnston and Doering (2009). Those authors were exploring the power law relationship between $Ra$ and $Nu$, that is still a matter of ongoing theoretical and experimental research. They found that above $Ra = 10^7$, the scaling law is of the form $Nu \approx 0.138 \times Ra^{2/7}$. Figure 3.5 shows the results of both the high $Ra$ and low $Ra$ simulations. Even at high $Ra$ the TLBM results are close to those of Johnston and Doering (2009). The dotted blue line is a theoretical prediction based on the assumption of maximum entropy production (MEP). This will be discussed in detail in the next chapter.

To give a sense of perspective, an image of the temperature field for a system with $Ra = 10^8$ is shown in Figure 3.6. This image shows the system at an early stage when the initial plumes have not yet morphed into a single pair of system-sized convection cells.

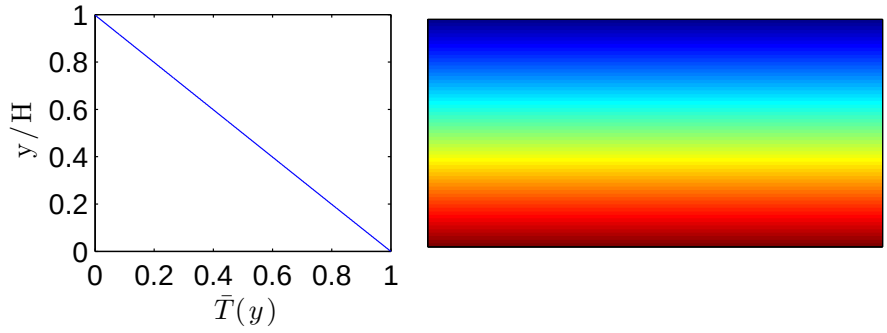


(a)

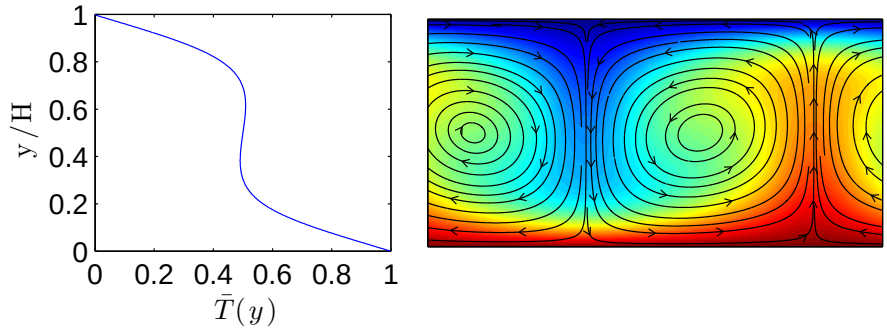


(b)

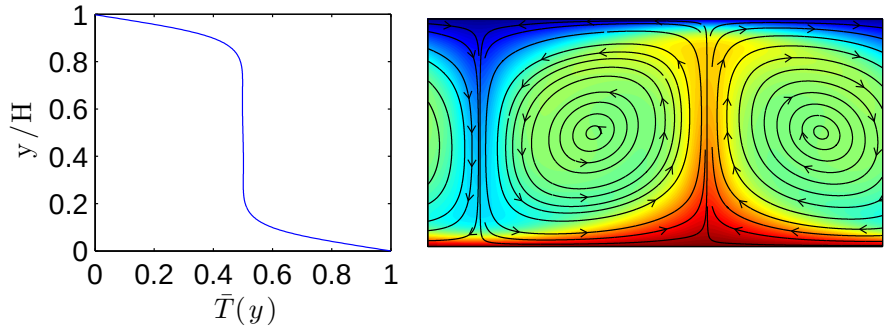


(c)

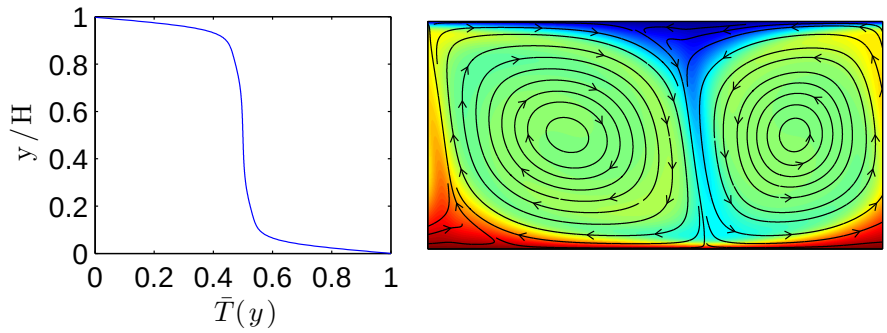


(d)

Figure 3.3: Mean horizontal temperature as a function of vertical coordinate, and temperature fields for fixed boundary temperature convection systems of different Rayleigh numbers. Flow streamlines are also displayed showing the characteristic boundary layers and convection rolls. a) $Ra = 10^3$, below the critical Rayleigh number ($Ra_c \approx 1706$) there is no convective motion and heat transport occurs purely by diffusion, b) $Ra = 10^4$, c) $Ra = 10^5$, d) $Ra = 10^6$. Note that the boundary layers become increasingly well defined with increasing Rayleigh number.

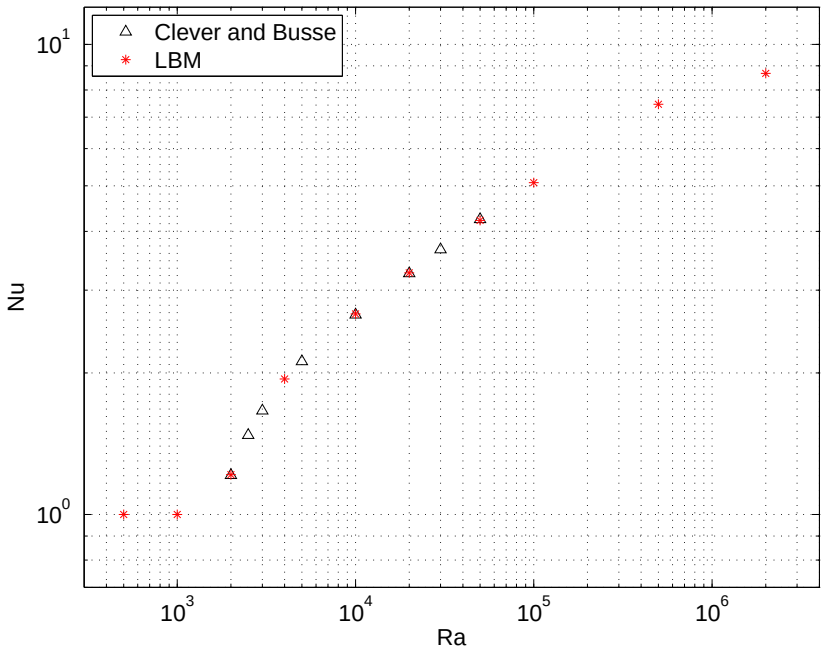


Figure 3.4: Nusselt number as a function of Rayleigh number for a fixed temperature convective fluid system with an aspect ratio of 2. Red asterisks correspond to values from TLBM simulations and black triangles to the benchmark solution of Clever and Busse (1974).

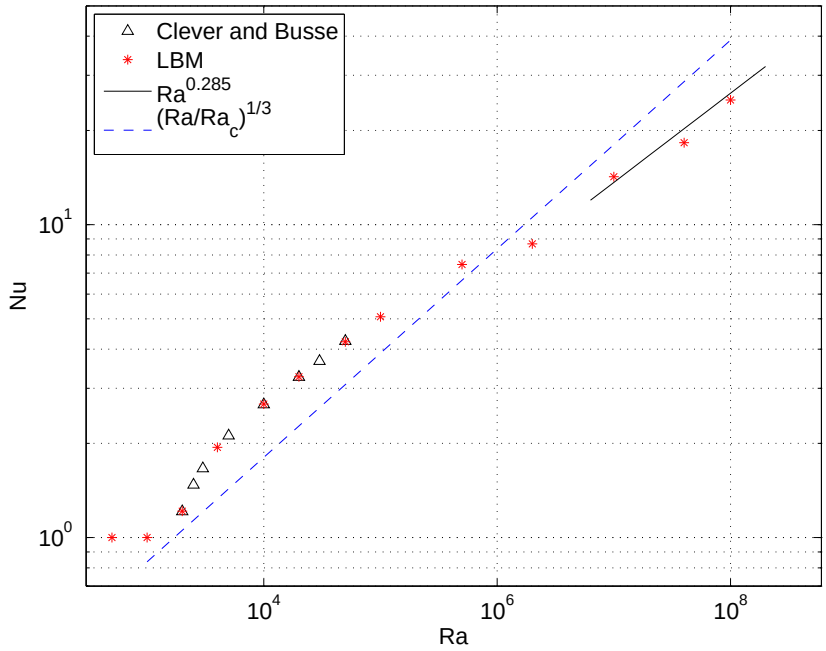


Figure 3.5: Nusselt number as a function of Rayleigh number for a fixed temperature convective fluid system with an aspect ratio of 2. Black triangles correspond to the benchmark solution of Clever and Busse (1974), red asterisks correspond to values from TLBM simulations, the black line is the scaling law observed in the direct numerical simulations of Johnston and Doering (2009) and the blue dashed line is the MEPP prediction of Ozawa et al. (2001).

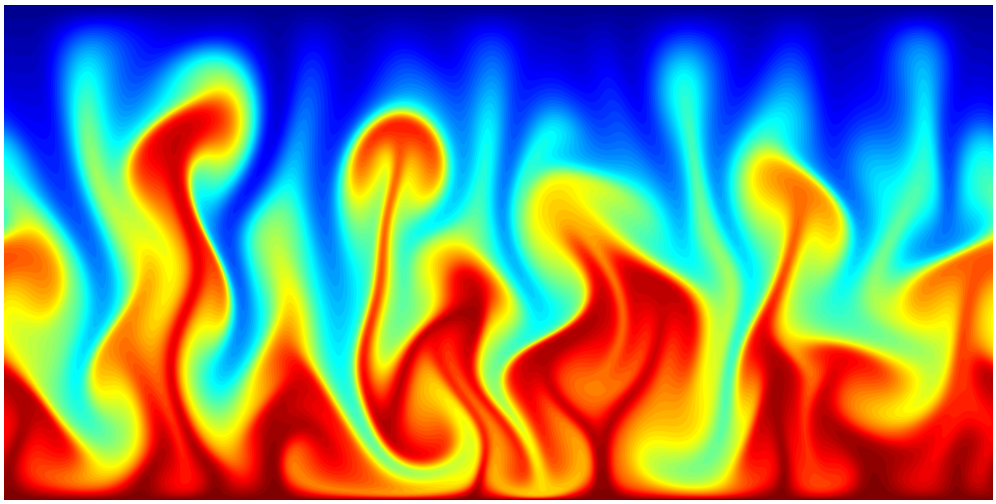

Figure 3.6: Temperature field of a fixed temperature NC system with $Ra = 10^8$. The snapshot shows the system during the early transient phase, during which the first set of convective plumes are growing towards the cold upper boundary.

### 3.4.3 Constant Boundary Fluxes

In the previous section the total temperature difference across the system was prescribed and the Rayleigh number was varied by altering the domain size $H$, viscosity $\nu$ and thermal diffusivity $\chi$ (while keeping $Pr = \nu/\chi$ constant). In such a situation the system has the freedom to adjust its total heat flux, but not its boundary temperatures. The BCs will add or remove as much heat as is required to maintain those boundary temperatures. Hence such BCs are often described as infinitely conducting, since the boundary heat flux can in principle be arbitrarily large. Of course it is limited by the rate at which the fluid can import, transport, and export heat. In this section, rather than fix the boundary temperatures, the rate at which heat enters and leaves the system will instead be prescribed.

So now the boundary heat flux is constant, but the total temperature difference across the system is free to vary. As well as a benchmark test, it is natural to ask whether this kind of BC produces any elementary differences in the transport or hydrodynamic properties of the resulting flow compared to the constant temperature BCs. In fact this has already been investigated by Johnston and Doering (2009), who compared the behaviour of constant flux and constant temperature systems using direct numerical simulations. They concluded that above $Ra \sim 10^6$, the imposition of different BCs has no effect on the steady state flow (at least in terms of the relationship between $Ra$ and $Nu$). In chapter 5 a third type of variable BC will be applied, in which the boundary flux is a function of temperature (both the temperature difference and heat flux can vary), and it will be shown whether this has an impact on the scaling of $Ra$ and $Nu$.

Returning to the benchmarking task, before making assessments of the model performance, the definitions of $Ra$ and $Nu$ must first be modified. The magnitude of heat injected into the lower boundary and extracted at the top boundary at each time step will be denoted by $Q$. Since the boundary temperatures are no longer constrained, the previous definition of the Rayleigh number can no longer be used as a measure of thermal driving force. Instead it can be modified by making use of the temperature gradient that would arise if all heat transport occurred through diffusion. By re-arranging Fourier's

law it is found that

$$\frac{Q}{A} = -\frac{\chi \Delta T_{diff}}{H} \tag{3.45}$$

$$|\Delta T_{diff}| = \frac{QH}{\chi A}. \tag{3.46}$$

A constant flux forcing parameter can now be defined using this expression for a characteristic temperature difference (Johnston and Doering, 2009; Otero et al., 2002; Verzicco and Sreenivasan, 2008):

$$\hat{R} = \frac{\beta g_0 \Delta T_{diff} H^3}{\nu \chi} \tag{3.47}$$

$$= \frac{\beta g_0 H^3}{\nu \chi} \frac{QH}{\chi A} \tag{3.48}$$

The Nusselt number takes on the following form:

$$Nu = \frac{Q/A}{\chi \left\langle \overline{\Delta T} \right\rangle / H} \tag{3.49}$$

The temperature difference used here $\left\langle \overline{\Delta T} \right\rangle$, is the time and horizontally averaged (at each boundary) temperature difference that the system exhibits, in contrast to $\Delta T_{diff}$, the total temperature gradient that would exist if the fluid was motionless and only able to transport heat via diffusion. The heat flux across the two boundaries is fixed (the average bulk flux will in general exhibit transient fluctuations but a suitable time average must always yield a value equal to the boundary flux), leaving only the steady state temperature difference $\left\langle \overline{\Delta T} \right\rangle$ as a free variable. Combining the above expressions yields

$$\hat{R} = \frac{\beta g_0 Q H^4}{\nu \chi^2 A}$$

$$= \frac{\beta g_0 \Delta T H^3}{\nu \chi} \frac{Q/A}{\chi \Delta T / H}$$

$$= RaNu \tag{3.50}$$

Thus $\hat{R}$ now becomes the dimensionless driving parameter. Note that the previous definitions for $Ra$ and $Nu$ are still compatible with the BCs in this section but they involve unnecessary calculation steps compared with the modified definitions given here.

It is now possible to simulate the constant flux system for a range of driving fluxes

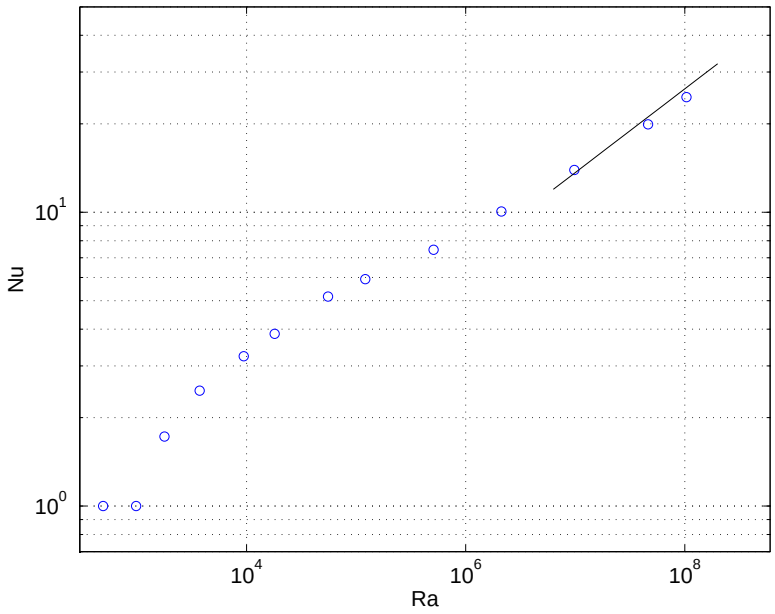


Figure 3.7: Nusselt number as a function of Rayleigh number for a fixed heat flux convective fluid system with an aspect ratio of 2. Blue circles correspond to values from TLBM simulations, and the black line corresponds to the scaling law observed in the direct numerical simulations of Johnston and Doering (2009).

and compare the results to those of Johnston and Doering (2009). Figure 3.7 shows the familiar scaling behaviour, once again demonstrating that the TLBM can simulate convective flows with similar accuracy to traditional CFD techniques.

These results also show that above $Ra \sim 10^7$ the system is indifferent to the type of BCs imposed. Whether the flux or temperature difference is prescribed seems to make no difference to the macroscopic transport properties. In fact this makes intuitive sense because any state of dynamical equilibrium has to be characterised by non-varying $Q$ and $\Delta T$ and having found that steady state, if the same conditions were enforced by fixing $Q$ instead of $\Delta T$ (or vice versa), the system wouldn't 'sense' any difference.

Nevertheless there is a difference between the two BCs for lower values of $Ra$ (see Figure 3.9). The constant flux systems seem to achieve higher Nusselt numbers for the same Rayleigh numbers compared to the constant temperature case. This is caused by a slightly more efficient flow structure that is permitted in the constant flux case since it can exhibit a non-uniform boundary temperature profile. Having higher temperatures near upward plumes and lower temperatures near downward plumes compared to a fixed temperature equivalent, allows the convection cells to extend slightly further vertically, allowing the ratio of total to diffusive heat transport to increase. The flow structure is

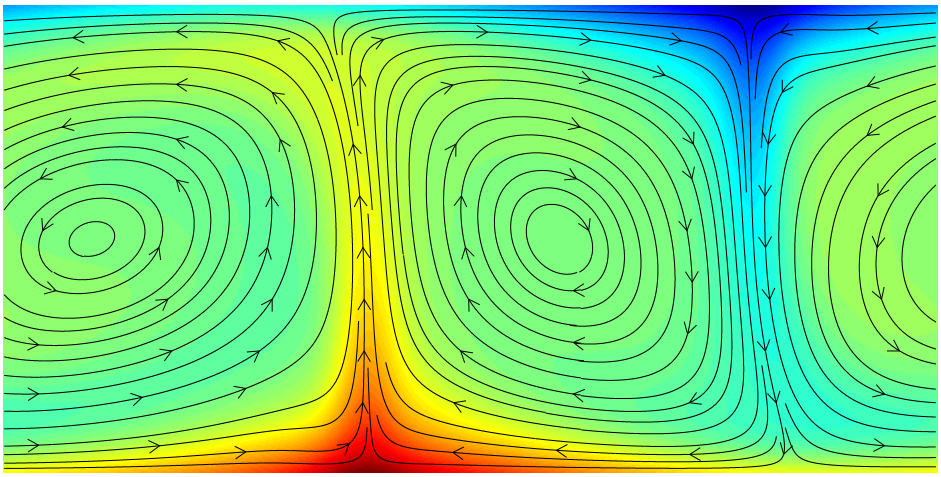

Figure 3.8: Temperature field for a fixed flux NC flow with $Ra = 1.2 \times 10^5$. Note the apparent lack of distinctive boundary layers compared to the fixed temperature systems (see Figure 3.3). This flow structure allows fixed flux systems of low $Ra$ to achieve higher magnitudes of convective transport than equivalent fixed temperature systems.

illustrated in Figure 3.8. This 'advantage' disappears when the system is more turbulent because the boundary layers are then so thin that any increase in convection cell size that the fixed flux systems might attain becomes negligible.

Finally, Figure 3.9 shows both the fixed temperature and fixed flux results. The slightly augmented Nusselt numbers of the fixed flux systems compared to those of fixed temperature are clearly visible here. What is also shown is the agreement between both sets of results and the scaling law of Johnston and Doering (2009) at higher Rayleigh numbers. The agreement is not perfect since resolving all flow features accurately for these turbulent systems is a formidable task, and it could be that certain small scale effects are not captured in the TLBM simulations. Furthermore there is considerable intermittency in the variables of these systems due to their chaotic nature, and this noise makes it more difficult to extract well-behaved averages for $Nu$ in particular.

## 3.5 Conclusions

This chapter has described in detail the TLBM of He et al. (1998) and Peng et al. (2003), and established its validity as a CFD method for thermal flows. The equations of motion for a single-phase thermal fluid were presented and de-dimensionalised, showing

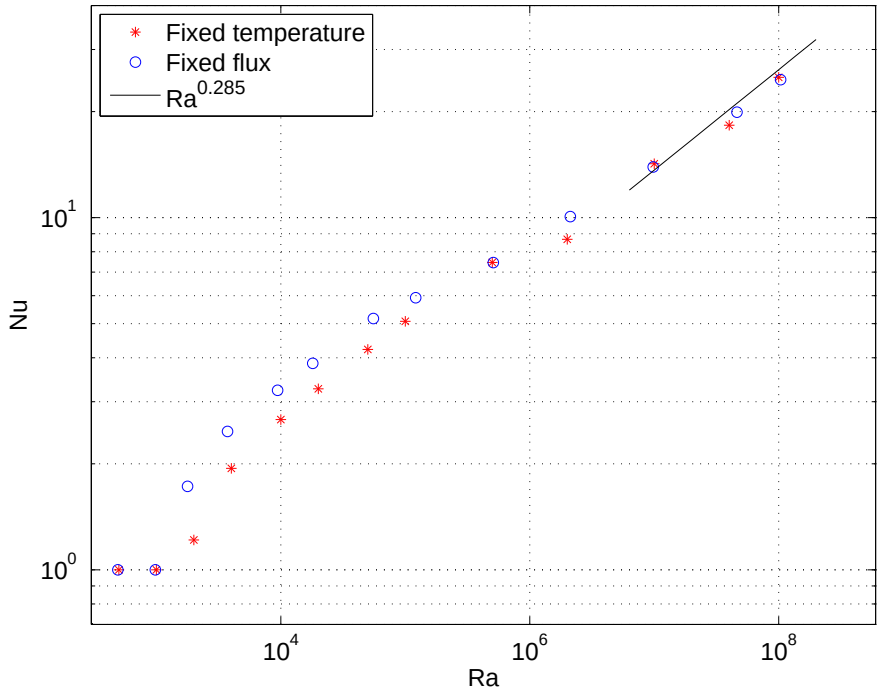


Figure 3.9: Nusselt number as a function of Rayleigh number for fixed temperature and fixed heat flux convective fluid systems with an aspect ratio of 2. Red asterisks correspond to fixed temperature BCs and blue circles to fixed flux BCs. The black line is the scaling law observed in the direct numerical simulations of Johnston and Doering (2009).

that the behaviour of such fluids depends only upon two dimensionless groups, the Prandtl number, the ratio of momentum to thermal diffusivity and the Rayleigh number, a measure of thermal driving force. The exact construction of the TLBM was then presented including the necessary BCs for the extra distribution function. A set of benchmark tests were then carried out, demonstrating that, in accordance with literature results, the TLBM can indeed simulate buoyancy-induced flows accurately.

Having established the validity of the method, it is now possible to begin using TLBM simulations to analyse the thermodynamic properties of pattern-forming systems. Specifically, the focus of the next two chapters will be the Maximum Entropy Production Principle (MEPP). Can such a principle predict the steady states of NC systems? If so why should this be the case? If not, are there any other variational principles using thermodynamic measures which could offer more predictive utility? These lines of enquiry will be addressed in the following chapters.

# Chapter 4

# What Can Maximum Entropy teach us about Convection?

Natural convection (NC) occupies a privileged position in the world of non-linear and non-equilibrium physics. When driven out of equilibrium, NC systems form sustained patterns: convection rolls (see Figure 3.8). Why does the system structure itself in this way? Disequilibrium induces fluxes of matter and energy and the effect of those fluxes is to reduce the gradients that produced them. The system is constantly acting in such a way as to bring itself back to an equilibrium state. In doing so it affects its environment because the environment provides the driving forces.

In the case of NC, by transporting heat from a hot to a cold boundary, the action of the fluid is bringing the composite system of the fluid plus external heat reservoirs, closer to equilibrium. In a real system those reservoirs would eventually come to the same temperature as a result of the system funnelling thermal energy from one end to the other. Ultimately all three components (system plus two reservoirs) would be of equal temperature with no discernible order or structure. The march to this inevitable end state is the essence of the second law of thermodynamics.

However the second law only states that the whole system will come to equilibrium, it does not provide any details concerning *how* it gets there. Systems in equilibrium remain in equilibrium. Systems not in equilibrium come to equilibrium with time. Thankfully we live in a universe that is currently not in equilibrium but is on its way there. Many (perhaps the majority) of the most critical scientific problems facing society today involve

systems that are not in equilibrium. Unfortunately, while equilibrium thermodynamics enjoys its deserved and enduring position as a foundation of physical theory (or perhaps statistics depending on your persuasion), non-equilibrium thermodynamics has a long way to go before it can lay claim to being established, predictive and well understood.

Of course important results have been proven, mainly in the last century, such as Onsager's reciprocal relations (see e.g., Kondepudi and Prigogine, 1998) and the non-equilibrium Boltzmann equation (Equation 2.1). But these theories tend to apply to linear systems or require assumptions of local equilibrium. Are there any general tendencies concerning the manner in which systems achieve equilibrium states, whether they are slightly or very far from equilibrium? Instinctively it feels like there should be due to the obvious and ubiquitous reproducibility and regularity that we can observe in most non-equilibrium systems. At the moment, theories that describe such regularities tend to work well for a subset of systems but have a relatively narrow range of applicability (for example, fluid dynamics theory does not translate to ecological systems). A theory or body of theories which could unite all non-equilibrium systems and predict certain properties of their behaviour would be an extraordinary achievement of far-reaching utility.

And so it was that the Maximum Entropy Production Principle (MEPP) emerged and created waves of excitement and anticipation. Simply put, the MEPP postulates that non-equilibrium systems of many degrees of freedom will adjust their steady state to that which maximises the rate of entropy production, subject to basic physical constraints (such as mass and energy conservation). On the face of it, the MEPP appears somewhat ambiguous and indeed it has received criticism because of this. However it has also enjoyed significant triumphs. Some pioneering, early analytical work on the problem of NC suggested that convecting fluids adjust their flows so as to maximise heat flux (Malkus, 1954a; Malkus and Veronis, 1958; Malkus, 1954b). If the boundary temperatures are fixed then this is equivalent to maximising entropy production (see Equation 4.1). However, that is absolutely not the end of the story when it comes to entropy production and NC, as will become clear later in this chapter.

Setting aside NC for a moment, in recent years the MEPP has found application in a range of fields. It has shown utility for predicting the steady state behaviour of several non-equilibrium systems including crystal growth (Hill, 1990; Martyushev and Axelrod,

2003), electrical current flow (Zupanović and Juretić, 2004), ecosystems (Vallino, 2010) (also see articles within Kleidon et al., 2010) and plant functional optimisation (Dewar, 2010). For a review, please see Martyushev and Seleznev (2006). Inspired by these achievements, it has been hoped that the MEPP may after all be *the* unifying principle of non-equilibrium thermodynamics.

It has been particularly successful in an area somewhat related to NC: the analysis of atmospheric heat transport (O'Brien and Stephens, 1995; Ozawa et al., 2003; Paltridge, 1978). These works, as well as others, found that certain transport properties of the atmospheric circulation of several planetary bodies including Earth can be reliably predicted using a simple 2-box model of the planetary energy balances and the application of the MEPP. A similar model will be explored in chapter 5.

Despite its accomplishments, there has been criticism of the principle since it has no rigorous theoretical basis. In fact some early proponents of the MEPP have (in the last decade or so) changed position on the philosophical role of the principle. For example Dewar (2003) appears to present the MEPP as an elementary principle of nature and attempts to derive it from a minimal set of statistical assumptions. In contrast Dewar (2009) takes a more cautious tone, emphasising instead the information theoretic interpretation of the MEPP in which the uncertainty of the observer is maximised. Furthermore, when it comes to fluid dynamical systems, entropy minimisation, as well as maximisation, has been observed (Niven, 2010; Paulus Jr. and Gaggioli, 2004). Which extremum emerges seems to depend in a non-trivial way upon the BCs and particular flow being studied. Even in the case of NC flows - which are often highlighted as a case in point for the MEPP (e.g., Meysman and Bruers, 2010) - entropy production *minimisation* can also emerge, and this is something that will be explored in this chapter.

## 4.1 Ozawa's Scaling Law

An explicit application of the MEPP to NC will now be explored in detail. The focus will be upon the work of Ozawa et al. (2001), who derived a scaling relation for the two key dimensionless groups describing NC flows, $Ra$ and $Nu$ (see Equation 3.22 and Equation 3.42 or below for definitions). The system in question is a heated fluid held between two parallel plates (the analysis applies to 2D or 3D systems). Initially it

will be assumed that the two horizontally oriented boundaries will be held at constant temperatures, but in section 4.2 systems with fixed boundary heat fluxes will also be considered.

One of the principle qualities of the MEPP is that it can help identify which aspects of a system's dynamics are relevant to a certain aspect of its behaviour. For example, in the work on atmospheric heat transport (Ozawa et al., 2003; Paltridge, 1978), one of the interesting consequences of the simple model was that the large scale transport properties seemed to be invariant to the physical properties of the materials involved (since the model did not include such details and yet still produced accurate predictions). In the derivation to be re-produced below, certain properties of the system in question are also ignored, and yet the predictions of the model represent a reasonable first approximation to experimental results.

With NC, as in many fluid dynamical systems, even if the equations of motion cannot be solved exactly, it is frequently found that a small number of dimensionless parameters (such as $Ra$ and $Nu$, see section 3.1) are sufficient to describe the hydrodynamics of the system. This is the basis of dynamical similarity, and for any two NC flows, if $Ra$ and $Pr$ are equal, the resulting flows will be identical even if they vary on specific physical properties. It has been proposed that the following relationship applies to NC systems: $Nu \approx 0.138 \times Ra^{0.285}$ for $Ra \geq 10^7$ and $Pr \approx 1$ (Johnston and Doering, 2009). However, this scaling law is still an empirical relation. It would be advantageous to be able to derive such correlations from a reasonable model of the transport properties of the system. This is precisely what was done by Ozawa et al. (2001), and the key steps in their derivation will now be described.

Since the boundary temperatures are fixed, maximum entropy production (MEP) implies maximum heat flux through the system,

$$\frac{dS}{dt} = Q_{ab}\left(\frac{1}{T_b} - \frac{1}{T_a}\right) = Q_{ab} \times const = max \tag{4.1}$$

$$Q_{ab} = max \tag{4.2}$$

Note that here the focus is solely upon the entropy produced through the process of the quantity of heat $Q_{ab}$ per unit time changing from temperature $T_a$ to $T_b$. It is convenient to think of the expression as representing the net outward flux of entropy from the fluid system (equal to the internal entropy production), since in steady state, an amount of

entropy $Q_{ab}/T_a$ enters the system and an amount $Q_{ab}/T_b$ leaves. So the change $dS/dt$ refers to the entropy change of the system's environment due to entropy production within the system.

It is also clear that the above expression differs from the original identity due to Clausius: $dS = \delta Q_{rev}/T$. One could call into question the reversibility of the process of fluid convection (such heat transfer is certainly not carried out quasi-statically). However, Equation 4.1 has become standard in the literature and even though it's not identical to the Clausius definition, it could simply be re-named if necessary (there are already numerous different entropies). The point is that the quantity expressed by Equation 4.1 could be used to predict steady state properties of non-equilibrium systems. That utility is not contingent on whether the quantity is identical to other definitions of entropy or what it is named.

At this stage additional constraints are required to place a limit on the total heat flux $Q_{ab}$. Ozawa et al. (2001) employed a simplified physical picture of the system's hydrodynamics. They assumed it would arrange itself into two thin boundary layers next to the upper and lower boundaries with convective motion transporting heat between these layers. They assumed that within each boundary layer the fluid would be motionless and the heat would be moving purely by diffusion. In the interior of the boundary layers, the heat was assumed to move by convective transport with negligible temperature gradient.

Since it is known that a layer of heated fluid will undergo NC once the Rayleigh number exceeds a critical value, stability of the boundary layers implies that the Rayleigh number of those sections of fluid must be exactly the critical value (if it was higher, further convection would set in and the boundary layer would become thinner). They assumed nothing about the interior fluid dynamics. Therefore transport of heat was limited by the rate at which it could travel by diffusion only, i.e., the overall temperature gradient, size of the cavity and the thermal diffusivity of the fluid.

The expression relating $Nu$ to $Ra$ as per Ozawa et al. (2001) will now be derived. The total heat flux through the boundary layers can be written as:

$$\frac{Q_{ab_{max}}}{A} = \chi \frac{\Delta T}{2\delta} \tag{4.3}$$

where $\delta$ is the height of each boundary layer (there are two of them). The stability of the boundary layers implies that those two regions of fluid alone can be characterised by the critical Rayleigh number:

$$Ra_c = \frac{\beta g_0 \Delta T (2\delta)^3}{\chi \nu} \approx 1706 \tag{4.4}$$

If $\delta$ is written in terms of the critical and overall Rayleigh numbers,

$$\frac{Ra}{Ra_c} = \left(\frac{H}{2\delta}\right)^3 \tag{4.5}$$

$$\delta = \frac{H}{2}\left(\frac{Ra_c}{Ra}\right)^{1/3}, \tag{4.6}$$

the boundary layer thickness can be eliminated by inserting this into Equation 4.3. An expression for the maximum heat flux can then be found:

$$\frac{Q_{ab_{max}}}{A} = \frac{\chi \Delta T}{H}\left(\frac{Ra}{Ra_c}\right)^{1/3} \tag{4.7}$$

Finally, if this is inserted into the definition for the Nusselt number (Equation 3.49), a rather elegant relation is revealed,

$$Nu = \left(\frac{Ra}{Ra_c}\right)^{1/3}. \tag{4.8}$$

Within these constraints, it is possible to calculate the maximum possible heat flux for a given temperature gradient.

## 4.2 How does the Maximum Entropy Production Principle Measure up?

It is claimed that the values for $Nu$ calculated using Equation 4.8 show good agreement with experimentally measured values (Ozawa et al., 2001). This agreement is shown in Figure 3.5, where the 1/3 scaling law provides a rough approximation for the correlation between $Ra$ and $Nu$. However it is very approximate, and when $Ra > 10^6$, the relationship begins to break down. But the MEPP values should show *better* agreement with the known results as $Ra$ increases, because the boundary layers become better defined with increasing $Ra$ (see Figure 3.3). In contrast, at $Ra < 5 \times 10^3$, the boundary layers

are relatively large and are not clearly distinguished from the convection region, so the assumptions of the MEPP derivation might not be completely valid. Instead of a value of 1/3, it has been shown that as the convection becomes more turbulent ($Ra \geq 10^7$), the scaling exponent seems to be $0.285 \approx 2/7$ (Johnston and Doering, 2009).

So while the MEPP prediction appeared to be accurate, it seems to provide only a first approximation, since it does not accurately capture the simple low $Ra$ flows, or the more turbulent ones. Indeed it is clear that it is not possible for a simple power law alone to capture all the scaling in Figure 3.5 since the low $Ra$ results do not form a straight line, and there appears to be two scaling laws present at least. It is likely that at low $Ra$, the assumption of well-defined boundary layers would need to be relaxed. For these flows there is considerable spatial overlap between the regions where diffusion dominates (near the boundaries), and where convection dominates (the interior). And for higher $Ra$, while the boundary layers and convective regions may be relatively well distinguished, the internal dynamics of the interior region are by no means trivial but would probably need to feature in any model of the system. Finding simple parameterisations for the heat transfer occurring here is challenging, as evidenced by the large body of literature concerned with analytical treatments of such flows.

At this stage it is worth considering some of the many other investigations of convection using both analytical and numerical methods. In the middle of the 20$^{\text{th}}$ century, Malkus (1954b) performed a theoretical study of thermal convection. It was found that NC flows appear to maximise their rate of heat flux, subject to basic hydrodynamic constraints. Since that seminal work, many other theoretical investigations have used the same maximum flux assumption with various analytical techniques to produce scaling relations between $Nu$ and $Ra$ including $Nu \propto Ra^{1/3}$ and $Nu \propto Ra^{1/2}$, with varying dependencies on the Prandtl number (Doering and Constantin, 1996; Grossmann and Lohse, 2000; Howard, 1963; Kraichnan, 1962).

So it seems that NC flows do seem to arrange themselves in such a way as to maximise their net vertical heat flux. Returning to Figure 3.3, it is clear that under the constraint of fixed boundary temperatures, the systems are trying to maximise the temperature gradient at the boundaries. But as noted before, whether this translates to maximisation of heat flux as $Ra$ increases depends on how the fluid parameters are being adjusted. If the viscosity is reduced with other parameters held constant, the heat flux does indeed

increase. But if the viscosity is reduced at constant Prandtl number, then the thermal diffusivity is also decreased and this results in a *reduction* of heat flux even though the thermal driving force experienced an increase.

To clarify this further, it would be beneficial to first review the definitions of $Ra$ and $Nu$:

$$Ra = \frac{\beta g_0 \Delta T H^3}{\nu \chi} \tag{4.9}$$

$$\begin{aligned} Nu &= \frac{Q_{diff} + Q_{conv}}{Q_{diff}} \\ &= 1 + \frac{Q_{conv}}{\chi \Delta T / H} \end{aligned} \tag{4.10}$$

It has been established that increases in $Ra$, however they are executed, lead to increases in $Nu$. But here it should be noted that $Nu$ only represents the ratio of total to diffusive heat flux. While it is proportional to the total heat flux, it can increase even when the heat flux decreases. For example, imagine the thermal diffusivity $\chi$ is decreased. The Rayleigh number increases, so too must the Nusselt number. Clearly the reduction in the denominator of $Nu$ causes an increase, but what about any changes in $Q_{conv}$? In fact it decreases but by a smaller factor than $\chi$. The decrease stems from the fact that even with the same temperature gradients at the boundary and the same convection in the interior, the diffusive heat transport at the boundary is reduced because of the reduction in diffusivity. So if the Nusselt number had been interpreted as being analogous to the heat flux, it might have led to false conclusions.

What about variations in the fluid viscosity? Reducing the viscosity increases the Rayleigh number. How does it affect $Nu$? Less friction allows greater fluid motion, delivering more heat from one boundary to another and thus the heat flux increases. An increase in heat flux also means an increase in entropy production.

What about when the boundary heat flux is held constant instead of the temperature difference? In that case reducing the viscosity causes a decrease in the total temperature difference. Physically, this is because more efficient heat transport mechanisms require smaller driving gradients. This behaviour is illustrated in Figure 4.1, where a schematic shows the changes that occur when a system is taken from the diffusive state through the critical Rayleigh number. The resulting changes in boundary temperatures and fluxes are shown.

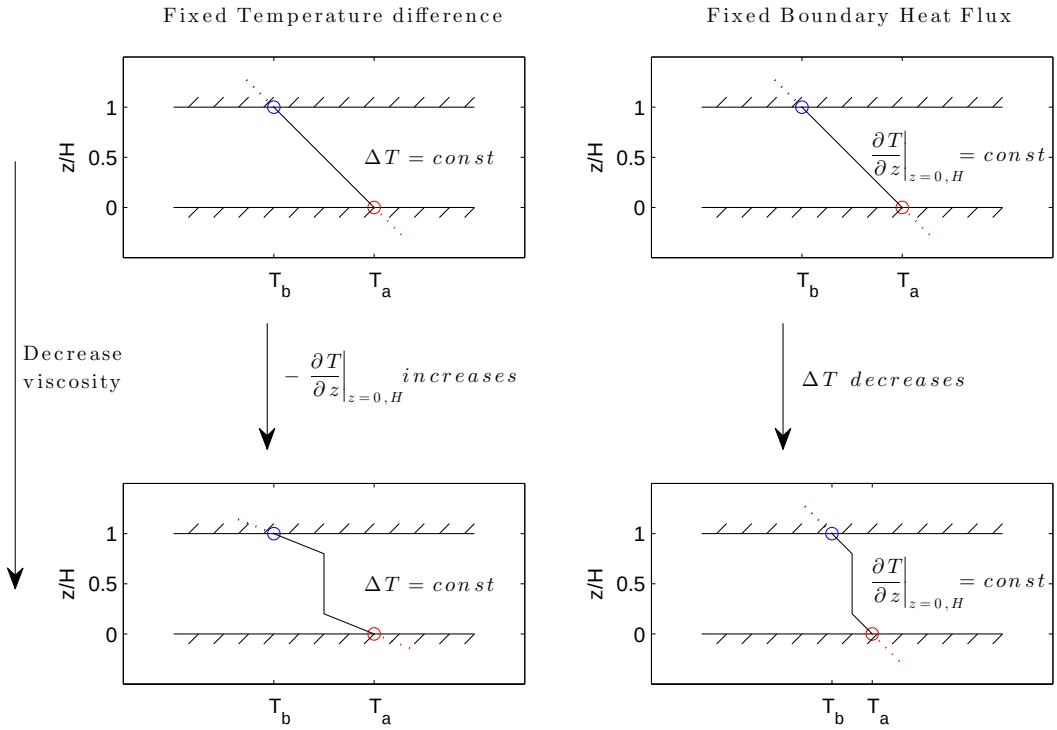


Figure 4.1: An illustration of the changes in transport properties of NC systems with two different types of fixed BCs. Note that going from the upper configurations to the lower set, the fluid viscosity is reduced while keeping the thermal diffusivity constant. This takes the Rayleigh number from $Ra < Ra_c$ to $Ra > Ra_c$, causing the onset of convection. Thus on the left, the temperature difference $\Delta T$ remains constant while the boundary temperature gradient (heat flux) changes, and on the right, the boundary temperature gradient remains constant while the temperature difference changes.

Clearly an extremum principle concerning the most basic interpretation of entropy production cannot offer a unifying theory for NC systems. Indeed the theoretical and conceptual foundations of the MEPP are far from universally accepted (Martyushev and Seleznev, 2006). The state selection version of the MEPP suggests that any non-equilibrium system which can settle into a range of steady states, will choose that state which has the MEP. However above the critical Rayleigh number, fixed flux NC systems settle into states of lower entropy production than the maximum.

In recent years, it has become increasingly clear that the MEPP shouldn't be viewed as a principle of nature, but rather a useful information theoretic tool to un-bias model predictions (Dewar, 2009; Dyke and Kleidon, 2010). Any dynamical system consists of a set of states defined by its external constraints plus a set of rules for the evolution of those states as a function of time. For most problems of interest, there are a vast

number of microscopic states that all produce similar macroscopic properties. Often the objective is to follow the trajectories of these bundles of microscopic states into the future and garner predictions about the macroscopic state of the system at those future points in time.

The information-theoretic concept of MaxEnt (Jaynes, 1957) begins with the assumption that our knowledge of which individual microscopic state a system will be in, is minimal. This allows one to begin to define properties of the probability distribution of the microscopic phase space paths, since minimising the state of knowledge is equivalent to maximising the Shannon information entropy, $S_I = -\sum_i p_i \ln p_i$. The exact phase space trajectory of the system is not known but in any real experimental or field scenario a set of measurements or parameters would provide a limited amount of information. This information could serve as constraints for the process of maximising $S_I$. The resulting distribution $p_i$ can then be employed to make predictions about the likely future states of the system by taking suitable expectation values for any relevant measurement over the states $i$, weighted by their probabilities $p_i$.

If those predictions prove correct, then there can be some confidence that the constraints that were used during the entropy maximisation procedure are sufficient to define the macroscopic evolution of the system. If the predictions are not correct, or not sufficiently well-defined (have a broad distribution), then it means more constraints are required to fully resolve the relevant macroscopic physics of the system. This procedure is the essence of the Bayesian, information theoretic approach to statistical mechanics. It is more general than equilibrium statistical mechanics because it is not restricted to systems that have reached equilibrium. The MaxEnt procedure has a strong intuitive appeal and indeed the famous probability theorist Edwin Jaynes believed that its basic logic underpins the foundations of the scientific method. I feel inclined to agree since we must always deal with incomplete information and we should always assume maximum uncertainty about those aspects of a system we do not understand or cannot measure. New measurements and theories introduce new constraints to our models and this increases the accuracy of our predictions. The process iterates and our state of knowledge increases with time (hopefully).

While the information-theoretic foundations of MaxEnt seem quite concrete, their relationship to the MEPP is still a matter of debate (Dewar, 2009). Some have argued that

for any given set of phase space paths of a non-equilibrium system, the vast majority of those paths should correspond to the maximum possible rate of thermodynamic entropy production (Equation 4.1), subject to whatever physical constraints the system is placed under (Dewar, 2003). Indeed it seems that the mathematical basis of the MEPP is essentially the same as the Gibbs derivation of the probability distribution for equilibrium systems. However the physical basis for this proposition has not been properly justified and a universally accepted derivation of the MEPP from MaxEnt is still lacking. Therefore one certainly shouldn't look to the MEPP as an encompassing principle of nature, a non-equilibrium version of the second law if you will.

As a final note, there is some evidence to suggest that the formation of organised structures in non-equilibrium systems can actually slow down the rate of approach to equilibrium. Experiments with simple reaction-diffusion systems performed by Awazu and Kaneko (2004) showed that pattern-formation caused a temporary decrease in the rate at which a chemical system relaxed to equilibrium. When a particular set of structures finally disintegrated, the rate of evolution towards equilibrium increased. So the default assumption that dissipative structures form and persist 'in order to' facilitate more rapid equilibration may not be generally true.

## 4.3 Conclusions

This chapter has critically evaluated the validity of the MEPP, specifically with regards to its application to the problem of heat transfer in fluid convection systems. The dimensionless groups used to describe the flow characteristics of thermal fluids can be modified in a variety of ways and the entropy production does not always increase with the dimensionless thermal driving parameter $Ra$. Furthermore when different BCs are used, such as fixed heat flux BCs, the entropy production decreases with $Ra$ due to the decline of the temperature difference $\Delta T$ with increasing $Ra$. This decrease in $\Delta T$ stems from the increased heat transfer efficiency of fluids with for example, a lower viscosity, meaning that the fixed flux imposed on the system can be achieved with a smaller driving temperature difference.

The state selection principle of the MEPP would imply that any NC system should settle into the state of MEP. But as just discussed, at $Ra > Ra_c$, fixed flux systems select

states of lower entropy production than the maximum due to the reduced temperature difference of the convective state compared to the purely diffusive state.

It seems to have been assumed in the literature (e.g., Meysman and Bruers, 2010) that at the bifurcation point (the critical Rayleigh number), convection is selected as the more stable steady state because it has higher entropy production. But as shown, for a system with fixed flux BCs, entropy production actually decreases below that of the static diffusive state beyond the bifurcation point, as the system settles on to the convective branch. I am not aware of any such detailed assessment of the role of BCs on the entropy production of convective fluids currently in the literature. Virgo (2010) discussed the role of BCs with regard to the MEPP but does not discuss convection in any depth. Therefore there is a need for some degree of clarification such that the general opinion shifts, from the default assumption that NC is a prime example of the MEPP to one that acknowledges the whole variety of entropy extremisation that can be observed in such systems.

In the next chapter another NC system will be investigated but it will have an extra element of freedom with respect to its BCs. It will be able to not only adjust its boundary heat flux but also its boundary temperature difference. Such an arrangement means that there is a peak in entropy production at intermediate values of heat flux. A direct interpretation of MEPP might suggest that the system should always choose a flux value of MEP. With the help of the TLBM, such a system will be simulated and it will be seen how it responds to its new found freedom.

# Chapter 5

# Negative Feedback Boundary Conditions

In the previous chapter it was argued that for natural convection (NC) fluid systems with fixed boundary conditions (BCs), maximum entropy production (MEP) does not seem to represent a universal steady state attractor. Some systems appear to minimise their rate of entropy production whereas others appear to exhibit maximisation, depending on how the BCs of the system are set up. What was evident though, is that the entropy production either increases or decreases monotonically as a single parameter of the system (such as the fluid viscosity or temperature difference) is varied.

In the previous two chapters only fixed temperature or fixed flux BCs were considered. Such systems have the freedom to adjust either their heat flux or temperature gradient, but not both. With one of these two fixed, any changes in the other variable will produce either increases or decreases in entropy production. What if the BCs are configured such that neither the heat flux or the temperature difference is prescribed? Such BCs are relatively simple and are often referred to as negative feedback BCs (Virgo, 2010), the reason for which should become clear in the following sections.

This form of model BC was first used in the middle of the last century to construct idealised models for atmospheric heat transport (Paltridge, 1978). While the original works made use of planetary atmosphere models consisting of 10 boxes through which heat was transported, the results are essentially unchanged if a model of 2 boxes is used. One box represents the equator of a planetary atmosphere and the other represents

the poles. It is assumed that both receive a solar energy flux, with the equatorial box receiving a higher flux due to its larger area exposed to radiation.

It is also assumed that both boxes are able to radiate heat away. The rate at which heat leaves the boxes is assumed to be a linear function of their temperatures (see Figure 5.1). If fixed heat capacities are defined for the two boxes, it is possible to calculate the energy balance for the entire system. What emerges is a range of steady states, each with a unique set of values for the box temperatures and the rate at which heat is being transported. Details of how the heat is funnelled from one box to the other (equator to poles) are excluded from the model. Instead a single variable representing the rate at which heat is transported is used to parameterise the physical mechanisms operating.

The range of steady states is bounded by the following two extremes: the equator-pole heat flux could be very low, causing a large temperature difference to build up between the boxes, or the equator-pole heat flux could be very high, bringing the temperatures of the two boxes closer together. Because of this trade-off between heat flux and temperature difference, changes in entropy production are not as simple as those for fixed BC systems. Instead of monotonic increases or decreases, there is actually a peak in entropy production at intermediate heat flux values. It was postulated that this peak might represent some kind of attractor for atmospheric steady states, and comparison with real data seemed to support this (Ozawa et al., 2003; Paltridge, 1978). The agreement even seems to extend to other planetary bodies including Mars and Titan (Lorenz, 2010).

Thus there is some evidence to suggest that the MEPP applies to atmospheric heat transport, although this is still a hotly contested area. The atmosphere is the epitome of a complex system involving a huge number of feedbacks, non-linear effects and different spatial and temporal scales. In essence it has a huge number of degrees of freedom, so uncovering exactly why such a system might maximise its entropy production is difficult to say the least.

However, the BCs of the 2-box model could be applied to a much simpler system: the 2D fluid systems that were investigated in previous chapters. Applying negative feedback BCs to the TLBM is straightforward. The system would have the same macroscopic energy balance as the 2-box model, but the internal dynamics would be fully resolved.

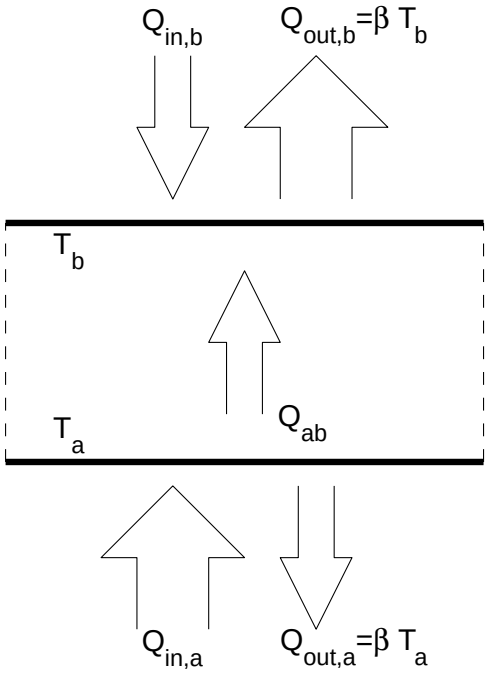


Figure 5.1: Schematic of a negative feedback BC system showing the various steady state fluxes, which comprise the boundary energy balances. Boundaries are periodic in the horizontal direction and upper and lower walls enforce the no-slip velocity condition.

Simulating the system would reveal whether the MEP state is also an attractor for simple convecting fluids, as it seems to be for atmospheres. Indeed some authors have hinted at this in the past (Kleidon, 2009), though the simulations of the following sections do not seem to have been performed previously. Before carrying out these experiments, it is important to first explicitly define the system and consider the details of the TLBM BCs required.

## 5.1 The Model System and its Macroscopic Variables

As in previous chapters, the model system is a 2-dimensional fluid enclosed between two solid plates. In the horizontal direction the system's boundaries are periodic. The upper and lower walls receive inward heat fluxes $Q_{in,b}$ and $Q_{in,a}$ respectively, and are also able to radiate heat away from the system. The outward fluxes have the functional form $Q_{out,i} = \beta T_i$ where $i \in \{a, b\}$ and $\beta$ is a parameter. Figure 5.1 shows a schematic of the system.

Heat flows through it by a combination of diffusion and NC, and it is assumed that it is a Boussinesq fluid (see section 3.1).

Ignoring the internal details of the system and regarding it as a black box that has reached a state of dynamic equilibrium, the energy balances at the two boundaries can be expressed,

$$Q_{in,a} - Q_{ab} - \beta T_a = 0 \tag{5.1}$$

$$Q_{in,b} + Q_{ab} - \beta T_b = 0 \tag{5.2}$$

where $Q_{ab}$ is the net heat flux away from and into the lower and upper boundaries respectively. Adding these two equations yields

$$Q_{in,a} + Q_{in,b} - \beta(T_a + T_b) = 0 \tag{5.3}$$

Writing the two temperatures in the form $T_a = T_0 + \Delta T/2, T_b = T_0 - \Delta T/2$, the equation above can be used to find the system's average temperature $T_0 = (T_a + T_b)/2$,

$$T_0 = \frac{Q_{in,a} + Q_{in,b}}{2\beta}. \tag{5.4}$$

To find an expression in terms of $\Delta T$ Equation 5.2 can be subtracted from equation Equation 5.1,

$$Q_{in,a} - Q_{in,b} - 2Q_{ab} - \beta(T_a - T_b) = 0 \tag{5.5}$$

$$Q_{in,a} - Q_{in,b} = 2Q_{ab} + \beta\Delta T. \tag{5.6}$$

It can now be seen that in fact the system has only a single macroscopic degree of freedom. The equation above shows that once the temperature difference is determined, the heat flux is also then determined (or vice versa). If there existed a relation between the heat flux and the temperature difference then the steady state of the system would be fully determined by the values of the boundary parameters and Equation 5.6. Such a relation does not exist for NC systems (at least not for all values of $Ra$).

However, the extrema of the heat flux and temperature difference can be calculated. In the case of zero flux through the fluid, $Q_{ab} = 0$ and thus $\Delta T_{max} = (Q_{in,a} - Q_{in,b})/\beta$. The opposite case is that of perfect mixing, $\Delta T = 0$, for which $Q_{ab_{max}} = (Q_{in,a} - Q_{in,b})/2$.

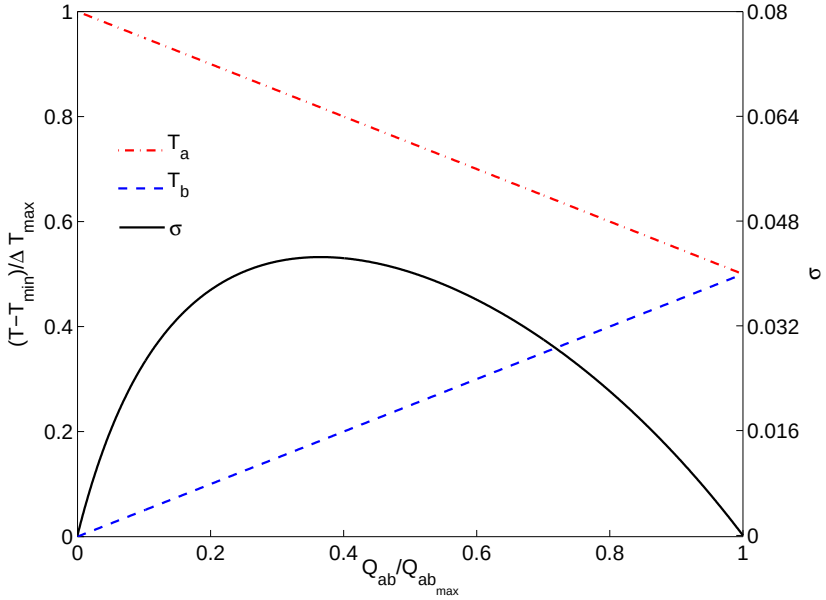


Figure 5.2: Macroscopic transport properties of the model system. External flux parameters are fixed at $Q_{in,a} = 0.1, Q_{in,b} = 0.01, \beta = 0.1$. The numerical value of the boundary heat flux $Q_{ab}$ is varied between its lower and upper extremes, 0 and $(Q_{in,a} - Q_{in,b})/2$. The resulting boundary temperatures $T_a$ and $T_b$ can then be calculated.

At this stage it could be assumed that the flux $Q_{ab}$ depends linearly on the temperature gradient, i.e., $Q_{ab} = k_e \Delta T$ where $k_e$ is an effective thermal diffusivity. This relation would hold true if heat were being transported purely by diffusion, whereby $k_e$ would just be the thermal diffusivity of the system's material. However a key characteristic of NC heat transfer is that it has a non-linear response to driving forces. Therefore the linear approximation does not hold.

Instead, one can get a sense of the system's transport properties by choosing a set of values for the flux parameters ($Q_{in,a} = 0.1, Q_{in,b} = 0.01, \beta = 0.1$), varying the boundary flux linearly between its extrema, i.e., $Q_{ab} \in [0, (Q_{in,a} - Q_{in,b})/2]$, and calculating the resulting boundary temperatures.

This behaviour is illustrated in Figure 5.2, which shows the boundary temperatures as a function of $Q_{ab}$. This figure illustrates the single degree of freedom that the system has (in terms of macroscopic energy balance). Larger heat fluxes $Q_{ab}$ result in lower temperature differences and vice versa. A relation between $Q_{ab}$ and $\Delta T$ would be a sufficient constraint to completely determine the steady state of a given system. However

in the absence of such a relation, the system has the freedom (in principle) to choose any value of $Q_{ab}$.

Also shown in Figure 5.2 is the entropy production rate $\sigma = Q_{ab}\,(1/T_b - 1/T_a)$. It has a maximum at an intermediate value of $Q_{ab}$. This contrasts with the cases of fixed BCs in which the entropy production changes monotonically with boundary heat flux or temperature difference.

As discussed in the previous chapter, it has been hoped that the MEPP may be a unifying principle of non-equilibrium thermodynamics. However evidence was presented suggesting that different variational principles involving entropy production seem to apply to NC depending on the BCs used. Ozawa et al. (2003) found that certain transport properties of the atmospheric circulation of several planetary bodies can be reliably predicted using a simple application of the MEPP and (Kleidon, 2009) suggested that in a simple convective fluid system like the one described in this chapter, the characteristic peak seen in Figure 5.2 should define the steady state heat flux of the system.

In the following sections, by modelling such a system, this hypothesis will be tested. However there is an apparent inflexibility of the MEPP when applied to this NC system. The entropy production peak (visible in Figure 5.2) occurs without any incorporation of the particular physical properties of the fluid used in the system. It comes purely from an analysis of the steady state energy balance. The boundary parameters feature in this energy balance but the fluid parameters do not. Surely a more viscous fluid would adopt a different steady state heat flux than one that was less viscous? In section 5.3 it will be shown exactly how the system responds in this respect. First, a method for constructing suitable BCs for the TLBM of chapter 3 will be described.

## 5.2 Definition of Boundary Conditions

Careful consideration of the BCs for the internal energy distributions must be taken as they are not uniquely defined for this new system. There are essentially two alternatives for applying the relevant boundary heat fluxes at each integration step. The first method, to be referred to as the *vari* method involves a simple point-by-point application of the BC. For the boundary grid nodes, after the bounce-back stage of the algorithm and before the collision step, the three inward-pointing internal energy distribution functions

underwent the following forcing step:

$$g'_{j,k} = g_{j,k} + 6\omega_j \frac{Q_{in_i} - \beta T_{i,k}}{W} \tag{5.7}$$

where $j$ indexes the distribution function (for a lower boundary, $j \in \{2, 5, 6\}$ and for an upper boundary, $j \in \{4, 7, 8\}$), $i \in \{a, b\}$ denotes the upper or lower boundary, $k$ denotes the grid node ($T_{i,k}$ is the temperature of node $k$ on the boundary $i$ calculated after streaming and bounce-back) and $W$ is the total grid nodes in the horizontal direction. The factor of 6 in the equation above stems from the division of heat flux between the three inward-pointing distributions. For example at an upper boundary, the fraction of the additional internal energy assigned to the direction $\mathbf{e}_7$ would be

$$\frac{\omega_7}{\omega_4 + \omega_7 + \omega_8} = 6\omega_7. \tag{5.8}$$

With this form of BC the temperature at either boundary is not constrained to be horizontally uniform.

The second BC type, referred to as the *uni* method, assumes that the boundary of the system has perfect thermal conductivity in the horizontal direction such that there is always a horizontally uniform temperature profile. The first stage is to calculate the mean boundary temperature after streaming and bounce-back. Then, the total heat flux into the boundary can be calculated,

$$Q_{tot_i} = Q_{in_i} - \beta \overline{T_i}. \tag{5.9}$$

Recall the expression for the total internal energy at grid node $k$,

$$\rho_k \epsilon_k = \sum_{j=0}^{8} g_{j,k} \tag{5.10}$$

where $\rho_k$ and $\epsilon_k$ are the mass and internal energy densities of grid node $k$. Summing this over the entire length of the boundary gives an expression for the total boundary internal energy

$$E = \sum_{k=0}^{W-1} \rho_k \epsilon_k \tag{5.11}$$

The new boundary internal energy after the heat flux step can now be calculated,

$$E' = Q_{tot_i} + E \tag{5.12}$$

$$= Q_{in_i} - \beta\overline{T_i} + \sum_{k=0}^{W-1} \rho_k \epsilon_k. \tag{5.13}$$

It only remains to calculate the new boundary internal energy $\epsilon'$ resulting from this inward flux of heat. Remember that the incoming energy is to be distributed such that every boundary grid node will have this new temperature. Thus $\epsilon'$ does not depend on the node index $k$. Equation 5.11 can be used here,

$$\sum_{k=0}^{W-1} \rho_k \epsilon' = E'$$

$$= Q_{in_i} - \beta\overline{T_i} + \sum_{k=0}^{W-1} \rho_k \epsilon_k$$

$$\epsilon' \sum_{k=0}^{W-1} \rho_k = Q_{in_i} - \beta\overline{T_i} + \sum_{k=0}^{W-1} \rho_k \epsilon_k \tag{5.14}$$

$$\epsilon' = \frac{Q_{in_i} - \beta\overline{T_i} + \sum_{k=0}^{W-1} \rho_k \epsilon_k}{\sum_{k=0}^{W-1} \rho_k}. \tag{5.15}$$

The inward-pointing (for a lower boundary, $j \in \{2, 5, 6\}$ and for an upper boundary, $j \in \{4, 7, 8\}$) internal energy distributions can then be modified before the collision step according to

$$g'_{j,k} = g_{j,k} + 6\omega_j \rho_k \left(\epsilon' - \epsilon_k\right) \tag{5.16}$$

All simulations were initialised in a state of zero fluid velocity at the mean temperature (Equation 5.4), with a uniform internal energy distribution and a small degree of random noise. Runs were concluded when the system's key variables (boundary temperatures, Rayleigh and Nusselt numbers) showed no further variation with time. In the more turbulent cases ($Ra > 10^6$), in which the key variables showed no sign of becoming stationary, but instead showed oscillatory behaviour, a long time average was taken.

## 5.3 New Results

The first set of experiments had the following boundary parameters: $Q_{in,a} = 0.1, Q_{in,b} = 0.01, \beta = 0.1$. The following system properties were varied: grid size $H$, viscosity $\nu$ and

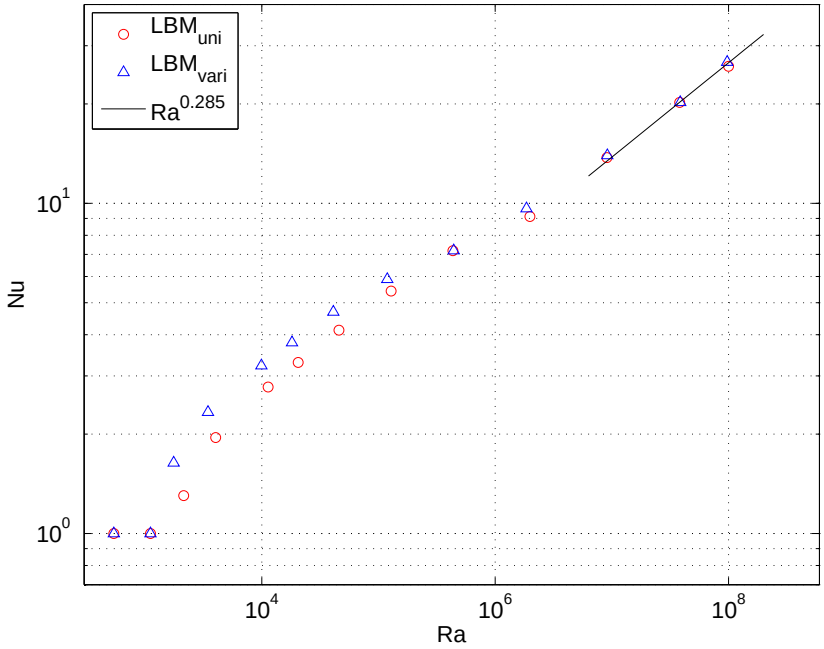


Figure 5.3: Dimensionless heat flux ratio $Nu$ as a function of dimensionless thermal driving force $Ra$ for NC systems with negative feedback BCs. Red circles correspond to systems with uniform boundary temperature profiles and blue triangles correspond to systems with a variable boundary temperature profile. The solid line shows the empirical scaling law $Nu \approx 0.138 Ra^{0.285}$ due to Johnston and Doering (2009).

thermal diffusivity $\chi$, while keeping the ratio $Pr = \nu/\chi$ constant. The reason that both the grid size and the viscosity were varied is that the most turbulent simulations require a significantly enhanced resolution to resolve the small scale flow features. For the simpler, laminar flows, all features can be simulated adequately with much coarser grids. If the grid size had been kept constant, carrying out all the simulations would have required an inordinate amount of time.

The scaling of the dimensionless groups $Ra$ and $Nu$ will first be considered. Figure 5.3 displays these results for the negative feedback system. The $Ra - Nu$ relation appears to be identical to the fixed temperature and fixed flux data (shown in Figure 3.9), and adheres to the same scaling law proposed by Johnston and Doering (2009) when $Ra \geq 10^7$. Notice also that at lower Rayleigh number the simulations that permitted a non-uniform boundary temperature profile (vari) were able to achieve an augmented Nusselt number compared to those with uniform boundary temperatures (uni). This is similar to the slight differences between fixed flux and fixed temperature systems over the same range of $Ra$ values. The fixed flux BCs also allowed a slightly higher

heat transport since the convection rolls could penetrate into the region which would normally be occupied by boundary layers in the fixed temperature systems. A similar explanation applies here to the difference between the *uni* and *vari* systems.

So in terms of the standard dimensionless measures, the fluid seems to behave identically to a system with fixed BCs. This implies some kind of hydrodynamic invariance to BCs. Intuitively this seems to make sense because in steady state, the boundary fluxes and temperatures are constant. In such a state, there would be no physical difference if it were chosen to prescribe the temperature, and adjust the flux to achieve that, or the flux such that the relevant temperature was achieved (with the exception of the subtle differences at low Rayleigh number).

Moving on from hydrodynamics, the steady state heat fluxes $Q_{ab}$ and temperature differences $\Delta T$ can now be assessed, relative to the entropy production peak. Figure 5.4 shows this data. Plotted in the figure are the steady state temperature differences $\Delta T$, normalised by the maximum possible temperature difference $\Delta T_{max} = (Q_{in,a} - Q_{in,b})/\beta$, as a function of the steady state heat flux $Q_{ab}$, normalised by its maximum $Q_{ab_{max}} = (Q_{in,a} - Q_{in,b})/2$. The first thing to notice about the data is that all points lie considerably to the right of the entropy production peak. So the system transports much more heat than it would in a state of MEP. Secondly, it can be seen that there is significant spread among the points, so a steady state attractor does not appear to exist. But what is it that dictates the steady state properties of a system as a function of its physical properties (viscosity, coefficient of thermal expansion and system size for example)?

Imagine a system in steady state, with a flux and temperature difference that have been measured. If all the fluid properties were kept constant but the system size $H$ was increased, an increase in $Q_{ab}$ would be observed (and a concomitant decrease in $\Delta T$). A larger system experiences stronger convection because the resistance of the whole fluid body to motion is reduced. So as a system is made larger, its steady state flux moves to the right on Figure 5.4 (and $\Delta T$ decreases).

Instead, an increase in fluid viscosity $\nu$ could be enforced. Such an increase weakens convective motion due to increased frictional resistance. As a result this change would shift a point on Figure 5.4 up and to the left due to the decrease in heat flux and increase in temperature difference. If the viscosity is increased further, eventually the fluid would become so 'thick' that fluid convection would stop altogether and heat transfer through

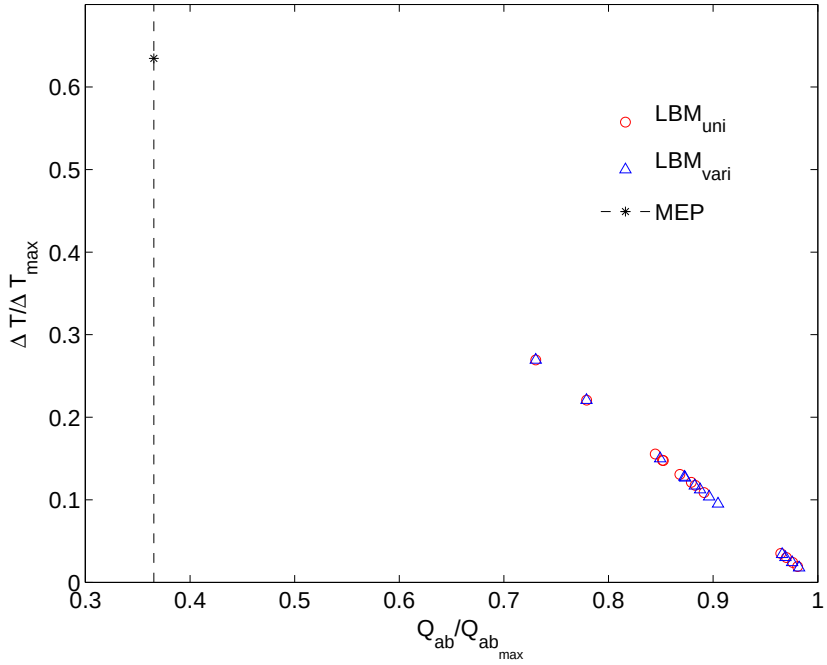


Figure 5.4: Normalised steady state temperature difference as a function of heat flux for TLBM simulations with negative feedback BCs. Red circles and blue triangles show results from the *uni* and *vari* simulations respectively. The black dotted line shows the heat flux value corresponding to a state of MEP and the black asterisk shows the corresponding value of the temperature difference. As predicted from the energy balance equations (and displayed in Figure 5.2), higher heat fluxes result in a lower temperature difference.

the system would occur purely by diffusion. At this point any more increases in viscosity would have no effect on the heat flux because that flux would then be constrained purely by the fluid's thermal diffusivity.

In contrast, decreasing the viscosity has the effect of increasing a system's heat flux, and this would continue until the system tends to the hard limit of $\Delta T \to 0$ at which point the transport of heat is so strong that the two boundaries would have almost equal temperatures. Since the temperature difference is the driving force for convection and heat transfer in general, the system cannot attain the limit $\Delta T = 0$ since there would then no longer be a driving force (the flux would reduce until a gradient developed again, at which point the flux would also re-initiate and an oscillatory negative feedback cycle would set in).

Finally, the case of increasing the viscosity at constant Prandtl number should be considered (increasing both the viscosity and thermal diffusivity). It might be expected that the flux would simply decrease since a more viscous fluid has a greater convective

resistance. Indeed this is true, but a proportionate increase in thermal diffusivity means that boundary heat flux is also increased (for the same local temperature gradient). In fact the increase in heat flux from the augmented thermal diffusivity actually outweighs the loss in flux due to increased viscosity. The net effect is that a point on Figure 5.4 would move down and to the right with this change, even though the Rayleigh and Nusselt numbers would decrease. Note that the Nusselt number has decreased even though the magnitudes of the total and diffusive fluxes have increased. Once again, it is clear that the Rayleigh and Nusselt numbers encompass several hydrodynamic effects and on their own, do not give us a complete description of the steady state.

So NC systems seem to be insensitive to their entropy production, MEP does not appear to be a steady state attractor. But only steady states that transport significantly more heat than the MEP value have been observed. Might it be possible to observe heat fluxes that are less than the peak or of a similar value? It has been established that a system's state can be shifted around Figure 5.4 by altering the physical properties of the fluid. Can a system be moved arbitrarily far to the left of the figure?

In fact this is possible if the assumption of constant Prandtl number is relaxed. Then the thermal diffusivity can be set very low and the viscosity very high (large Prandtl number). This would yield a fluid that would not undergo convective motion but also would not conduct a great deal of heat. Although heat would be moving by diffusion only, it would be possible to observe values of $Q_{ab}$ as far to the left of Figure 5.4 as required. As $\chi \to 0, Q_{ab} \to 0$, the lower limit of heat flux.

There is also a more elegant alternative. So far the BC parameters have been kept constant. Changing them will have a direct impact on the energy flows of the system. The primary driving force for heat flux through the fluid system (as opposed to heat instantly leaving the boundaries of the system through the outward fluxes), is the flux difference $Q_{in_a} - Q_{in_b}$. Looking back at Equation 5.6, it is clear that increasing this flux difference will have the effect of increasing both $Q_{ab}$ and $\Delta T$. However at present the aim is to find situations in which the relative heat flux is lower than intermediate values.

If the parameter $\beta$ were increased, the dependence of the outward fluxes on boundary temperature would be increased. Hence a larger fraction of the total energy being received by the system would be re-emitted at the boundaries, and a smaller fraction would be funnelled through the fluid than an equivalent system with a smaller value of

$\beta$. Note also that changing $\beta$ does not affect the range of flux values: $Q_{ab} \in [0, (Q_{in,a} - Q_{in,b})/2]$. What is affected is the range of temperature differences: $\Delta T \in [0, (Q_{in,a} - Q_{in,b})/\beta]$.

All $\Delta T$ values (and indeed the mean temperature $T_0$) will experience a decrease with increasing $\beta$. However since this is a linear re-scaling of all values, the position of the entropy production peak remains unchanged (as long as only $\beta$ is adjusted). Thus if systems with different $\beta$ values are simulated, the results can be compared with other data sets as long as the heat flux and temperature difference values are normalised by their relevant maxima.

At this stage it is possible to notice an apparent issue. If the fluid properties are kept similar to those used previously and $\beta$ is increased, the mean temperature will be decreased significantly. Surely then, the fluid will not convect because the temperature differences in the new system will be far too small to induce convective motion?

This problem can be alleviated however. There are no constraints on the fluid properties (other than $Pr = 1$) so the viscosity and thermal diffusivity can simply be reduced proportionately to the reduction in mean temperature, such that the system returns to a convective regime. With this in mind, simulations were carried out with two additional values for the parameter $\beta$ and the results are shown in Figure 5.5.

Note that each of the three data sets represents a range of Rayleigh numbers: $Ra \in [2 \times 10^3, 5 \times 10^5]$ (more turbulent simulations were not carried out for the two additional data sets and so those higher $Ra$ results from the first data set are omitted from Figure 5.5). These results show that the system does indeed seem indifferent to entropy production. With suitable adjustments of parameters, steady states have been observed spanning the whole range of flux values, and one of the data sets even passes straight through the MEP flux value.

This, combined with the results in the previous chapter, constitutes sufficient evidence that entropy production rate has no bearing on the steady state properties of NC systems. Previous work that suggested such a link seems to have missed the fact that $Nu$ can increase even when total heat flux decreases and that $Ra$ can also increase even when the entropy production shows a decrease. To describe a NC system fully, all of its physical properties must be taken into account. While the dimensionless groups $Ra$ and

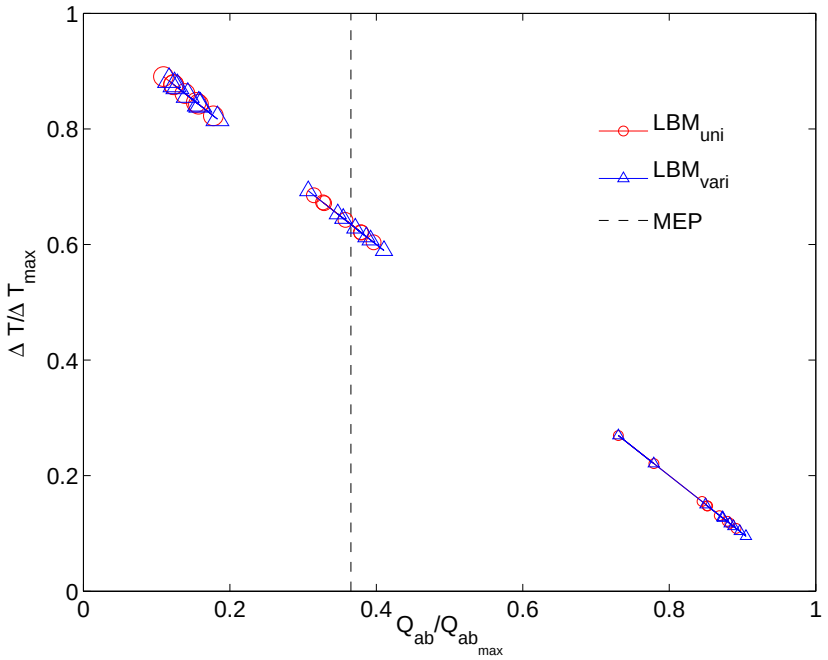


Figure 5.5: Normalised steady state temperature difference as a function of normalised heat flux for TLBM simulations with negative feedback BCs. Red circles and blue triangles show results from the *uni* and *vari* simulations respectively. The black dotted line shows the heat flux value corresponding to a state of MEP. As predicted from the energy balance equations (and displayed in Figure 5.2), higher heat fluxes result in a lower temperature differential. On this figure there are three separate data sets, each corresponding to a different value of the parameter $\beta$, but all had common values for the other BC parameters, $Q_{in,a} = 0.1, Q_{in,b} = 0.01$. The leftmost cluster of points represent simulations with $\beta = 4$, the central cluster $\beta = 1.3$, and the rightmost cluster $\beta = 0.1$.

$Nu$ are useful for the purposes of dynamical similarity, they do not convey every detail. Nor in fact can we summarise the steady state with just the heat flux and temperature difference (the two components of the entropy production).

## 5.4 Can the Maximum Entropy Production Principle be Trusted?

Even though the MEPP has failed for NC, it has succeeded for the problem of atmospheric heat transport (O'Brien and Stephens, 1995; Ozawa et al., 2003; Paltridge, 1978). Why is it that it was successful for that system and not for simpler NC systems? A physically rigorous explanation as to why it seems to work so well for atmospheres (and

indeed why it should work in general) is still lacking. However, the most obvious difference between atmospheric transport and the single-phase fluid systems dealt with in this chapter, is the significant reduction in the degrees of freedom of the simpler system. To say it is more constrained is an understatement. And this is precisely why taking into account the physical specifics of the system is so important.

If MEP is indeed an attractor for atmospheres, changing the thermal expansion of oxygen for example, is likely to be insufficient to shift the system away from that attractor. In fact in the MEP literature the phrase "What if the sea was made of vinegar?" is frequently mentioned pertaining to the suggestion made at a workshop that since the 2-box model doesn't take account of the particular physical properties of the atmospheres that it models, it would make no difference to the predictions if the water oceans were replaced by vinegar oceans. And since several different planetary atmospheres have been shown to exhibit MEP, this seems to hold true; it does not matter what materials or properties comprise the atmosphere, when it comes to atmospheric circulation, MEP appears to be the selection rule (Kleidon et al., 2006; Ozawa et al., 2003).

The MEP peak for the simple NC system also doesn't take into account the physical particulars of the fluid. But that system is much simpler than an atmosphere. In fact it is approximately as constrained as a linear diffusive system. Even though the functional relationship $Q_{ab}(\Delta T)$ is not known, it might be expected that it is of the form $Q_{ab} = \alpha \Delta T^{\gamma}$, where the physical properties of the fluid and the nature of the heat transfer process are embedded within the two parameters $\alpha$ and $\gamma$. If this relationship was revealed, there would no longer be any question of MEP because the system's macroscopic properties would be completely predictable. So it is possible that the 2D fluid system is too constrained to have the real freedom needed to express MEP, but the theoretical knowledge of its behaviour is not quite sufficient to completely resolve it.

The empirical scaling law, $Nu \approx Ra^{2/7}$ of Johnston and Doering (2009) for systems with $Ra \geq 10^7$ could be used as a constraint:

$$Nu = \frac{Q_{ab}}{\chi \Delta T / H} \approx 0.138 \times Ra^{2/7} \tag{5.17}$$

$$Q_{ab} \approx 0.138 \frac{\chi \Delta T}{H} Ra^{2/7} \tag{5.18}$$

Introducing this into Equation 5.6 yields, after some re-arrangement,

$$\begin{aligned} Q_{in,a} - Q_{in,b} &= 2(0.138\frac{\chi\Delta T}{H}Ra^{2/7}) + \beta\Delta T \\ &= 0.276\frac{\chi\Delta T}{H}\left[\frac{bg_0\Delta T H^3}{\chi\nu}\right]^{2/7} + \beta\Delta T \\ &= 0.276\frac{\chi}{H}\Delta T^{9/7}\left[\frac{bg_0 H^3}{\chi\nu}\right]^{2/7} + \beta\Delta T \\ &= \phi\Delta T^{9/7} + \beta\Delta T. \end{aligned} \tag{5.19}$$

This defines a fixed relationship between the macroscopic parameters of the system $(Q_{in,a}, Q_{in,b}, \beta)$ and the steady state temperature difference $\Delta T$ (as long as $Ra \geq 10^7$). When such a relationship exists (another case is when $Ra < Ra_c$ and the heat transport is diffusive and linear), an extremum principle such as the MEPP is no longer required because macroscopically, there are no remaining degrees of freedom. The system's dynamics are fully resolved and all the physical properties of the fluid are embedded within $\phi$. While Equation 5.19 is not universally applicable, the idea was simply to show that the only missing piece in this puzzle is the function $Q_{ab}(\Delta T, \phi)$, which if known, would allow the system to be completely described.

The results and conclusions of this and the previous chapter imply that MEP is unfortunately not a useful guide when it comes to 'simple' NC systems. How does this bear on the general position of the MEPP? It has a significant body of proponents, critics and bench-sitters, so the MEPP will be a feature of non-equilibrium thermodynamics for some time yet, whether it is 'correct' or not. My own position is that the information-theoretic interpretation of the MEPP is the correct one. There is no doubt that in any physical model, one should assume maximum (not just partial) uncertainty about those aspects of a system about which there is no knowledge or understanding. The problem is then a matter of rigorously working out the consequences of this.

In some models it may be straightforward and the assumption of maximum information entropy may easily translate to maximum thermodynamic entropy production. However in most cases, it is not so simple. It may be that some of the successes of the MEPP are actually cases in which a diligent choice of force and flux automatically reveals maximisation of entropy production. There are many simple non-equilibrium systems which behave in predictable ways and one can imagine adapting a variational principle like the MEPP into a variety of problems. This is rather speculative and the success

of the MEPP for atmospheric heat transport is not in doubt, so my words come with a degree of caution.

## 5.5 Conclusions

I have spent the first half of this thesis analysing heated fluid systems and their thermodynamic transport properties. While these systems are interesting, it is more or less impossible for them to exhibit life-like behaviour (unless we can simulate self-reproducing hurricanes perhaps). My main motivation for the previous two chapters was to establish the role of thermodynamic entropy production in predicting the steady states of complex fluid systems. Since I have uncovered no evidence that entropy production represents an attractor for such systems, I cannot assume that this variational principle will serve as a guide for how similar and also more complex systems will behave.

The relevance of entropy production to biology should however not be ignored. It may be that in years to come a comprehensive theory for the flows of entropy (or its negative, information) through biological and ecological systems is discovered. The presence of life on Earth has pushed it into a state of much greater disequilibrium than would have occurred without life (the primary example being the high concentration of atmospheric oxygen). Might it be possible to observe anything remotely similar in simple physicochemical systems? The second half of this thesis aims to begin to answer such a question. I will use the modelling framework presented thus far as a platform to build more complex models of thermal, reactive fluid systems. These systems will exhibit a richer pattern-forming phenomenology and it will be seen whether their transport properties throw up any surprises.

# Chapter 6

# Doing Chemistry with an Isothermal Lattice Boltzmann Model

So far the behaviour of single-phase, single component fluids undergoing flows due to energy gradients have been explored. It has been shown that the thermodynamic characteristics of these systems are not trivial and cannot be straightforwardly predicted from the boundary conditions or macroscopic energy balance expressions. However, such systems are fundamentally limited in terms of their diversity of emergent patterns. A principal aim of this thesis is to explore the ways in which non-equilibrium systems make use of additional degrees of freedom. To that end, the complexity of the Lattice Botlzmann Model (LBM) simulations will now be ramped up to a new level, that of extra chemical species and reactions between them. Fully resolving a chemically reacting fluid flow is a daunting task to say the least and there are many different levels of description that could be chosen from the microscopic (usually treated with molecular dynamics simulations) to the bulk level (described by a small number of macroscopic state variables).

In fact, like many others my interest lies in an intermediate length scale, the so-called mesoscopic. Following the trajectories of individual molecules is impossible for all but the smallest systems. However it is undesirable to coarse grain all the interesting details out of the system. This was the essence of the previous justification for adopting the

LBM and it applies once again here. Introducing additional passive scalar species to the LBM is simple and actually this was already done in one form in chapter 3 for the internal energy. Introducing reactions between components is something that has not been as comprehensively explored in the literature as say, flows through porous media, although this is beginning to change. Most modern studies of reactive LBMs involve specific engineering problems, most commonly the combustion of a fuel in a chamber (Chen et al., 2008). There are some elemental studies however (Ayodele et al., 2011; Zhang and Yan, 2012).

In chapter 3 I introduced the Thermal LBM (TLBM) in which internal energy is modelled as an additional component with its own set of discrete distribution functions. The equilibrium distributions used for this component ensure that at the macroscopic level, the internal energy obeys the advection-diffusion equation of a passive scalar, i.e., the extra component does not influence the fluid flow unless some form of extra coupling is introduced (this was done through the buoyancy force term). Analogous to the advection and diffusion of heat, dissolved solutes also have very little influence on the flow of their solvent assuming their concentration is low.

A vast number of biochemical reactions occur in aqueous solution. However, much of the previous modelling work focussing on chemical systems, particularly with regard to the origin of life and astrobiology, has been performed under a well-mixed solution assumption (for example, the pioneering work of Kauffman, 1996, on autocatalytic chemical reaction networks). The models do not incorporate any spatial aspect. Furthermore the dynamics of chemical reaction networks on their own do not seem to offer any universal answers to how life-like behaviour can emerge from a non-living system (Vasas et al., 2012). Including space as a variable has proved very fruitful in uncovering fascinating and novel chemical phenomena, a primary example of which is the 2-dimensional Gray-Scott (GS) model (Pearson, 1993), that originally had no spatial aspect (Gray and Scott, 1985). In the past it was rather difficult to model such systems due to limited computational power and the large increases in memory required for multi-component, spatially resolved systems. In this respect, the LBM will prove its utility, since extra components only cause a linear increase in memory requirements. Additionally there is only a meagre increase in algorithm complexity when one wishes to include additional chemical species and reactions.

## 6.1 Theoretical Considerations

This section will describe the additions required to bring chemistry into the LBM. In this chapter only isothermal, 2-component systems will be considered. This will allow some elementary tests of the new LBM's performance to be performed. Furthermore it will allow the extra elements of the algorithm to be introduced step-by-step.

The distribution functions for extra chemical species diffusing and advecting within the solvent fluid behave just as the mass density and internal energy density,

$$h_i^\sigma\left(\mathbf{x}+\mathbf{e}_i\Delta t, t+\Delta t\right) - h_i^\sigma(\mathbf{x},t) = -\frac{1}{\tau_\sigma}(h_i^\sigma - h_i^{eq,\sigma}) \tag{6.1}$$

undergoing completely analogous streaming and collision steps. This is because the distribution functions representing the chemical species also obey the continuous Boltzmann equation (Equation 3.7). On its own, the above algorithm is essentially a numerical solution method for the diffusion equation (repeated propagation and spreading of mass). The new index $\sigma = 1, 2, ..., n$ corresponds to the $n$ different passive scalar species. In the above expression $h_i^\sigma(\mathbf{x},t)$ is the distribution function for the component $\sigma$, and $\tau_\sigma$ is the relaxation parameter, controlling the diffusivity of that component.

In this chapter the focus will be on static fluids (no flow-induced advection). As a result the equilibria for the new distribution functions have the following form:

$$h_i^{eq,\sigma} = \omega_i \psi_\sigma \tag{6.2}$$

expressing the fact that the equilibrium state should simply be the maximum entropy distribution of mass at a grid node. The concentration $\psi_\sigma$ of species $\sigma$ is given by:

$$\rho(\mathbf{x},t)\psi_\sigma(\mathbf{x},t) = \sum_{i=0}^{8} h_i^\sigma(\mathbf{x},t) \tag{6.3}$$

The diffusivity of component $\sigma$ is calculated from the relaxation parameter,

$$D_\sigma = \frac{1}{3}\left(\tau_\sigma - \frac{1}{2}\right)c^2 \tag{6.4}$$

At this stage a mechanism for chemical change is required. The LBM has been applied to

reactive systems, but in a limited number of examples compared to the multi-phase, non-reactive versions. Simulating a non-equilibrium, reacting flow system is difficult. The exact kinetic mechanisms underlying the dynamics of fluid flow and chemical reaction and the resulting phenomena emerging from the combination of the two are very much an active area of research (particularly in the case of combustion). However, the level of description relevant to this thesis, and to which the LBM is ideally suited is the meso-level. Therefore molecular-level dynamics will be ignored and it will be assumed that the law of mass-action kinetics holds at the level of the individual grid node in the LBM. In its most basic form, the law of mass action states that the overall rate of an elementary, irreversible reaction $aA + bB \rightarrow cC + dD$ is given by

$$r = k[A]^a[B]^b, \tag{6.5}$$

where $[A]$ represents the concentration of species $A$. This law will be used for defining the additional reaction term in the collision stage of the Reactive LBM (RLBM). The exact form of the reaction term to be added to the collision step (Equation 6.1) will be given in the following sections.

The accuracy of the RLBM can now be assessed. There will be two key tests of its performance: A linear system for which an analytical solution exists, and a non-linear system, the results of which will be compared with the literature.

## 6.2 Benchmark Tests

### 6.2.1 Two-species Linear Reaction in a Closed System

#### 6.2.1.1 Analytical Solution

The first assessment will be the simplest possible: the irreversible decay of a reactant $A \rightarrow B$ in a closed system with no fluid motion. The equations of motion for this system

are

$$\frac{\partial \hat{\psi_A}}{\partial \hat{t}} = D_A \hat{\nabla}^2 \hat{\psi_A} - k\hat{\psi_A} \tag{6.6}$$

$$\frac{\partial \hat{\psi_B}}{\partial \hat{t}} = D_B \hat{\nabla}^2 \hat{\psi_B} - k\hat{\psi_B} \tag{6.7}$$

$$\tag{6.8}$$

where $k$ is a rate constant. These are somewhat similar to the 2D heat equation with a source term and can be solved analytically with the help of Fourier transforms. The first step is to de-dimensionalise using a reference concentration $\psi_{A_0}$, characteristic length $L$ and time scale $t_d = L^2/D_A$, which corresponds to the time required to diffuse over length $L$ (Ayodele et al., 2011). The equation for species $A$ now becomes:

$$\begin{aligned}
\frac{t_d}{\psi_{A_0}} \frac{\partial \hat{\psi_A}(\hat{x}, \hat{y}, \hat{t})}{\partial \hat{t}} &= \frac{t_d}{\psi_{A_0}} \left( D_A \hat{\nabla}^2 \hat{\psi_A}(\hat{x}, \hat{y}, \hat{t}) - k\hat{\psi_A}(\hat{x}, \hat{y}, \hat{t}) \right) \\
\frac{\partial \psi_A(x, y, t)}{\partial t} &= \frac{L^2}{\psi_{A_0} D_A} \left( D_A \hat{\nabla}^2 \hat{\psi_A}(\hat{x}, \hat{y}, \hat{t}) - k\hat{\psi_A}(\hat{x}, \hat{y}, \hat{t}) \right) \\
\frac{\partial \psi_A(x, y, t)}{\partial t} &= \nabla^2 \psi_A(x, y, t) - \phi^2 \psi_A(x, y, t)
\end{aligned} \tag{6.9}$$

where carets indicate dimensional variables and $\phi^2 = L^2 k/D_A$ is the Thiele modulus, a dimensionless parameter which measures the ratio of the characteristic reaction time to that of mass diffusion. For systems which are very large, have a high rate constant or a low mass diffusivity, $\phi^2 \gg 1$ and chemical reaction will be the dominant process. When $\phi^2 \ll 1$ due to some combination of small characteristic length or high diffusion rates, the dynamics of the system are diffusion dominated. Transforming the above equation into the frequency domain makes it amenable to analytical solution:

$$\frac{d\Psi_A(\xi, t)}{dt} = -\xi^2 \Psi_A(\xi, t) - \phi^2 \Psi_A(\xi, t) \tag{6.10}$$

where $\Psi_A(\xi, t)$ is the Fourier transform of $\psi_A(x, y, t)$, $\xi$ is frequency (incorporating both of the two coordinate axes). This equation has the following solution:

$$\Psi_A(\xi, t) = Ce^{-\xi^2 t} e^{-\phi^2 t} \tag{6.11}$$

The constant $C$ corresponds to the Fourier transform of the initial condition: $\Psi_A(\xi, 0)$. The solution thus reads

$$\Psi_A(\xi, t) = \Psi_A(\xi, 0) e^{-\xi^2 t} e^{-\phi^2 t}. \tag{6.12}$$

The final solution will be the inverse Fourier transform of Equation 6.12:

$$\psi_A(x, y, t) = \left[\psi_A(x, y, 0) * f(x, y, t)\right] e^{-\phi^2 t} \tag{6.13}$$

where $f(x, y, t)$ is the inverse Fourier transform of $F(\xi) = e^{-\xi^2 t}$:

$$f(x, y, t) = \frac{1}{4\pi t} e^{-\frac{x^2+y^2}{4t}} \tag{6.14}$$

Note that the process of Fourier transformation has caused multiplication in Equation 6.12 to become a convolution operation in Equation 6.13. Carrying out the convolution operation yields the final solution:

$$\begin{aligned} \psi_A(x, y, t) &= \left[\delta(x - x_0)\delta(y - y_0) * \frac{1}{4\pi t} e^{-\frac{x^2+y^2}{4t}}\right] e^{-\phi^2 t} \\ &= \frac{1}{4\pi t} e^{-\frac{(x-x_0)^2+(y-y_0)^2}{4t}} e^{-\phi^2 t} \end{aligned} \tag{6.15}$$

where it has been assumed that the mass of the species $A$ is initially concentrated at the point $(x_0, y_0)$, in which case $\psi_A(x, y, 0) = \delta(x - x_0)\delta(y - y_0)$ (Ayodele et al., 2011). This exact solution will allow the accuracy of the RLBM to be assessed.

#### 6.2.1.2 Reactive Lattice Boltzmann Model Implementation

Simulating this 2-component system is straightforward with a RLBM. There are two equations for the streaming and collision of the chemical species distributions:

$$h_i^A\left(\mathbf{x} + \mathbf{e}_i\Delta t, t + \Delta t\right) - h_i^A(\mathbf{x}, t) = -\frac{1}{\tau_A}(h_i^A - h_i^{eq,A}) - \omega_i k \psi_A \tag{6.16}$$

$$h_i^B\left(\mathbf{x} + \mathbf{e}_i\Delta t, t + \Delta t\right) - h_i^B(\mathbf{x}, t) = -\frac{1}{\tau_B}(h_i^B - h_i^{eq,B}) + \omega_i k \psi_A, \tag{6.17}$$

that encompass the two processes of diffusion and chemical reaction. The equilibrium distributions are given by Equation 6.2, since there is no fluid motion.

#### 6.2.1.3 Test Results

Insight into the accuracy of the RLBM on this elementary system can now be gained. The assessment will be similar to that performed in Ayodele et al. (2011), one of the few recent works to assess the performance of RLBMs. The assessment does differ from that work slightly. In order to avoid the use of initial conditions with large discontinuities, all test simulations will be initialised at dimensionless time $t_i = 1 \times 10^{-4}$, and run through to $t_f = 2 \times 10^{-4}$. This avoids the (non-fatal) numerical instabilities that occur as a result of significant gradients of mass density. Such gradients are inevitable if the simulation is initiated simply with unit concentration of reactant at the central grid node. In the simulations presented in later chapters, the systems will never involve extreme discontinuities of mass or momentum and therefore it is un-representative to perform a benchmark test that begins with such a condition.

The simulation will be run for a range of relaxation parameters $\tau_A$. Note that for comparison with the analytical solution, the species $B$ and its concentration field is actually irrelevant (since it does not affect the reaction rate), so it was not represented in the simulations. The rate constant $k$ was also varied. In order to compare the same physical problem across different parameter combinations, the dimensionless group $\phi^2$ must be kept constant for all simulations ($\phi^2 = 2 \times 10^4$, in line with Ayodele et al. (2011)). The dimensionless end time $t_f$ must also be the same for all simulations. To keep $\phi^2$ constant, the characteristic length $L$ (grid size) was appropriately adjusted for each $[\tau_A, k]$ pair (Ayodele et al., 2011). The error is calculated using:

$$E = \sqrt{\frac{\sum_{x,y} \left[\psi_{A,exact}(x,y) - \psi_{A,sim}(x,y)\right]^2}{\sum_{x,y} \psi_{A,exact}(x,y)^2}}. \tag{6.18}$$

Figure 6.1 shows this error as a function of $\tau_A$ and $k$.

The figure shows that lower reaction rates and higher diffusivities lead to lower errors. It seems that the method cannot reproduce the correct dynamical behaviour if the reaction rate is very large (compared to the diffusion rate). This makes intuitive sense because it is well established that the LBM is accurate and isotropic for diffusion-only systems, whereas its accuracy for reactive systems is still being explored. It is likely that a more sophisticated implementation of the reaction term in the LBM evolution equation would

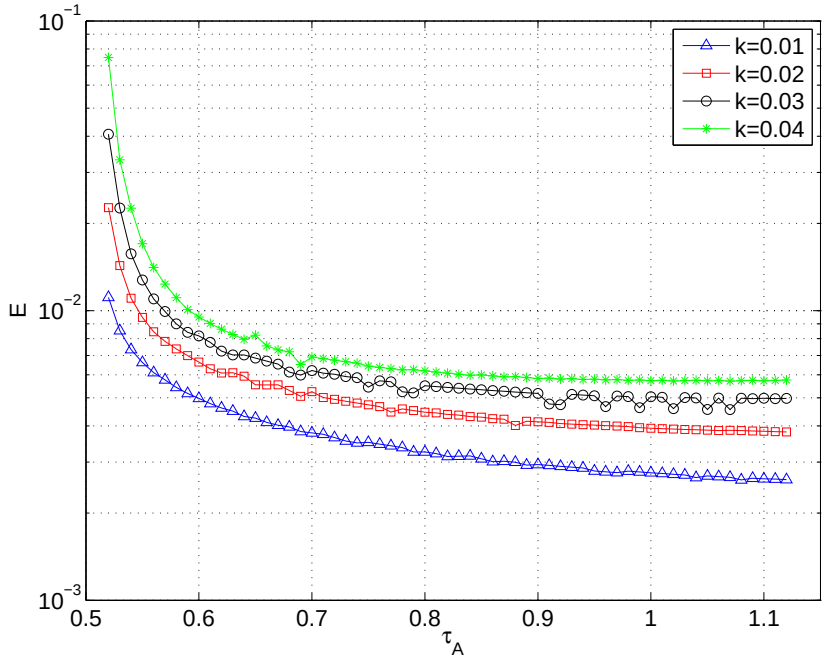


Figure 6.1: Numerical error of RD simulations as a function of relaxation parameter $\tau_A$ for several reaction rates $k$. For each simulation the dimensionless parameters $\phi^2$ and $t$ were kept constant allowing an objective comparison between $[\tau_A, k]$ combinations.

be required to alleviate this issue. However, when $\tau_A \geq 0.9$, the error is still less than 0.6%. With regards to the reduction in error with increasing $\tau_A$, this is probably due to the concomitant increase in grid resolution $L$, required to maintain $\phi^2$ at a constant value. What can be learned from this assessment is that it will be advantageous to make use of large grids and to use relaxation parameters $\tau_\sigma \geq 0.9$.

### 6.2.2 Two-species Non-linear Reaction in an Open System

#### 6.2.2.1 Reaction-Diffusion Dynamics

The next system to be considered stands alongside NC as a pinnacle of pattern formation in a non-equilibrium system: GS reaction diffusion (RD) systems. The umbrella term RD, applies to an ensemble of fascinating physico-chemical scenarios in which two or more chemical species spread and transform due to the simultaneous processes of mass diffusion and chemical reaction (these systems exist in both the theoretical and experimental realm). So in fact the system of the previous section was a RD system, albeit without lighting any fires in terms of interesting patterns.

The key, it seems, to many of the most interesting non-living and living phenomena in science is non-linearity. This behaviour often manifests itself in the form of exponential growth or exponential decay. Or in other words, positive feedback or negative feedback. Positive feedback is closely related to autocatalysis, wherein the presence of something makes its growth more likely. If a component of a system experiences positive feedback it will increase in magnitude until it exhausts whatever supplies it requires. In this sense an analogy can be drawn between chemical and biological systems. An autocatalytic substance will increase in concentration exponentially as long as the supply of input substances is not limited. If such a limit is imposed and the supply is sustained at a constant value, negative feedback will set in and the system will settle into dynamic equilibrium of some form. If the input substance is not replenished then the autocatalyst will no longer grow in concentration and may decay into lower enthalpy products and disappear altogether.

A similar dynamic occurs with any tragedy of the commons scenario in ecology. Organisms will flourish when they discover a plentiful source of vital nutrients. This source will inevitably be shared between many such organisms. Upon exploiting the resource (another organism in the case of heterotrophs), that resource will begin to recover (e.g., plants re-growing). With moderate consumption, a steady state may eventually emerge in which the production of new resource is balanced by predation. If however the predators are too enthusiastic with their feasting, they may begin to diminish the ability of the resource to replenish itself.

In fact that resource may collapse completely (if its ability to reproduce was made unviable because of a large reduction in its breeding population for example). At that point the predators will die back. Perhaps the resource may then recover and a periodic cycle of oscillations will set in (as captured by Lotka-Volterra dynamics). But it is also possible that the predators secure their own demise. The effect in biological populations is well documented and one could argue that as a species, we ourselves are currently entering into our own tragedy of the commons as we push the productive processes of the planet to the very last depths of possibility. In this and the next chapter, it will be shown that patterns formed in chemical systems can exhibit some of these ecological effects.

The most painless route into the annals of RD systems begins with the GS model (Gray

and Scott, 1985; Pearson, 1993). Despite its simplicity, this model can conjure stunning displays of coherent order. It comprises just two chemical species (it sometimes contains a third waste product, but its presence is not strictly required). They are imagined to be sandwiched in a thin (effectively two-dimensional) film by two porous plates. Within the layer, the two species are governed by the following equations

$$\frac{\partial \psi_A}{\partial t} = D_A \nabla^2 \psi_A - \psi_A \psi_B^2 + F(1 - \psi_A) \tag{6.19}$$

$$\frac{\partial \psi_B}{\partial t} = D_B \nabla^2 \psi_B + \psi_A \psi_B^2 - (F + R)\psi_B, \tag{6.20}$$

with the following autocatalytic reaction occurring: $A + 2B \rightarrow 3B$. There are the elements of the heat equation as before (rate of change of concentration depends upon local curvature of concentration), and also a non-linear reaction mechanism in which the presence of 2 $B$ particles with an $A$ particle stimulates the conversion of that $A$ particle to a third $B$ particle. The rate law is again based upon mass action kinetics (Equation 6.5).

Finally there are also processes in place to add reactant $A$ and remove product $B$. These are not so strong that they fix the concentrations of the two species. But they do impose a negative feedback effect. Notice that the supply of $A$ diminishes as $\psi_A \rightarrow 1$. In addition, the removal of $B$ diminishes as $\psi_B \rightarrow 0$. Physically, it is assumed that there is a reservoir of $A$ at concentration 1 in contact with the system. Particles of $A$ diffuse in at a rate proportional to the concentration difference $(1 - \psi_A)$, and the parameter $F$ quantifies the resistance to inward flux of $A$ from the reservoir. The same applies for the removal of $B$ except in that case, it is assumed that the diffusive resistance of the reservoir barrier is greater for removing $B$, by an amount $R$ (if $R = 0$, then removal of $B$ occurs just as fast as the supply of $A$).

In terms of parameters, it has been found that the most interesting dynamics occur when $D_A/D_B = 2$, $F \in [0, 0.082]$ and $R \in [0.02, 0.07]$. The pattern-forming phenomena actually occurs in an interface region (technically the saddle-node bifurcation line) of the model's $[F, R]$ phase space (see Figure 6.2 for a sneak preview). Either side of the critical region one finds only homogeneous states. The first consists of $\psi_A = 0, \psi_B = 1$ for $F \gg R$ (since the supply of $A$ is large and the removal of $B$ is relatively low, there is constant, rapid conversion of $A$ to $B$). The second consists of $\psi_A = 1, \psi_B = 0$ for $F \ll R$ (the removal of $B$ is so fast that the conversion reaction is relatively slow, insufficient

to reduce $\psi_A$ significantly). This is a simplified description and there are further subtle complexities to the system.

Within the critical region between these two extreme cases, an incredible variety of structures form including chaotic waves, spirals, lamellae, tubes and solitions. Unfortunately the governing equations currently have no analytical solution. A linear stability analysis could be performed but there would be nothing particularly novel about that (such an analysis can be found in many good non-linear dynamics textbooks). The task here is to explore the performance of the RLBM. Thus the focus now moves to RLBM simulations of the GS RD system.

#### 6.2.2.2 Reactive Lattice Boltzmann Model Implementation

To extend the current RLBM to non-linear reactions and supply and depletion requires modest adjustments. The evolution equations of the two chemical species take on the following form:

$$h_i^A\left(\mathbf{x}+\mathbf{e}_i\Delta t, t+\Delta t\right) - h_i^A(\mathbf{x},t) = -\frac{1}{\tau_A}(h_i^A - h_i^{eq,A}) - \omega_i\psi_A\psi_B^2 + F(1-\psi_A) \quad (6.21)$$

$$h_i^B\left(\mathbf{x}+\mathbf{e}_i\Delta t, t+\Delta t\right) - h_i^B(\mathbf{x},t) = -\frac{1}{\tau_B}(h_i^B - h_i^{eq,B}) + \omega_i\psi_A\psi_B^2 - (F+R)\psi_B \quad (6.22)$$

Note that a rate constant $k$ is no longer required since the effects of tuning such a constant can be absorbed into the relative tuning of the other parameters of the system. The equilibrium distributions are identical to those in Equation 6.2 since the system is static once again.

#### 6.2.2.3 Test Results

Since an analytical solution cannot be computed, qualitative comparison must be relied upon. Fortunately, there has been a huge amount of research carried out on this quintessential system, and its behaviour has been thoroughly documented (see, e.g., Pearson, 1993). It is thus possible to compare the complete phase portrait of the system between RLBM simulations and the literature. The phase portrait was constructed by carrying out simulations in which the parameters $F$ and $R$ vary continuously across the

simulation domain. In this way it is possible to observe all the pattern-forming features of the system in a single simulation.

This assumes that features in one region cannot significantly influence the properties of the patterns in the rest of the domain. Such an assumption may be violated and it is possible that the homogeneous regions either side of the critical zone have the effect of squashing it from either side. However such issues are not particularly relevant to the current focus. The objective here is simply to ensure that the RLBM is capable of producing the full repertoire of patterns observed in the GS RD system. Therefore the small non-local influences of different regions of the simulation domain will be assumed negligible. Comparison of the results with the literature will support the validity of this assumption.

The initial condition consisted of

$$\psi_A(x, y) = 1 \tag{6.23}$$

$$\psi_B(x, y) = \begin{cases} 0 & \text{if } X > 0.2 \\ 1 & \text{if } X \leq 0.2 \end{cases} \tag{6.24}$$

where $X$ is a uniformly distributed random variable. Figure 6.2 displays the phase portrait produced by the RLBM. Comparison with similar figures in the literature (Pearson, 1993) imply that the RLBM can indeed reproduce the full spectrum of patterns and structures.

There is one remaining parameter, the choice of which is not defined by the specification of the model system. This parameter is the relaxation time $\tau_A$. Since the ratio of diffusivities for the GS system has to be fixed ($D_A/D_B = 2$), the second relaxation time $\tau_B$ is defined once $\tau_A$ is chosen. However there is complete freedom in the value chosen for $\tau_A$. Therefore, the effect of varying $\tau_A$ was investigated and the results are presented in Figure 6.3. This figure demonstrates the influence that the mass diffusion rate has on the system's emergent patterns.

A lower diffusion rate (lower value for $\tau_A$) - which means that reaction is given a stronger relative influence - leads generally to structures with smaller characteristic length scales and vice versa. The relaxation parameter has a lower bound of $\tau_A > 0.5$ (lower values would lead to negative diffusivities), but what about larger values? Do the spot patterns

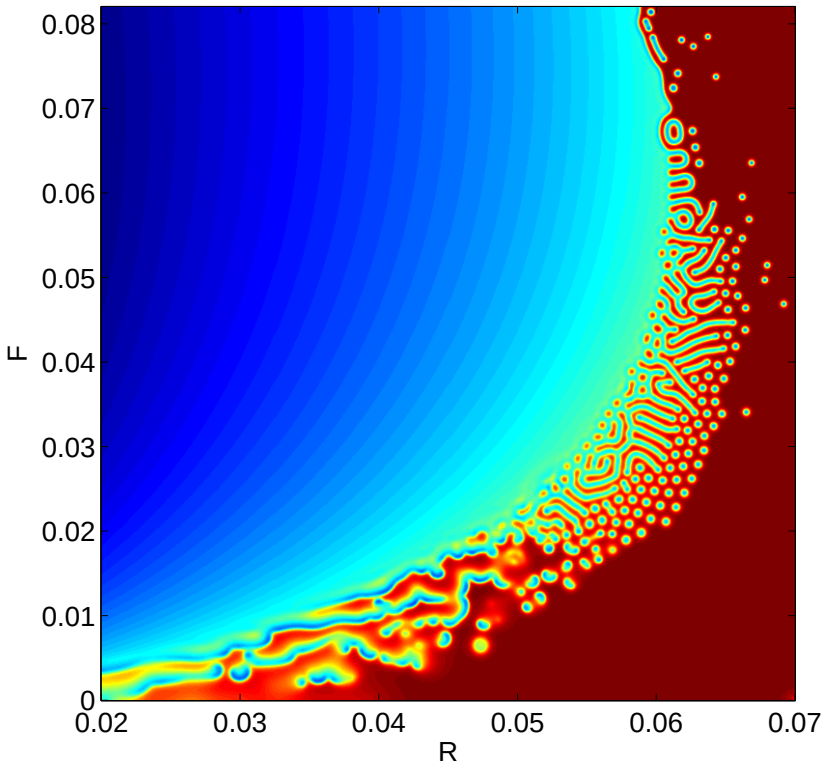


Figure 6.2: RLBM simulation of a GS RD system. The feed rate $F$ and depletion rate $R$ were varied continuously across the domain, allowing all the characteristic structures to emerge in a single simulation. The relaxation parameter is fixed at $\tau_A = 0.9$. The colourmap shows the order parameter $\phi(\mathbf{x}, t) = \psi_A(\mathbf{x}, t) - \psi_B(\mathbf{x}, t)$, with red corresponding to values of $\phi = 1$ and the deepest blue corresponding to $\phi \approx -0.5$.

and other structures just become arbitrarily large? In fact this enlargement of pattern length scales does continue as $\tau_A$, and hence the diffusivity, is increased even further. This is illustrated in Figure 6.4, which shows the same system again for $\tau_A = 3$. Since the mass diffuses at a higher rate, all the emergent structures swell in size. It seems that the mass of the two species diffuses so fast that the stable reaction fronts required for the formation of distinct structures are blurred out of existence except at very large length scales.

As well as demonstrating the abilities of the RLBM, the results of this section will be used to choose values of the relaxation parameters such that patterns of reasonable size emerge in the simulations of the next chapter.

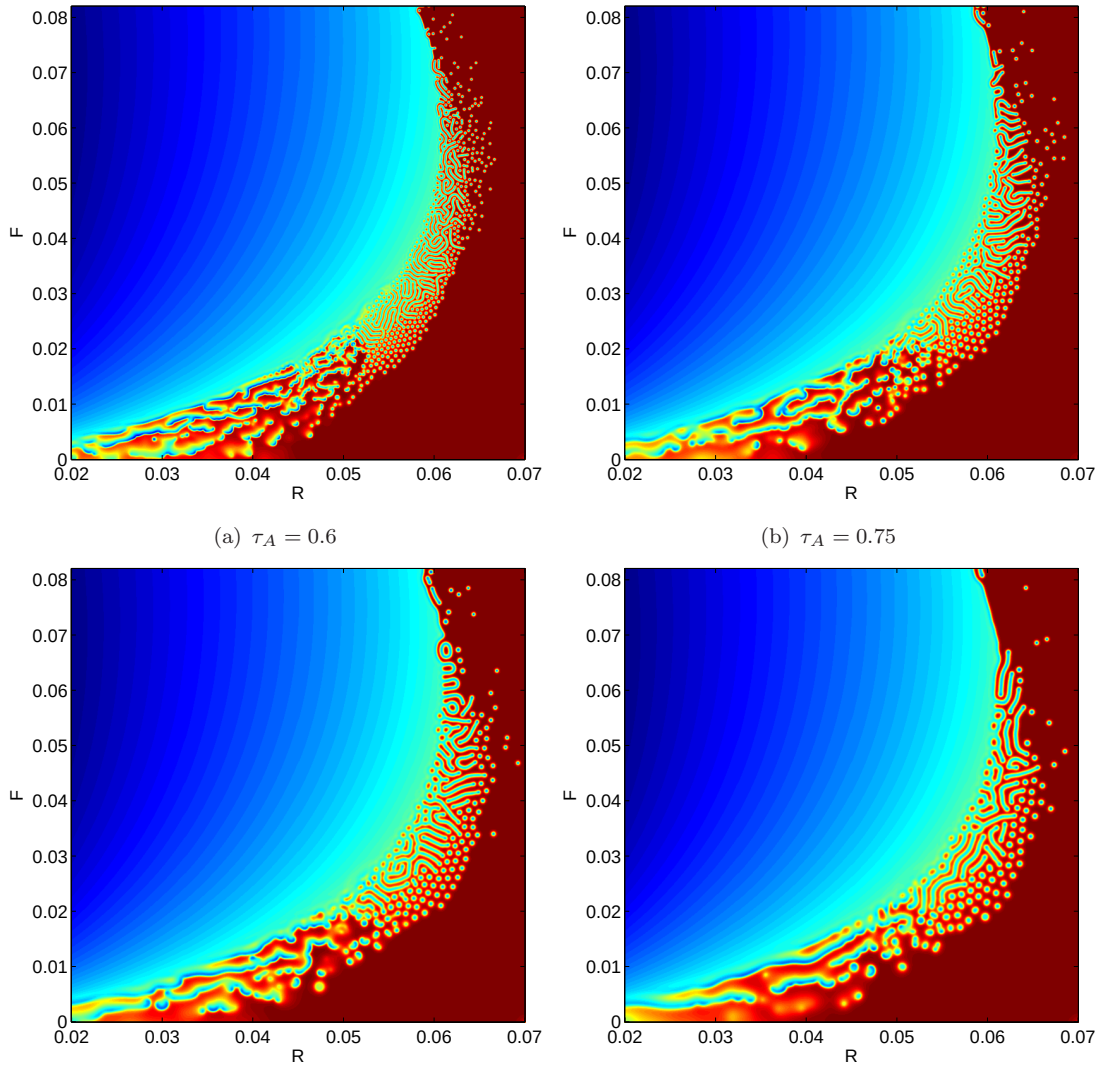


(a) $\tau_A = 0.6$

(b) $\tau_A = 0.75$

(c) $\tau_A = 0.9$

(d) $\tau_A = 1.05$

Figure 6.3: RLBM simulations of a GS RD system with different relaxation parameters $\tau_A$. The feed rate $F$ and depletion rate $R$ were varied continuously across the domain. The colourmap shows the order parameter $\phi(\mathbf{x}, t) = \psi_A(\mathbf{x}, t) - \psi_B(\mathbf{x}, t)$, with red corresponding to values of $\phi = 1$ and the deepest blue corresponding to $\phi \approx -0.5$.

## 6.3 Conclusions

In some respects the thesis up to this point represents a process of foundation building. Simulating non-isothermal, reactive fluid flows is a formidable task. There are all manner of ways in which highly simplified, heuristic models of such systems could be constructed. While useful and informative, such models run the risk of representing a different logic and reality to our own. Conversely the state of the art in computational

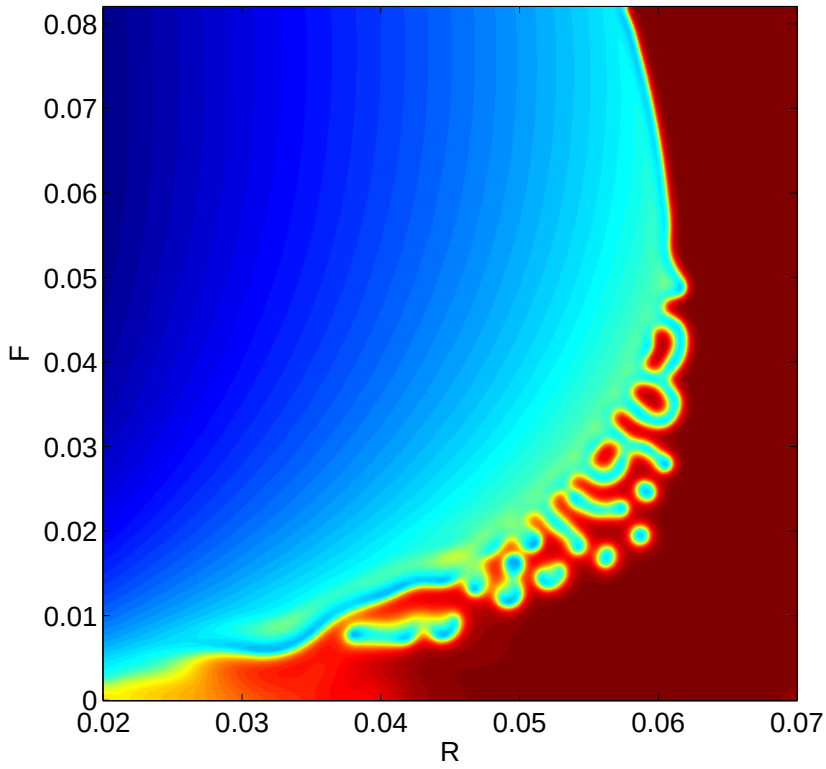


Figure 6.4: RLBM simulation of a GS RD system. The feed rate $F$ and depletion rate $R$ were varied continuously across the domain. The relaxation parameter is fixed at $\tau_A = 3$. The colourmap shows the order parameter $\phi(\mathbf{x}, t) = \psi_A(\mathbf{x}, t) - \psi_B(\mathbf{x}, t)$, with red corresponding to values of $\phi = 1$ and the deepest blue corresponding to $\phi \approx -0.5$.

physics techniques can simulate such systems with very high accuracy, but only for very short time scales, over extremely small length scales.

The RLBM as developed here, represents an excellent balance between these two options. Of course like any model, it comes with a set of assumptions. Furthermore there is no analytically tractable system with which one can assess the combined effects of reaction, diffusion and advection in the RLBM. However, this and previous chapters have shown that at its own level of description, the meso level, it can accurately simulate the following physical phenomena: diffusion of scalar fields, the advection of scalar fields by fluid flow, convective heat transfer and reactive mass change of passive scalar chemical species. The testing and analysis of the various versions of the model give confidence that systems combining all of the physical effects just listed can be simulated.

There doesn't seem to be any published work in which the GS RD model was enhanced to include thermal kinetics and advection by a fluid flow. But such a system would

surely reveal a considerable suite of phenomena, given that it has several extra levels of physical detail and degrees of freedom. Therefore the next chapter will explore exactly this kind of system.

# Chapter 7

# Turning up the Heat: Enthalpy Changes and Convection

It was shown in the previous chapter that the Reactive Lattice Boltzmann Model (RLBM) is capable of simulating simple reaction diffusion (RD) systems. In this chapter the simulations will be delving into somewhat new frontiers. The concept of enthalpy changes will be introduced. While the non-linear dynamics of RD systems are fascinating in their own right, they have been well studied and it is unlikely that there are significant new phenomena to be discovered without adding extra levels of complexity to the models. However what is generally missing is the next level of physical description. Hence in this chapter, thermal RD (TRD) systems will be the focus.

Chemical reactions occur because of scattering events between reactant molecules. They pass through intermediate, transition states somewhere between that of reactants and products, in which old bonds are broken and new ones formed. These intermediate states are higher energy, unstable states than either the reactant or product state. The system relaxes into the product state and the reaction is complete. In general the product state has a different energy than the reactant state, and the difference is known as the enthalpy of reaction $\Delta H$ (see Figure 7.1).

Furthermore, reaching the intermediate state requires an initial input of energy, known as the activation energy, $E_f$. The probability of a reaction thus depends critically on the activation energy and the local temperature. If the temperature is very low compared to the activation energy then the reaction will not take place. The difference in enthalpy

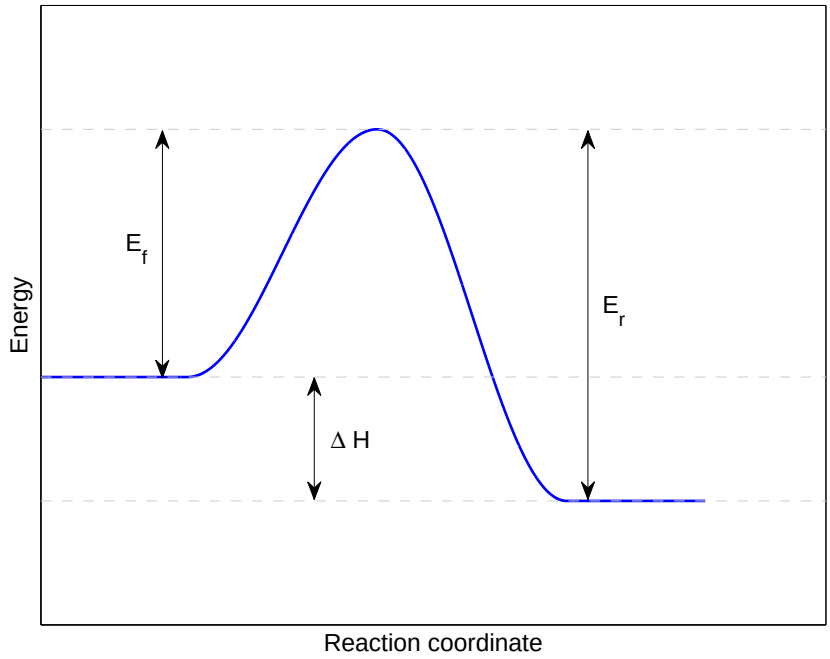


Figure 7.1: Schematic of a typical exothermic chemical reaction. The reactant state is represented by the initial portion of the curve and the product state by the final portion. The reaction coordinate approximately represents how far through the microscopic reaction process the reaction has proceeded.

between reactants and products manifests as a release or uptake of heat from the local environment of the reaction. How could all these chemical details be taken into account in the RLBM? This will be revealed in the next section.

## 7.1 Theoretical Considerations

Here the RLBM will be generalised to model systems with flows of the solvent fluid (in which the chemical species are dissolved). Another aim is to include the effects of chemical reactions on the temperature field and vice versa. It will thus be a Reactive Thermal Lattice Boltmann Model (RTLBM). To achieve these goals, the model must include the following elements: the fluid distribution functions $f_i$ using Equation 3.18, the internal energy distribution functions $g_i$ using Equation 3.13 with some extra terms taking account of enthalpy changes, and the distribution functions for an arbitrary number of passive scalars $h_i^\sigma$ (the exact form of the collision operation for these distributions will depend on the reaction scheme adopted). The equilibria for the fluid mass and internal

energy distributions will be of the same form that was used before: Equation 2.10 and Equation 3.14 respectively.

Analogous to the internal energy, the equilibria for the solute chemical species will be of the following form:

$$\begin{aligned} h_{i=0}^{eq,\sigma} &= -\frac{2}{3}\rho\psi_\sigma\frac{\mathbf{u}^2}{c^2} \\ h_{i=1,2,3,4}^{eq,\sigma} &= \frac{1}{9}\rho\psi_\sigma\left[\frac{3}{2}+\frac{3}{2}\frac{\mathbf{e}_i\cdot\mathbf{u}}{c^2}+\frac{9}{2}\frac{(\mathbf{e}_i\cdot\mathbf{u})^2}{c^4}-\frac{3}{2}\frac{\mathbf{u}^2}{c^2}\right] \\ h_{i=5,6,7,8}^{eq,\sigma} &= \frac{1}{36}\rho\psi_\sigma\left[3+6\frac{\mathbf{e}_i\cdot\mathbf{u}}{c^2}+\frac{9}{2}\frac{(\mathbf{e}_i\cdot\mathbf{u})^2}{c^4}-\frac{3}{2}\frac{\mathbf{u}^2}{c^2}\right] \end{aligned} \tag{7.1}$$

In order to specify the additional collision terms for the internal energy and chemical species distributions, it is convenient to focus on a specific case, the irreversible 4-component reaction: $aA + bB \rightarrow cC + dD$. Invoking the law of mass-action once more, the following expressions for the RTLBM collision step can be constructed:

$$h_i^A\left(\mathbf{x}+\mathbf{e}_i\Delta t, t+\Delta t\right) - h_i^A(\mathbf{x},t) = -\frac{1}{\tau_A}(h_i^A - h_i^{eq,A}) - \omega_i a m_A k(\mathbf{x},t)\psi_A^a\psi_B^b \tag{7.2}$$

$$h_i^B\left(\mathbf{x}+\mathbf{e}_i\Delta t, t+\Delta t\right) - h_i^B(\mathbf{x},t) = -\frac{1}{\tau_B}(h_i^B - h_i^{eq,B}) - \omega_i b m_B k(\mathbf{x},t)\psi_A^a\psi_B^b \tag{7.3}$$

$$h_i^C\left(\mathbf{x}+\mathbf{e}_i\Delta t, t+\Delta t\right) - h_i^C(\mathbf{x},t) = -\frac{1}{\tau_C}(h_i^C - h_i^{eq,C}) + \omega_i c m_C k(\mathbf{x},t)\psi_A^a\psi_B^b \tag{7.4}$$

$$h_i^D\left(\mathbf{x}+\mathbf{e}_i\Delta t, t+\Delta t\right) - h_i^D(\mathbf{x},t) = -\frac{1}{\tau_D}(h_i^D - h_i^{eq,D}) + \omega_i d m_D k(\mathbf{x},t)\psi_A^a\psi_B^b \tag{7.5}$$

where the $\omega_i$'s are the velocity distribution weights and $m_\sigma$ is the molar mass of species $\sigma$. Also note that a unit integration step $\delta t = 1$ has been assumed (a factor of $\delta t$ is required in the final terms of the above equations to maintain the correct units).

Since temperature must now be taken into account, the rate constant $k$ now takes on a more complicated, but physically representative form, known as the Arrhenius equation:

$$k(\mathbf{x},t) = Ae^{-E_f/T(\mathbf{x},t)} \tag{7.6}$$

where $A$ is known as the frequency factor, encompassing several effects related to the speed of the reaction such as the cross-sectional areas of the reactant molecules. Use of the Arrhenius equation reflects the fact that as the temperature increases, all physical processes start to become equally likely, since thermal energy is less of a limiting factor.

The rate law also now incorporates the kinetic barrier that a reaction must surpass in order to proceed fully: the activation energy $E_f$.

An additional term must also be included in the collision step for the internal energy distributions to represent heat release due to enthalpy changes. For the 4-component reaction above, the following expression applies:

$$g_i\left(\mathbf{x}+\mathbf{e}_i\Delta t, t+\Delta t\right) - g_i(\mathbf{x},t) = -\frac{1}{\tau_c}(g_i - g_i^{eq}) - \omega_i k(\mathbf{x},t)\psi_A^a\psi_B^b\Delta H, \qquad (7.7)$$

where $-\Delta H$ is the heat released per unit reaction rate (the presence of the minus sign is simply for the sake of convention, wherein an exothermic reaction leads to a lower energy state and $\Delta H < 0$). For multiple reactions additional $\Delta H$ terms would be required for each reaction.

With this simple scheme it is possible to implement a good approximation to a real chemical reaction system. It is possible that a Chapman-Enskog expansion might reveal that at the macroscopic level, the above system does not exactly reproduce the reaction-diffusion-convection equations since the reactions occur under an assumption of local well-mixed reactors. At each grid point it is assumed that the chemistry is effectively isolated from the perturbations due to net fluid flow and that the different species are well-mixed at the scale of the grid node. In reality reactions might proceed more slowly than this since the distribution functions streaming into each node do not equilibrate with each other completely during one integration step. But if the effect was simply a change in reaction rate then it would make no phenomenological difference because the error could be corrected simply with a linear adjustment of the rate law (by adjusting the magnitude of the frequency factor $A$).

Besides, highly turbulent flows will not be simulated, the Mach number will always be kept low. And the objective here is not quantitatively accurate, predictive solutions to specific differential equations. The interest lies in more basic phenomenological questions about the pattern-forming and transport properties of complex reacting fluids. Upon discovering an interesting new class of behaviour requiring intense further study, the method could be refined to be more physically rigorous.

Another assumption built into the above RTLBM is that there is no cross-diffusion between passive scalar species, i.e., their diffusion is independent of all the other species

and the internal energy. This is justified by the simple fact that they are assumed to be in dilute solution and thus the effect of cross-diffusion from other species will be negligible compared to self-diffusion and advection.

The scheme described above represents a complete RTLBM toolkit, able to simulate an immense variety of complex flow phenomena. It should not be understated the potential of this model (within the limits of its basic assumptions). It is now possible to simulate a huge range of reaction schemes and observe the basic interactions between the reactions, the temperature field, the resulting buoyancy induced flows and the various feedbacks between these different phenomena. Unfortunately there is no possibility to fully explore the space of behaviours and parameters now available. A rigorous exploration of the model would take a daunting amount of time, and it will only be possible to scratch the surface in this thesis.

Nevertheless, it is now feasible to begin to uncover some of the basic phenomena of this new model. The first scheme will be the simple decay reaction $A \rightarrow B$ that was assessed previously. The complexity of the model systems will increase gradually. In the following section the static fluid assumption will still be adopted. The focus will instead be on the interplay between the mass diffusion, reactions, and the production, depletion and diffusion of heat. Section section 7.3 will move on to systems involving fluid flow.

## 7.2 Two-Species Diffusive

### 7.2.1 Linear Closed System

For the two-component, single-stage reaction system, the collision operation becomes:

$$\begin{aligned} h_i^A\left(\mathbf{x}+\mathbf{e}_i\Delta t, t+\Delta t\right) - h_i^A(\mathbf{x},t) &= -\frac{1}{\tau_A}(h_i^A - h_i^{eq,A}) \\ -\omega_i\psi_A A_f e^{-E_f/T(\mathbf{x},t)} &+ \omega_i\psi_b A_r e^{-E_r/T(\mathbf{x},t)} \end{aligned} \tag{7.8}$$

$$\begin{aligned} h_i^B\left(\mathbf{x}+\mathbf{e}_i\Delta t, t+\Delta t\right) - h_i^B(\mathbf{x},t) &= -\frac{1}{\tau_B}(h_i^B - h_i^{eq,B}) \\ +\omega_i\psi_A A_f e^{-E_f/T(\mathbf{x},t)} &- \omega_i\psi_b A_r e^{-E_r/T(\mathbf{x},t)} \end{aligned} \tag{7.9}$$

where unit masses have been assumed for the chemical species and the enthalpy change is defined as the energy difference between the product and reactant states $\Delta H =$

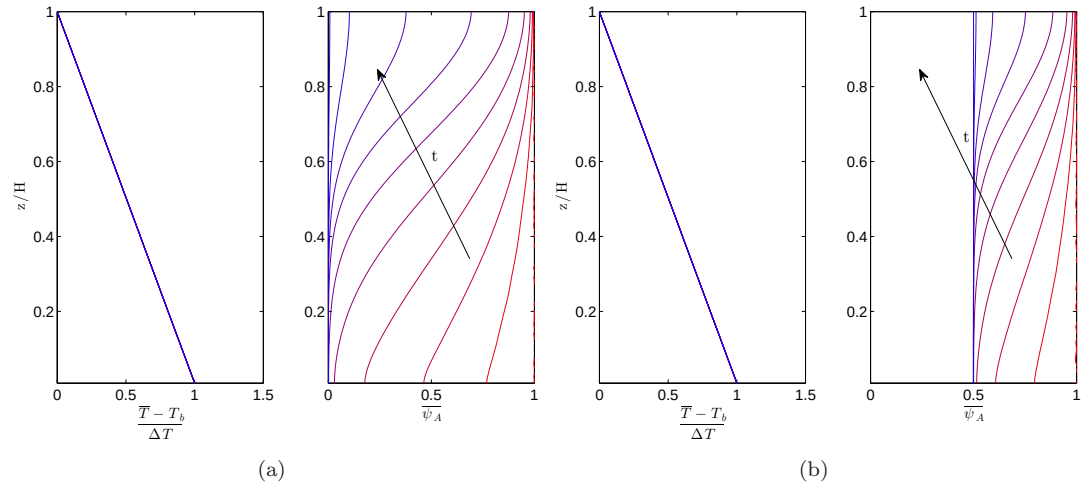


Figure 7.2: Temperature and concentration profiles for TRD systems. Simulations were initiated with $\psi_A = 1$ and $\psi_B = 0$, and $T(x,z) = T_b + \Delta T(H-z)/H$, with a small degree of noise. The parameters were varied as follows: a) $A_f = 1, A_r = 0, \Delta H = 0$, b) $A_f = 1, A_r = 1, \Delta H = 0$. Profiles are plotted for several different times through the simulation. The time intervals are logarithmically spaced due to the exponential decay inherent to these systems. Red indicates early times in the simulation, turning to blue as the simulation progresses.

$E_f - E_r$. Note that here the reaction has been allowed to be reversible by introducing the appropriate term in the equations. This means that the system no longer simply marches inexorably towards a state of pure $B$, but has the possibility to be cyclic in some sense. It is possible to control the following kinetic parameters: the two activation energies $E_f, E_r$ and the two frequency factors $A_f, A_r$. The forward frequency factor is set to $A_f = 1$ for simplicity, and $A_r \in \{0, 1\}$ is used as a reversibility switch. The activation energies will be varied.

Due to the form of the rate term, when $E_f/T(\mathbf{x},t) \gg 1$, the forward reaction will proceed very slowly and as $E_f/T(\mathbf{x},t) \to 0$, the reaction rate becomes no longer limited by local temperature. The system will be initialised with $\psi_A = 1$ across the whole domain with a small degree of noise. There will be none of species $B$ present and the temperature will vary linearly from $T_a = 2$ at the bottom of the domain to $T_b = 1$ at the top. The boundary temperatures will be maintained at these values but the temperature is free to vary internally.

For the first two experiments, $E_f = E_r = 10$, and both an irreversible and reversible version were simulated. The results are shown in Figure 7.2. In the simplest version

with an irreversible reaction, the concentration of $A$ diminishes across the whole domain. The rate of this depletion is highest at the bottom of the domain where the temperature is highest and lowest at the top, where the temperature is also lowest. One would expect nothing else from such a system: an exponential decay of reactant, modulated by the local temperature.

In the second experiment, the reaction is made reversible. A similar decay process occurs but after the initial transient, a state of dynamic equilibrium is reached, wherein the conversion of $A$ to $B$ is matched by the reverse process. The steady state concentration of the two species represents an equal division of the initial mass between the two species. Again, this matches the natural intuition for how such a system should behave. Since the two activation energies $E_f$ and $E_r$ are equal, temperature should not provide any bias for the steady state concentration profile, hence why it is a perfectly straight vertical line at $\overline{\psi_A} = \overline{\psi_B} = 0.5$.

Now more complicated scenarios in which the reactions alter the local internal energy balance will be considered. All four combinations of irreversible and reversible, exo- and endothermic were explored. The results are shown in Figure 7.3.

With the exothermic reaction in Figure 7.3(a), the same decay process observed before occurs, but with some subtle differences. The reaction proceeds fastest near the warmer end of the domain as before, but the temperature profile is significantly affected by the reaction. Since it releases heat, there is an initial rise in the temperature, particularly at the bottom of the system. Such a temperature increase has the effect of enhancing the reaction rate and the decay proceeds even faster, leading to the noticeable kink in the concentration profiles in the lower section. The reason there is a kink and not simply a straight line is that the temperature, while being raised by the reaction locally, was held constant at the boundary. So immediately above the boundary there was a small restriction in the reaction rate increase.

During the initial transient phase there is a small period of positive feedback in the lower part of the domain but this soon fades as the concentration $\psi_A \to 0$. The temperature profiles show that there was a large amount of heat released in the lower region during the positive feedback period. However, the rate of heat release declined as $\psi_A$ and the reaction rate also declined and with time, the temperature profile returned to a straight line between the fixed boundary temperatures.

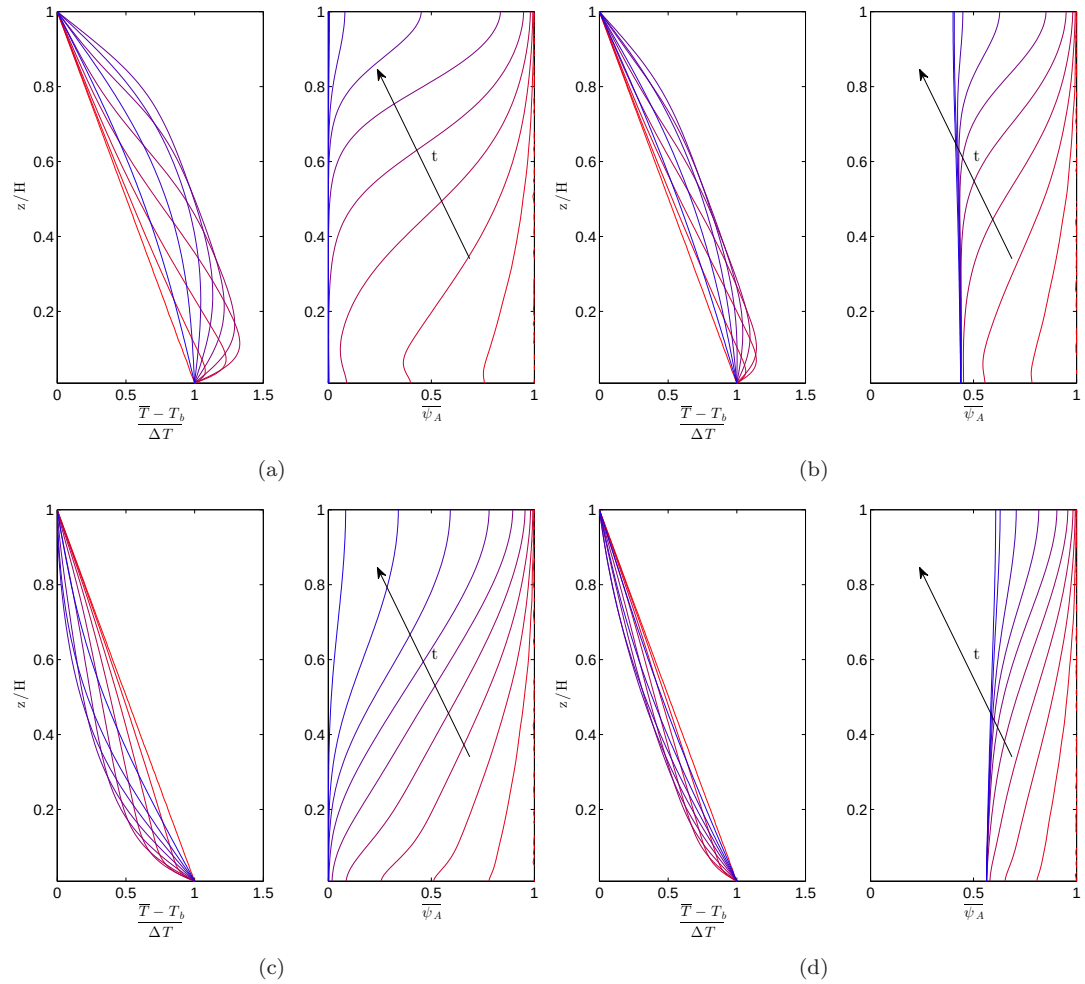


Figure 7.3: Temperature and concentration profiles for TRD simulations with varying kinetic parameters. Simulations were initiated with $\psi_A = 1$ and $\psi_B = 0$, and $T(x,z) = T_b + \Delta T(H-z)/H$, with a small degree of noise. The parameters were varied as follows: a) $A_f = 1, A_r = 0, \Delta H = -0.5$, b) $A_f = 1, A_r = 1, \Delta H = -0.5$, c) $A_f = 1, A_r = 0, \Delta H = 0.5$, d) $A_f = 1, A_r = 1, \Delta H = 0.5$. Profiles are plotted for several different times through the simulation. The time intervals are logarithmically spaced due to the exponential decay inherent to these systems. Red indicates early times in the simulation, turning to blue as the simulation progresses.

In the reversible version of this system (Figure 7.3(b)), similar phenomena occur, but there appears to be a significant amount of damping, and the steady state is different. The damping is caused by the reverse reaction effectively cancelling the action of the forward reaction. This applies also to the heat produced by the forward reaction. A fraction of that released heat is absorbed by the endothermic reverse reaction. So compared to the irreversible version, there is decreased heat release and a lower rate of $A \rightarrow B$ conversion. The steady state is an approximately equal split of mass between

the two species. There is slightly less of species $A$ present in the steady state because of the difference in activation energy between the forward and reverse reactions. Because the forward reaction has a lower activation energy, when the forward and reverse rates equalise, they do so with a slight bias towards a lower mass of $A$. There is also a small temperature dependence of this effect, with the steady state concentration of $A$ being slightly lower at the lower temperature of the top of the domain.

Turning to the endothermic, irreversible system in Figure 7.3(c), it is clear that the reaction is self-inhibiting and it proceeds fastest near the lower boundary where the temperature is held constant. Above this position, the reaction rate is reduced by its own heat uptake causing local cooling. The reaction proceeds slowly at the upper end of the domain due to the lower boundary temperature, so the rate of heat depletion is also lower but it still has an effect. Eventually all of the $A$ species decays.

Finally in Figure 7.3(d), with the addition of the reversible reaction, there is again significant damping of the dynamics compared to the irreversible case. The reverse reaction is now exothermic and has a cancelling effect upon the heat uptake of the forward reaction. In contrast with the exothermic version (Figure 7.3(b)), the steady state concentration of $A$ is now slightly higher than $\psi_A = 0.5$. The small bias towards higher concentrations of $A$ is caused by the slightly lower energy barrier of the reverse reaction. This can be seen by making use of the steady state condition (forward and reverse rates equal):

$$\begin{aligned} A_f e^{E_f/T}[A] &= A_r e^{E_r/T}[B] \\ \frac{[A]}{[B]} &= \frac{e^{E_r/T}}{e^{E_f/T}} \\ &= e^{(E_r - E_f)/T} \end{aligned} \tag{7.10}$$

Hence as the difference in activation energies diminishes to 0, the concentration ratio of the two species tends to 1.

This concludes the analysis of static, linear, 2-component, TRD systems. It has been shown that the addition of enthalpy changes in a system of variable temperature can induce different feedbacks. Exothermic reactions feed back positively on themselves, since they enhance their own reaction rate by raising the local temperature. Endothermic reactions have a retarding effect on themselves, and rely on external heat input to

compensate for localised cooling effects. The introduction of reversibility permits states of dynamical equilibrium wherein reaction rates are finite, but there are no net changes in concentration with time.

### 7.2.2 Non-linear Open System

This section will deal with a system with slightly richer dynamics, due mainly to its non-linear reaction term. It will take the classic Gray-Scott (GS) RD system (simulated in subsection 6.2.2), and relax the isothermal assumption. In the standard version of the model, the reaction rate depends only upon the concentrations of the two chemical species (see Equation 6.19). Now, rate constants of the Arrhenius type will be added, introducing a dependence upon activation energy and local temperature. This leads to the following form for the chemical species collision and streaming operation:

$$\begin{aligned} h_i^A\left(\mathbf{x}+\mathbf{e}_i\Delta t, t+\Delta t\right) - h_i^A(\mathbf{x},t) &= -\frac{1}{\tau_A}(h_i^A - h_i^{eq,A}) \\ &\quad -\omega_i\psi_A\psi_B^2 A_f e^{-E_f/T(\mathbf{x},t)} + F(1-\psi_A) \qquad (7.11) \\ h_i^B\left(\mathbf{x}+\mathbf{e}_i\Delta t, t+\Delta t\right) - h_i^B(\mathbf{x},t) &= -\frac{1}{\tau_B}(h_i^B - h_i^{eq,B}) \\ &\quad +\omega_i\psi_A\psi_B^2 A_f e^{-E_f/T(\mathbf{x},t)} - (F+R)\psi_B. \qquad (7.12) \end{aligned}$$

There are two free parameters: the activation energy $E_f$ and the frequency factor $A_f$. Vast regions of the available parameter space will produce trivial steady state behaviour such as the system being fully saturated with one of the two species or the reaction not occurring due to the temperature being too low for example. It also goes without saying that an exhaustive exploration of the parameter space of this new model would be a significant task. Therefore the parameters will be chosen such that much of the well-known dynamics of the model are retained, but the influence of thermal effects can be easily observed.

To that end, the frequency factor was calculated thus: $A_f = e^{E_f/T_0}$, where $T_0$ is the mean temperature of the simulation. This ensures that for the forward reaction, when $T = T_0$, the system reverts to its standard behaviour. But at temperatures either side of this, a thermal enhancement or modulation of the reaction rate can be observed. With fixed temperatures at the boundaries of the domain, the activation energy $E_f$ can be used to directly control the thermal influence upon the reaction dynamics. This

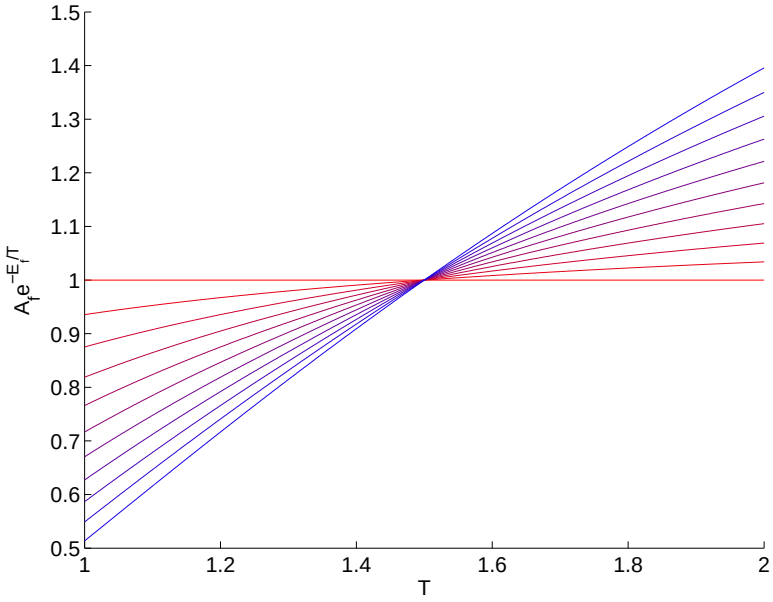


Figure 7.4: Changes in reaction rate as a function of temperature for different activation energies $E_f$. The frequency factor is calculated using $A_f = e^{E_f/T_0}$ where $T_0 = 1.5$ is the mean temperature. The range of activation energies plotted extends from $E_f = 0$ in red to $E_f = 2$ in blue.

is illustrated in Figure 7.4, which shows how the reaction rate constant changes with temperature and activation energy, with the form for $A_f$ given above.

For the supply and depletion parameters it was decided to focus on a single pair of values, $F = 0.03, R = 0.061$ since this causes the emergence of replicating spots, arguably the most life-like phenomenon exhibited by GS RD systems.

The simulation results produced by this system can now be evaluated. An activation energy of $E_f = 1.7$ was used (since this exerted a sufficiently strong thermal effect on the reaction rate), and boundary temperatures were fixed at $T_a = 1$ and $T_b = 2$. Initial conditions were identical to those used for isothermal RD systems in subsection 6.2.2. As an initial assessment, the reaction was prevented from releasing or absorbing heat, $\Delta H = 0$. The system formed several different types of structure, since the reaction rate was augmented in the lower region of the domain and reduced in the upper region due to the temperature profile. The system's behaviour is displayed in Figure 7.5.

Enhancing the reaction rate of a GS RD system has a similar effect to reducing both the diffusion rate and supply and depletion rates, effectively altering the position of the system on the phase portrait (Figure 6.2). This is why it is possible to see progressively,

spot patterns, worm-like structures, inverted spots and then a pure phase as one traces down through the domain in Figure 7.5. The effect is similar to moving along a line (in a west-southwesterly direction) through the phase portrait of the isothermal RD system. Near the lower boundary, the reaction proceeds so fast that stable structures cannot form.

Spots exist because of a stable balance between reaction, diffusion and addition and removal of particles. In the interior of a spot, the reaction is fast enough that the concentration of species $A$ is kept low, and $B$ high. Outside of a spot, the concentration of $B$ is lower and so the reaction is slow, slower than the rate at which $A$ is supplied and $B$ removed, causing the concentration of $A$ to remain high there. Moving from the outside of the spot to the inside there is a gradual change of conditions from one to the other and in the boundary layer between, species $A$ is diffusing inwardly and species $B$ outwardly. The rate of inward diffusion of $A$ (plus the external supply) is matched by the rate at which it is converted to $B$ inside the spot due to the reaction. And the production of $B$ within the spot is balanced by the removal of $B$ (due to external extraction) and outward diffusion away from the spot's vicinity where the reaction is proceeding at a lower rate. Under conditions of a higher reaction rate (due to higher temperatures), it becomes impossible for any region to have a high concentration of $A$ because the reaction consumes it immediately.

It has been shown that with variable temperature and a thermal rate term, variation in emergent structure within a system can be observed even when the supply and depletion parameters are kept constant (as a function of position). The focus will now move on to systems where the reaction itself influences the local temperature by releasing or absorbing heat, starting with an exothermic reaction, shown in Figure 7.6.

The emergence of multiple patterns can once again be seen but the heat released from the reaction soon begins to alter the temperature field. The heating effect enhances the reaction rate, destroying nearby structures, and a relatively thin interface front forms between the upper region of almost pure $A$ and the lower region of almost pure $B$. This front propagates upwards as the continued heating distorts the temperature profile. The reaction front only stalls near the upper boundary due to the temperature being held constant there. In the interior the temperature continues to rise without limit because the enhanced reaction rate causes further heating, enhancing the reaction

rate further, releasing more heat. In summary, making the reaction exothermic causes a strong positive feedback effect, that runs away with time. Attention can now turn to an endothermic reaction system, shown in Figure 7.7.

In contrast to the previous system, the absorption of heat by the reaction pushes the 'viable zone' for structure formation downwards, where the constant temperature boundary will supply as much heat as is needed to maintain that temperature. Eventually a steady state is reached in which reactive heat depletion is compensated for by heat supply from the boundary. In such a scenario there is still scope for the stable existence of a range of structures.

The differences between the exothermic and endothermic systems are stark. In the former, the effect of the reaction is to enhance the conditions for the reaction and in the latter, it worsens the conditions. A natural question is then: is there any similarity between these chemical systems and ecological systems? An organism's survival depends critically on the effect it has on its environment. Any organism has to consume some source of free energy, i.e., taking in low entropy energy and expelling that energy in a less useful, higher entropy form.

For modern organisms this energy comes in a variety of forms from solar radiation for phototrophs, to chemical potential gradients for chemoautotrophs (postulated to be the first organisms to emerge on Earth), and chemical potential gradients due to other organisms for heterotrophs (such as ourselves). The fate of the higher entropy waste products is crucial. Organisms can easily poison themselves if there is not some recycling mechanism available to remove those waste products or turn them back into something useful. Following the evolution of oxygenic photosynthesis, the Great Oxidation caused toxic poisoning for huge numbers of organisms including possibly those organisms producing the oxygen.

Fortunately for us this paved the way for the evolution of aerobic respiration, but for a certain period those early photosynthesisers were probably killing themselves. Life frequently solves this kind of problem through symbiosis. In the contemporary world ecosystems are a dense network of exchanges where the waste of one organism can represent the staple diet for another. Planet-wide cycles of material have emerged including the carbon, water and nitrogen cycles. In the absence of life these cycles would turn at a drastically reduced rate and the Earth would be a very different place.

Might it be possible to observe the emergence of any such similar symbiosis in an abstract model like the ones we've looked at in previous sections? What about dissipative structures that can proliferate into regions where they cannot form spontaneously, so-called precarious structures? It will be seen in the following sections that such phenomena can readily be observed in simple physico-chemical models.

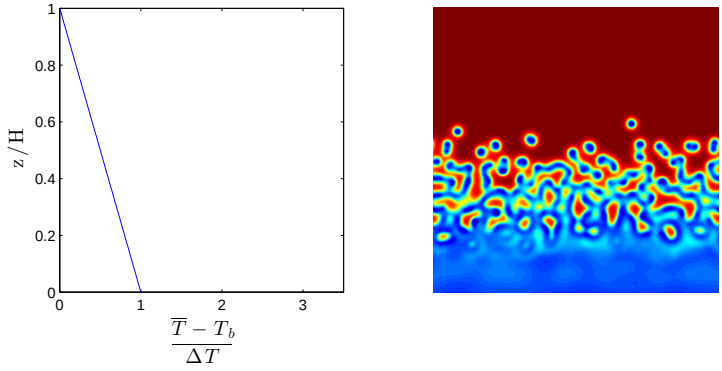


(a) $t = 750$

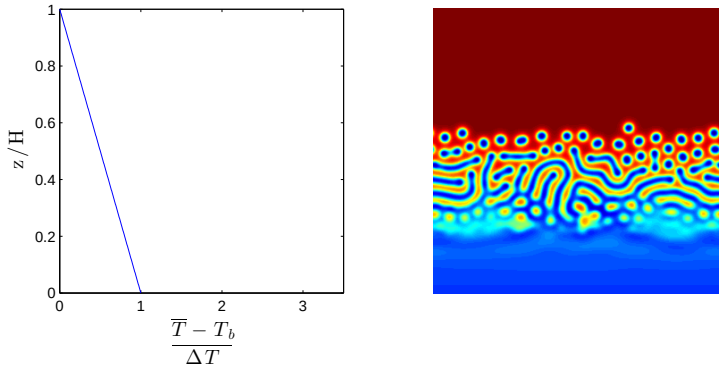


(b) $t = 2750$

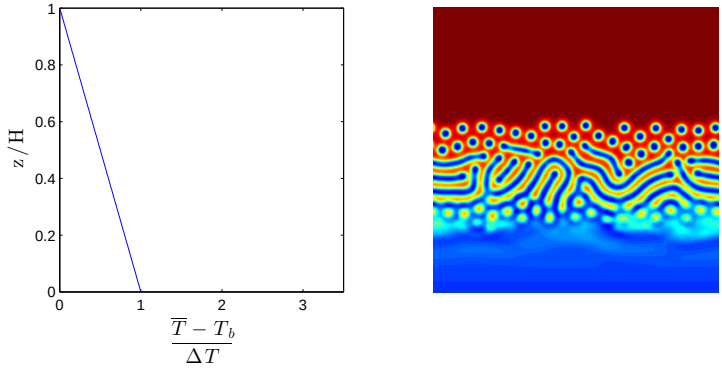


(c) $t = 9000$

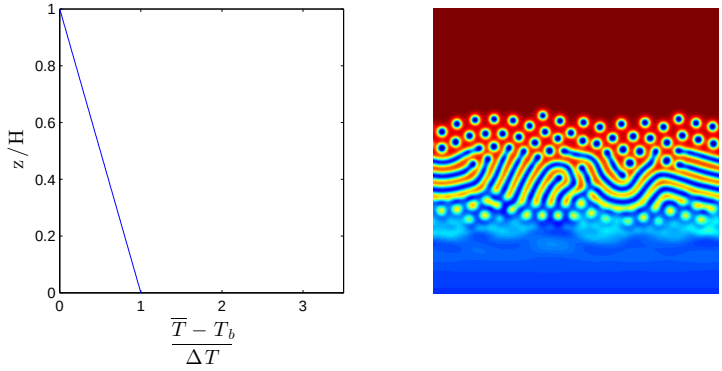


(d) $t = 30000$

Figure 7.5: Temperature profiles and chemical order parameter ($\psi_A - \psi_B$) fields for a thermal GS RD simulation at several different times through the simulation. There is no enthalpy change $\Delta H = 0$, and the time intervals are logarithmically spaced.

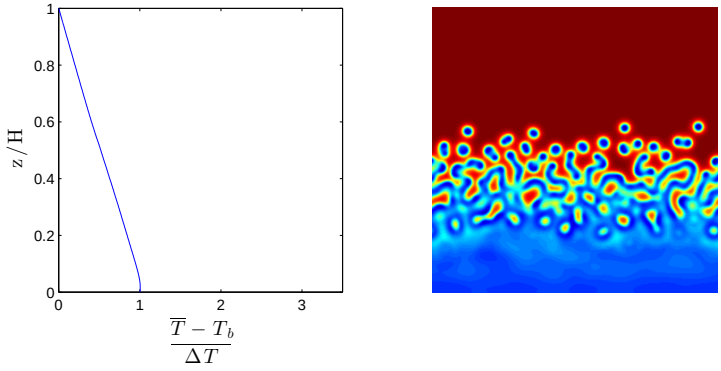


(a) $t = 750$

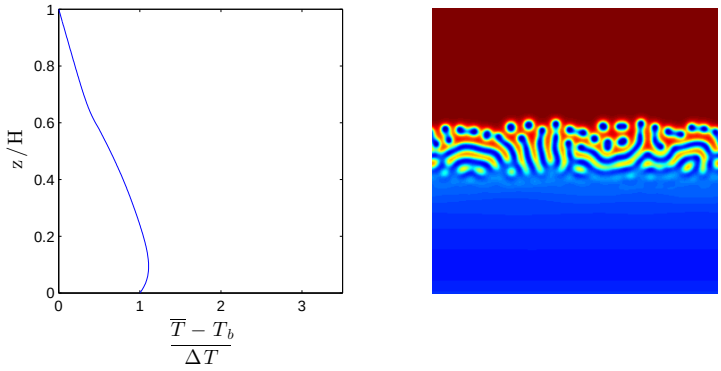


(b) $t = 2750$

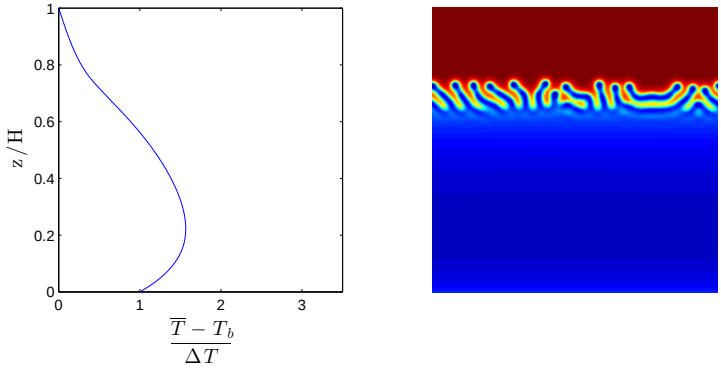


(c) $t = 9000$

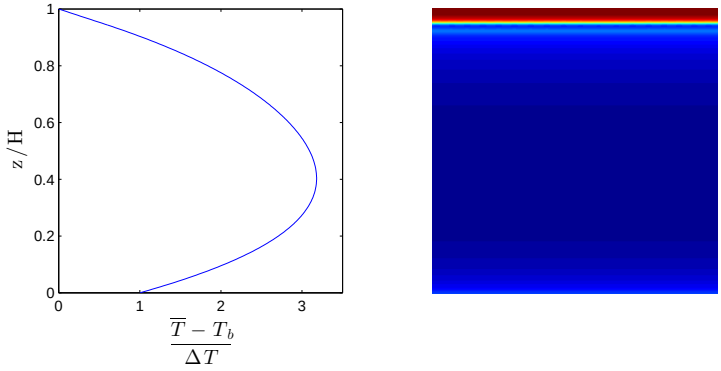


(d) $t = 30000$

Figure 7.6: Temperature profiles and chemical order parameter $(\psi_A - \psi_B)$ fields for an exothermic GS RD simulation at several different times through the simulation. The enthalpy of reaction is $\Delta H = -5 \times 10^{-3}$. The time intervals are logarithmically spaced. See an animation of this simulation in additional digital material.

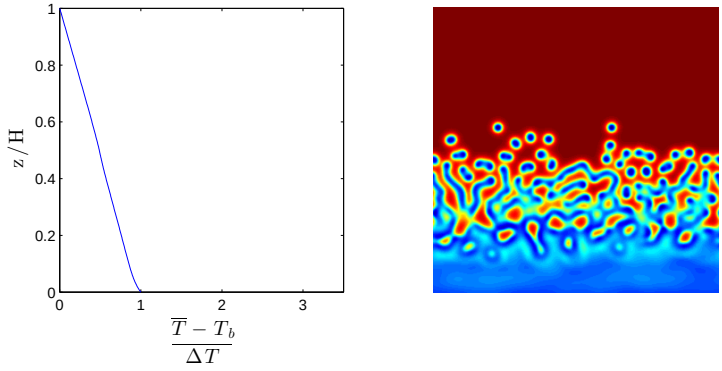


(a) $t = 750$

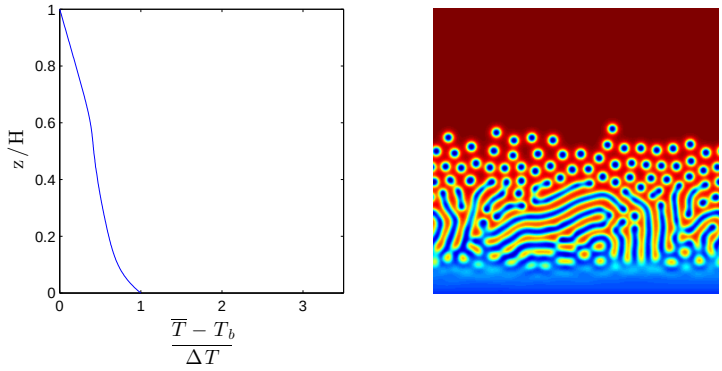


(b) $t = 2750$

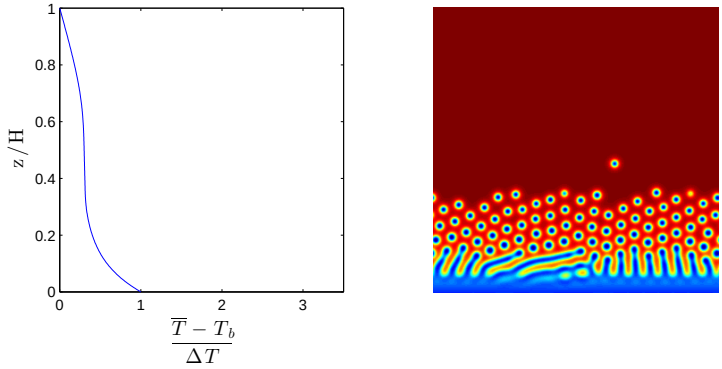


(c) $t = 9000$

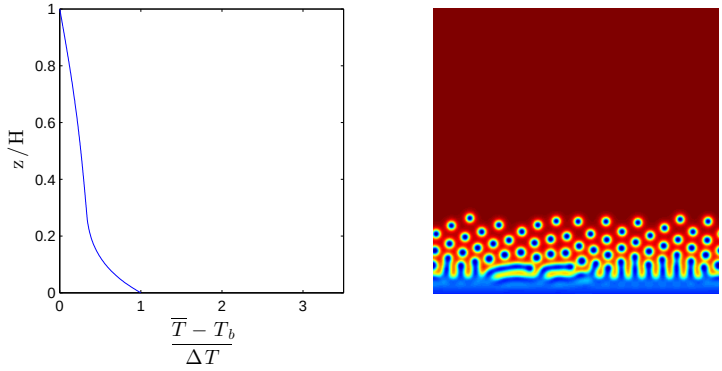


(d) $t = 30000$

Figure 7.7: Temperature profiles and chemical order parameter ($\psi_A - \psi_B$) fields for an endothermic GS RD simulation at several different times through the simulation. The enthalpy of reaction is $\Delta H = 5 \times 10^{-3}$. The time intervals are logarithmically spaced. See an animation of this simulation in additional digital material.

## 7.3 Two-Species Convective

In this section things will begin to get moving and the simulations will progress from still fluids to convective motion. A reasonable amount of work has been carried out on the simulation of reacting fluids, but primarily on very specific applications, usually with the goal of providing a predictive capacity for the design of functional mechanical devices (Chen et al., 2008). Some work has also been done on adding flow to simple RD schemes, but as far as I'm aware, they always involved forcing a prescribed flow upon a reaction scheme.

To allow fluid flows, the RTLBM will consist of: the mass density distributions that will undergo the standard collision operation as before (Equation 3.18), the internal energy distributions that will also undergo the standard collision operation of the form of Equation 7.7 and the chemical species distributions that will have equilibria of the form of Equation 7.1, and collision operations of the form of Equation 7.2.

### 7.3.1 Linear Closed System

Before hunting for the emergence of ecological phenomena, there is a simple question to be answered: what is the net effect of the presence of chemical species and the reversible reaction $A \rightleftharpoons B$ on the thermal transport properties of a fluid system? If they were non-reactive passive scalars or if the reaction was thermally neutral, the buoyancy driven convection seen in previous chapters would be unaffected by their presence. However when these assumptions are relaxed, and the processes of chemically-induced heat absorption/production and transport by advection are included, how does the system make use of these extra degrees of freedom? For cases of fixed temperature boundary conditions (BCs), is the heat flux enhanced? For fixed flux BCs, how is the steady state temperature difference affected?

In order to shed light on these questions, a series of experiments were conducted on systems of a single size, with two different sets of fluid parameters. In the first case, a fluid was used that would normally exhibit a Rayleigh number of $Ra = 5 \times 10^3$, and in the second case $Ra = 5 \times 10^4$. Experiments were performed with fixed temperature BCs and fixed flux BCs. The total mass of dissolved chemical species was varied. It was increased incrementally from 0 to a value that gave mean concentrations of $\overline{\psi_A} = \overline{\psi_B} = 4$. Each

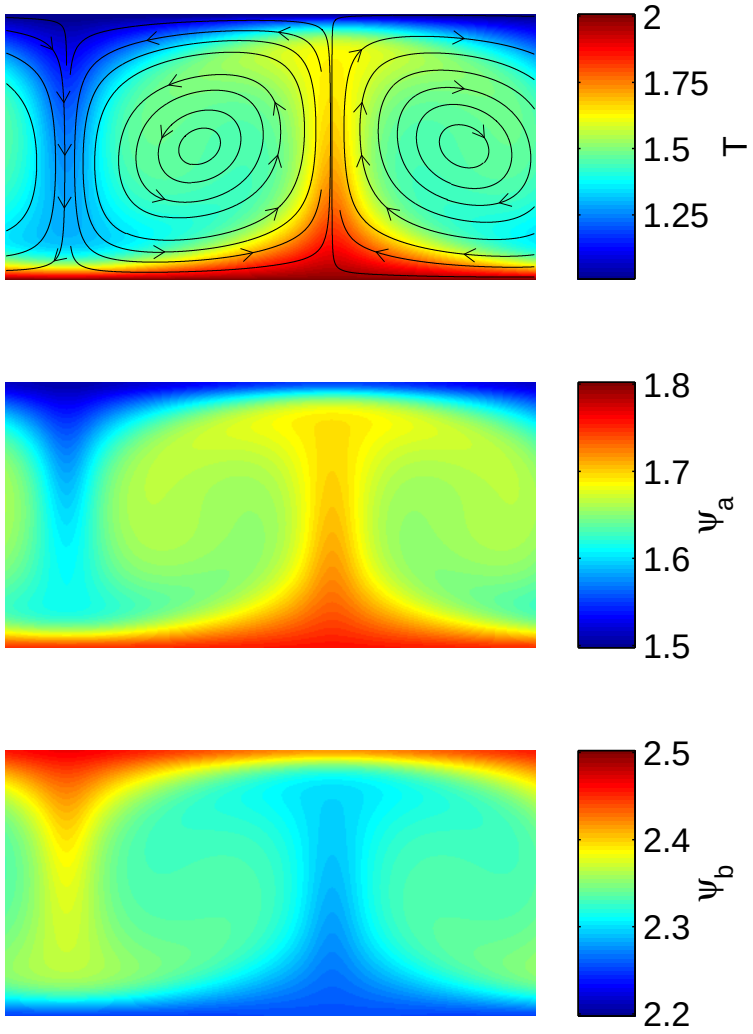


Figure 7.8: Steady state of a RTLBM simulation in which a passive scalar species $A$ can undergo a reversible decay reaction $A \rightleftharpoons B$ to a lower energy product $B$. The top image shows the temperature field with fluid velocity streamlines, the middle image the concentration field for the first component $\psi_A$, and in the lower image the concentration field for the second component $\psi_B$. The simulation was initialised with $\overline{\psi_{A0}} = \overline{\psi_{B0}} = 2$.

experiment was initiated with random homogeneous conditions and run until a steady state was reached.

Figure 7.8 shows the steady state configuration of a simulation with $Ra = 5 \times 10^4$ and $\overline{\psi_{A0}} = \overline{\psi_{B0}} = 2$. The system has arranged itself such that the endothermic reaction $B \rightarrow A$ dominates at the lower, hotter end of the domain, leading to a higher $\psi_A$ in that region. Conversely, the forward reaction dominates at the cooler end, giving rise to higher concentrations of $B$ near the upper boundary. This arrangement seems to be the one which would maximise the heat flux through the system. Having the endothermic

reaction dominate at the lower boundary means that the system invests heat energy in converting $B$ to $A$, this energy is carried by $A$ as it is advected by the flow before being released gradually as the reaction turns to $A \rightarrow B$ at the top boundary. Thus the system is using the two chemical species as an additional heat delivery mechanism alongside the advection and diffusion of heat itself.

It is useful to look quantitatively at this enhancement of heat transport. Figure 7.9 shows the different components of heat flux as a function of average chemical species concentration. The heat flux values are normalised by the total heat flux, so the figure displays the fractional contributions to the three different types of heat flux: diffusion, convection and advection by chemical species (and reactive heat release and absorption). For both types of BC, identical trends are exhibited. As the concentration of chemical species increases, the role played by them in heat transport increases, and the role of the other heat transport mechanisms diminishes. So the system is gradually switching over to a configuration wherein advection and reaction provides a more and more significant role in terms of heat transport. This makes intuitive sense because a higher concentration of chemical species means that the heat exchange as a result of reactions will increase, and the amount of heat that can be invested in the enthalpy of chemical species also increases.

This raises an interesting issue however: what is the limit of this trend? If the passive scalar concentration was increased further would the system continue to reduce the relative roles of convection and diffusion? Firstly there should be a lower limit for the diffusive heat transport (indeed in the fixed temperature case it is constant since the temperature difference and thermal diffusivity are constant), since all heat must enter and leave the system by diffusion. Secondly, the advection of chemical species relies on there being a sustained fluid flow. The fluid flow is induced by the temperature gradient and so in the fixed flux case as the system becomes 'more efficient' at transporting heat, it gradually diminishes the driving force for that transport.

What of the fixed temperature case? Here the temperature difference can never be diminished but if the reaction depletes significant amounts of heat from the hot boundary and releases large amounts at the cold boundary then this begins to reduce the driving force for convective motion. Having said that, a finding not shown in Figure 7.9 is that for this BC, the total heat flux increased with $\overline{\psi}$. While the presence of the passive scalars

enhanced the system's heat transport abilities, it used those new abilities to augment its total heat flux above that which would occur without the action of the chemistry. So it may be that if the reaction system erodes the overall temperature gradient within the system, the system compensates by simply extracting more heat at the boundaries (that are perfectly conducting and so can deliver arbitrary amounts of heat).

In conclusion, the system appears to have made use of its additional degrees of freedom to increase its heat transport abilities. There were higher fluxes for fixed temperature systems and lower temperature differences for fixed flux systems. This all implies that the system can transport heat more easily with the addition of the chemical species and reactions. This is not altogether surprising, but it does not support any kind of maximum entropy production (MEP) hypothesis because the entropy production of the fixed flux system decreases with increased heat transport efficiency. This effect is similar to that which was discussed in chapter 4, where it was noted that when the boundary flux is fixed and the system's convective resistance is decreased, a reduction of temperature difference occurs (except under certain, contrived changes in parameters).

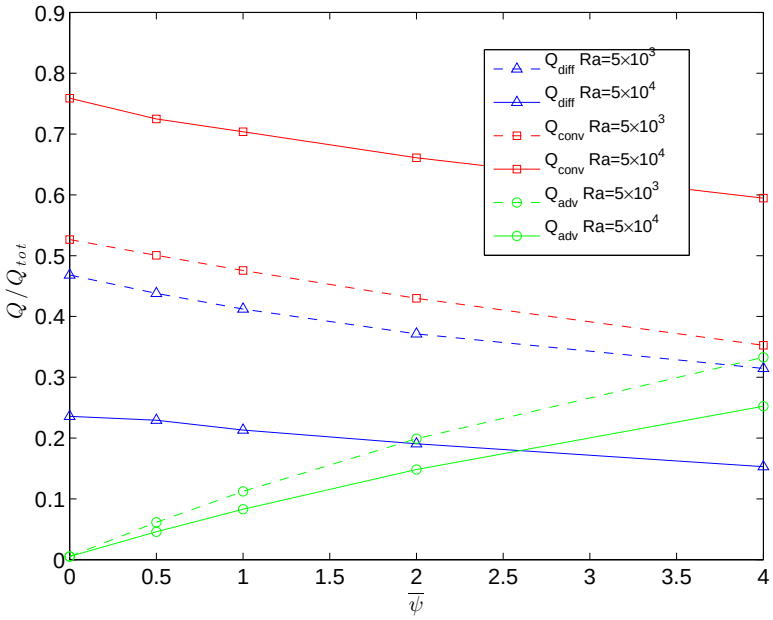


(a) Fixed Temperature

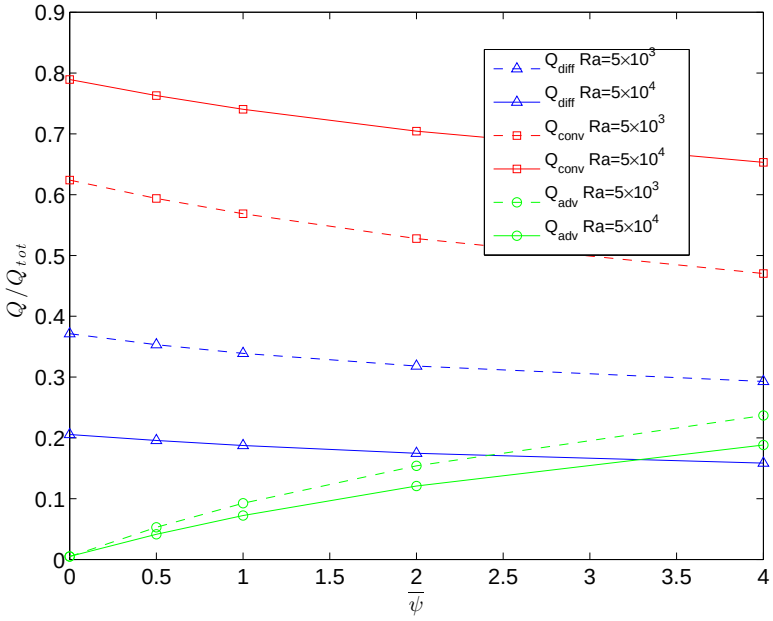


(b) Fixed Flux

Figure 7.9: Component heat fluxes as a function of average chemical species concentration for RTLBM simulations at two different Rayleigh numbers. The heat flux values (corresponding to diffusion in blue, convection in red and advection by passive scalar chemical species in green) are normalised by the total heat flux.

### 7.3.2 Non-linear Open System

This is a particularly fascinating and visually appealing part of the journey. In a convective fluid system within which the thermal GS RD model is embedded (dissolved), how do the dual pattern formation processes of convection and RD interact? Throughout this section it should be kept in mind the concept of stability, being robust to perturbations. It will be shown that both convective structures (convection cells) and RD spots can withstand a certain degree of tampering from other physical processes occurring in their vicinity. However it is also possible (probably more common) to find parameter combinations where the balance is tipped and patterns may be destroyed, only to emerge again if the perturbations recede.

Furthermore there will be examples in which emergent structures critically impact their surroundings, spelling either prosperity or disaster for their own persistence. Scenarios will be shown where there is a perpetual competition between different pattern-forming processes, all of which are being driven by gradients, but by existing they are also dissipating those gradients. Like biological organisms, the second law of thermodynamics is neither friend nor foe: without free energy flows, any ordered structure will eventually fall victim to fundamental statistical randomisation, but at the same time the dissipation of available energy is the driving force that perhaps defines the living state. Life is simultaneously driven by and must resist, free energy dissipation. So it is with these simple, non-living patterns.

#### 7.3.2.1 Thermally Neutral Reaction

It is sensible to begin with a system in which the RD dynamics do not influence the temperature field and fluid flow. As in subsection 7.2.2, $E_f = 1.7$ and $\Delta H = 0$ so that no heat is absorbed or produced by the reaction. The reaction will simply occur where the temperature is sufficiently high. The evolution of the system is shown in Figure 7.10.

Since the GS layer of the system does not influence the temperature field, a normal convection pattern forms along with a range of RD structures. The changes in RD structure formation are simply due to the temperature variation. In the hottest regions, the reaction takes over and there are regions of mostly $B$, and as the temperature declines

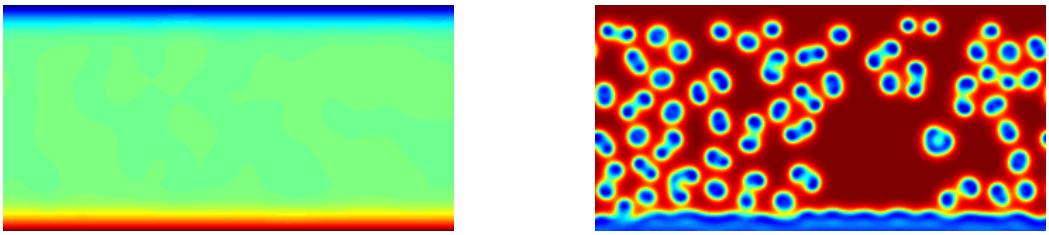

(a) $t = 500$

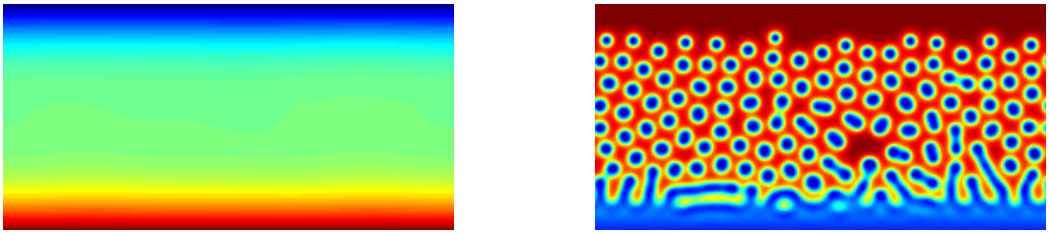

(b) $t = 2200$

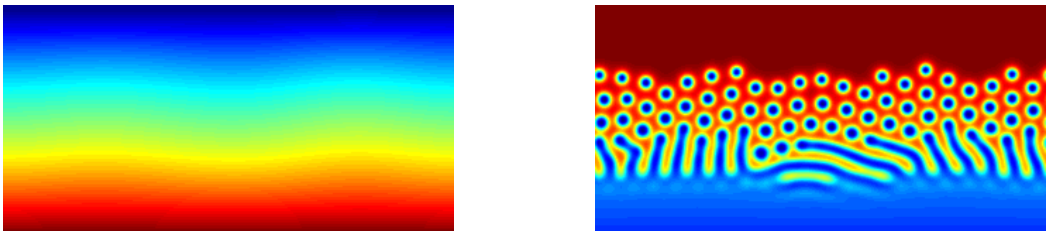

(c) $t = 10600$

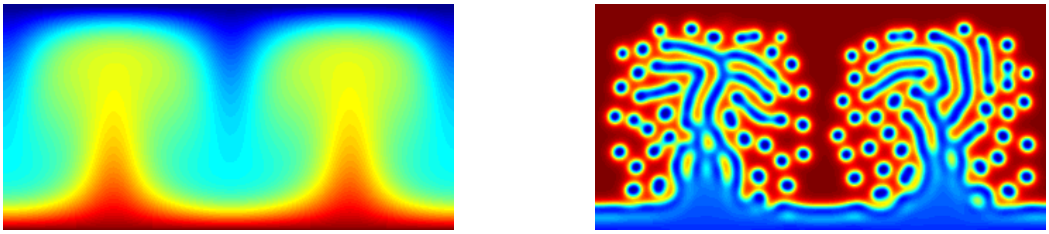

(d) $t = 50000$

Figure 7.10: Temperature and chemical order parameter ($\psi_A - \psi_B$) fields for a thermally neutral ($\Delta H = 0$), convective GS TRD simulation at several different times through the simulation. The time intervals are logarithmically spaced. See an animation of this simulation in additional digital material.

moving through one of the convection cells, there are worm-like structures, spots and then regions of almost pure $A$ where the reaction rate has diminished considerably.

Note that in this simulation the emergent configuration consisted of 4 convection cells. Given that the aspect ratio of the domain was fixed at a value of 2, it was more often the case that a 2-convection cell arrangement emerged. Throughout performing these simulations it was clear that the stability of these two steady states was relatively close.

However the 2-cell arrangement was slightly more stable, since in the presence of fluctuations, the 4-cell configuration sometimes lost stability and the system fell into the 2-cell attractor. Nonetheless, the number of convection cells did not significantly impact the basic phenomenology of the TRD dynamics when the whole simulation domain was differentially heated. In later sections, portions of the lower boundary will no longer be heated and in those cases the convection pattern is highly relevant to the system's evolution.

#### 7.3.2.2 Exothermic Reaction

The thermal neutrality assumption can now be relaxed and the same system but with an exothermic reaction: $\Delta H = -0.5 \times 10^{-3}$ will be simulated. This system's states are qualitatively very similar to those of the thermally neutral system shown in Figure 7.10. The additional heat released does however allow the pattern-forming region to extend slightly higher. The expansion is halted by the extraction of additional heat by the upper boundary. When the reaction is more strongly exothermic, a different arrangement of chemical concentration gradients begins to arise. This is illustrated in Figure 7.11, which shows a simulation with $\Delta H = -1 \times 10^{-3}$.

Now the steady state has shifted to one with higher average temperature and a large portion of the structure forming area has been enveloped by the $B$-dominant region. If $\Delta H$ is decreased further (greater heat release), there is a continuation of this trend and the B-dominant region eliminates essentially all of the finer structure that is normally observed in GS RD systems. Since the positive feedback between the temperature and reaction means that its rate is significantly enhanced, the effect is similar to a reduction in the other parameters relevant to GS RD dynamics: the feed rate $F$, the removal rate $R$ and the diffusion coefficients of the chemical species. Referring back to the standard phase portrait in Figure 6.2, this effect is roughly equivalent to moving down and to the left in the phase space, moving the system into a regime dominated by a simple interface and periodic concentration waves. Indeed this is what occurs in the strongly exothermic simulation. Further reductions in $\Delta H$ cause very strong positive feedback leading to divergence of temperature.

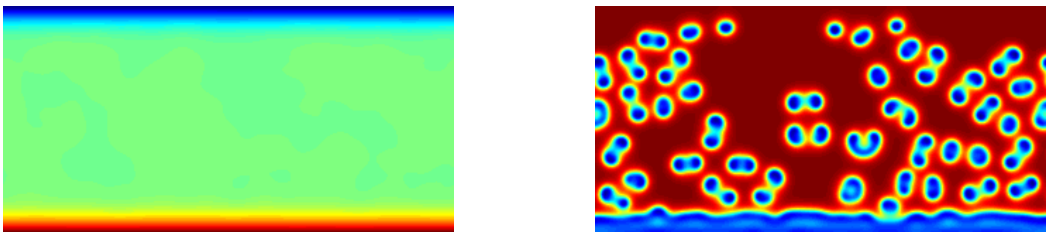

(a) $t = 500$

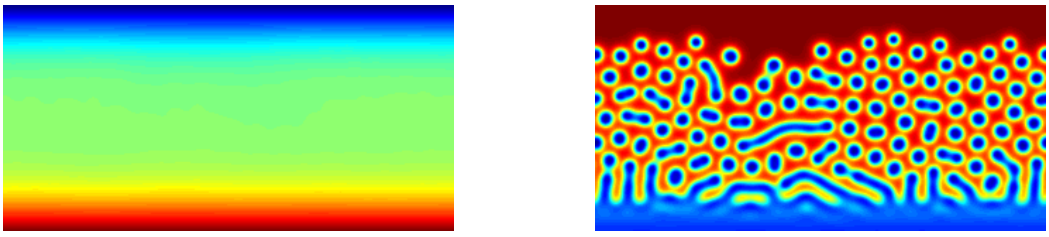

(b) $t = 2200$

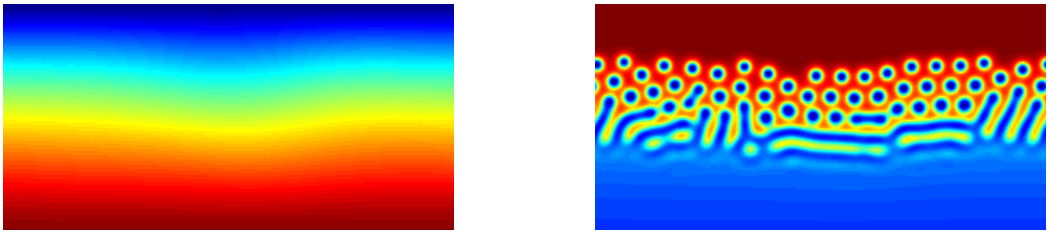

(c) $t = 10600$

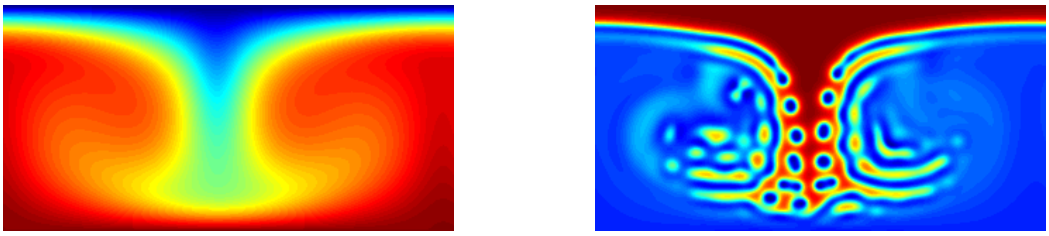

(d) $t = 50000$

Figure 7.11: Temperature and chemical order parameter $(\psi_A - \psi_B)$ fields for an exothermic, convective GS TRD simulation with $\Delta H = -1 \times 10^{-3}$ at several different times through the simulation. The time intervals are logarithmically spaced. See an animation of this simulation in additional digital material.

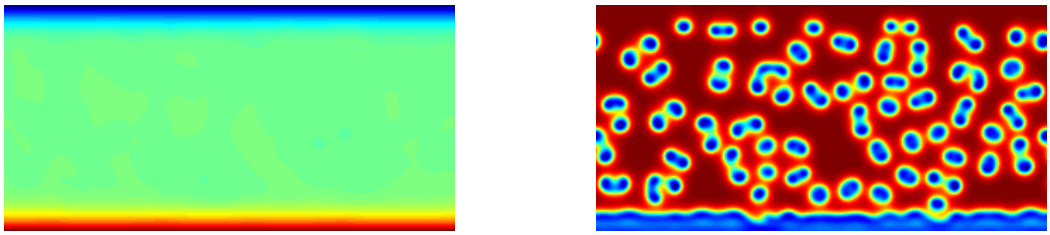

(a) $t = 500$

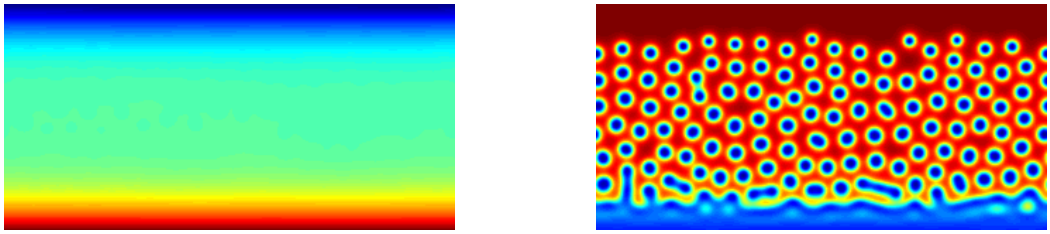

(b) $t = 2200$

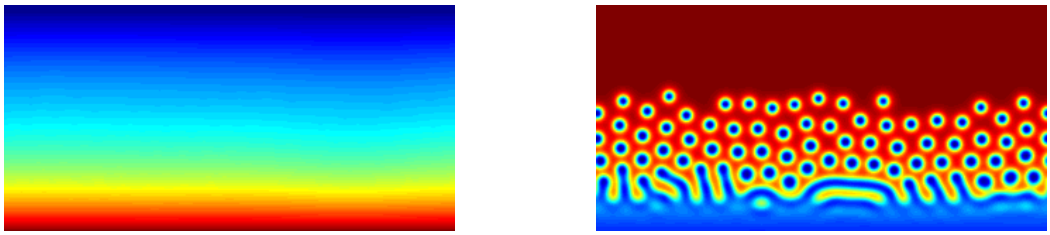

(c) $t = 10600$

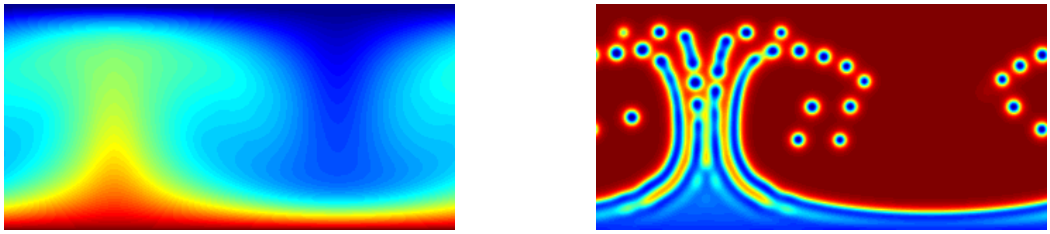

(d) $t = 50000$

Figure 7.12: Temperature and chemical order parameter $(\psi_A - \psi_B)$ fields for an endothermic, convective GS TRD simulation with $\Delta H = 2 \times 10^{-3}$ at several different times through the simulation. The time intervals are logarithmically spaced. See an animation of this simulation in additional digital material.

#### 7.3.2.3 Endothermic Reaction

Endothermic systems can now be considered. If the reaction enthalpy is adjusted to $\Delta H = 2 \times 10^{-3}$, a different configuration of patterns emerges, as shown in Figure 7.12. In contrast to the exothermic systems, the emergent structures here are self-limiting. Early in the simulation while the temperature is relatively high across the domain, RD spots replicate and proliferate. However, they soon have a dramatic cooling effect and 'die back' to the lower portion of the domain. This thermal damping is not strong enough

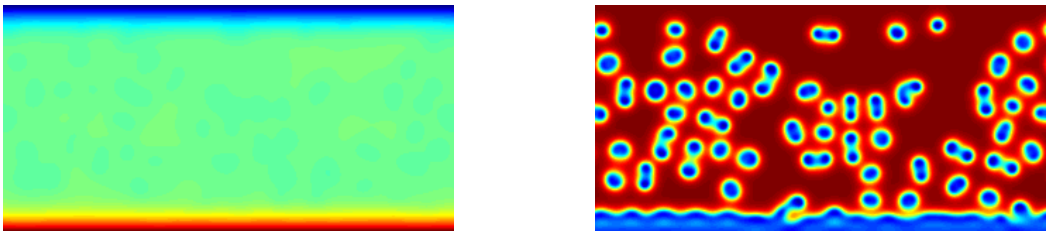

(a) $t = 500$

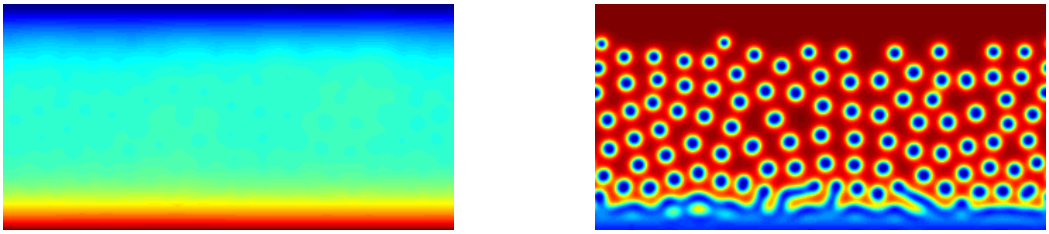

(b) $t = 2200$

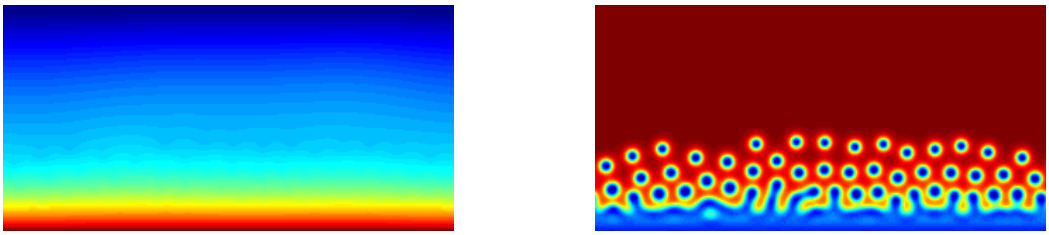

(c) $t = 10600$

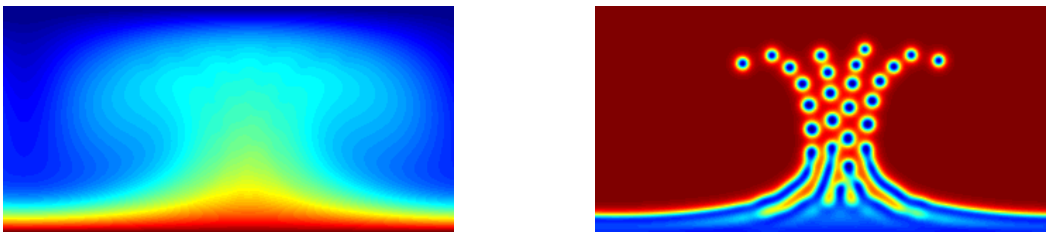

(d) $t = 50000$

Figure 7.13: Temperature and chemical order parameter ($\psi_A - \psi_B$) fields for an endothermic, convective GS TRD simulation with $\Delta H = 5 \times 10^{-3}$ at several different times through the simulation. The time intervals are logarithmically spaced. See an animation of this simulation in additional digital material.

to prevent the onset of convection however, and the characteristic double convection cell forms and persists. The heat flux from the lower boundary eventually adjusts such that the heat loss due to convective heat transport and the chemical reaction is compensated for.

If the reaction is even more strongly endothermic, such as in Figure 7.13, the pattern forming region is forced back further, and the heat absorbed by the reacting spots almost eliminates any rising convection plumes. Eventually, when the reaction is sufficiently

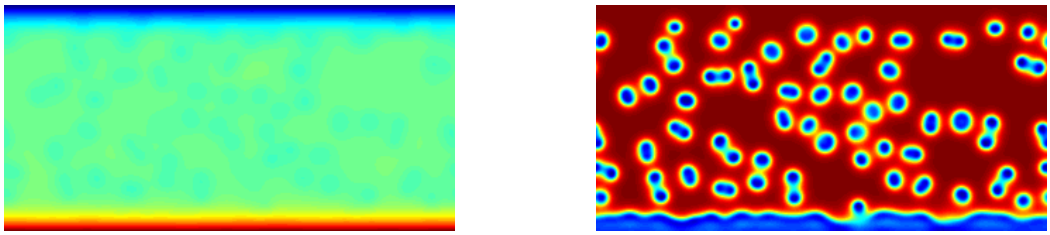

(a) $t = 500$

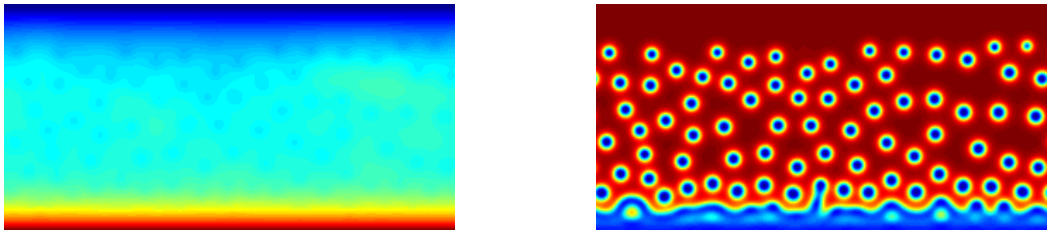

(b) $t = 2200$

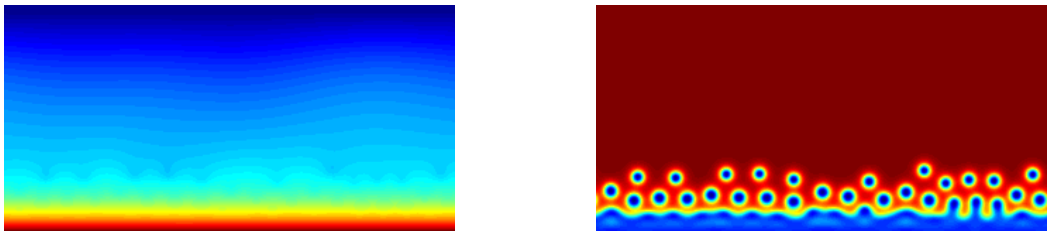

(c) $t = 10600$

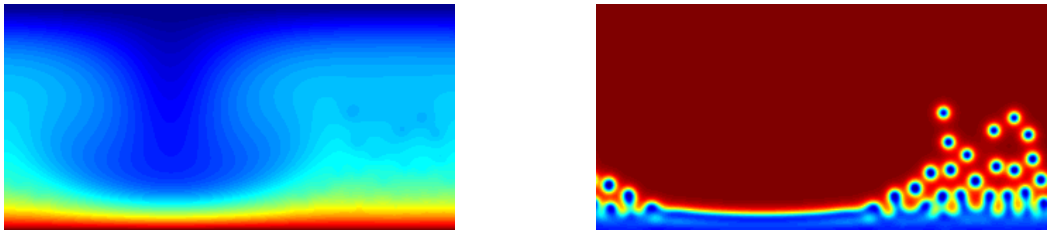

(d) $t = 50000$

Figure 7.14: Temperature and chemical order parameter ($\psi_A - \psi_B$) fields for an endothermic, convective GS TRD simulation with $\Delta H = 10 \times 10^{-3}$ at several different times through the simulation. The time intervals are logarithmically spaced. See an animation of this simulation in additional digital material.

endothermic, the bifurcation to convective motion can be almost entirely prevented, as shown in the simulation of Figure 7.14.

In this example, the RD spots effectively destroy the conditions for their own proliferation. They are thus forced to only grow and divide by the lower boundary where the large heat flux can counter the reactive losses. If the temperature was not held constant here, the reaction would cease across the entire domain. Despite the cooling effects of the spots, convective plumes sporadically appear when a fluctuation allows a local

heating event. Such plumes initially grow as they displace colder fluid above. However, since they draw up warmer fluid from below, they cause the RD spots to undergo rapid growth in the warm wake. The growth and division of the spots causes rapid cooling and what might have led to the setting in of convection is all but extinguished. This behaviour is best viewed through the animation provided in the additional digital material, associated with this thesis.

A stronger competitive dynamic of the form just described can be observed if the activation energy of the reaction is reduced to $E_f = 0.2$. Giving the reaction a weaker temperature dependence means that RD spots are less restricted by local temperature constraints. It is then possible to further increase the enthalpy of reaction to $\Delta H = 25 \times 10^{-3}$. As a result, there is a very strong, oscillatory dynamic involving a combination of several feedbacks. Snapshots from the simulation are shown in Figure 7.15, although the behaviour is best viewed with the corresponding animation in the additional digital material.

Due to the strength of the reactive heat absorption, the average temperature of the system is somewhat lower than even the low temperature upper boundary. This has the effect of increasing the driving force for convective motion between the central part of the domain and the warm lower boundary. With this strong gradient, small fluctuations in temperature can allow convective plumes to grow rapidly and begin transporting heat from the lower boundary to the central part of the domain. Because the lower boundary provides whatever heat is required to maintain its temperature, the convective plumes can transport significant quantities of heat. However this local abundance of heat is rapidly exploited by the RD spots, which are otherwise prevented from growing and dividing.

The convective plumes can sometimes withstand this heat loss temporarily, but eventually once the collection of RD spots grows to a certain size, their collective cooling effect dampens the convective flow back to the lower boundary.What makes this phenomena so intriguing is that here we have two characteristic pattern-forming processes, both competing for a supply of free energy in a perpetual conflict, which under certain conditions (such as the parameters used in Figure 7.15) appears to go on indefinitely.

Note that some RD spots are able to survive near the upper boundary. This is because the upper boundary is held at a constant temperature that ends up being higher than

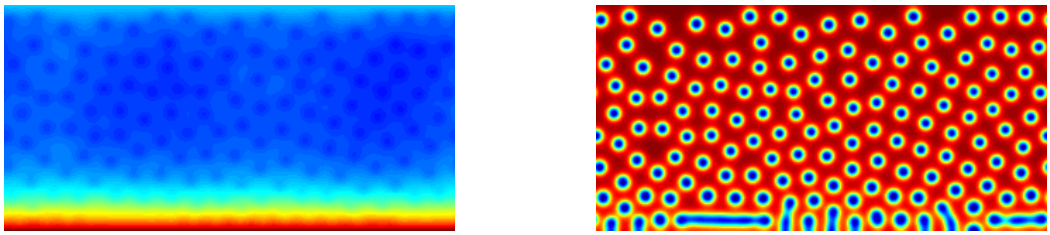

(a) $t = 500$

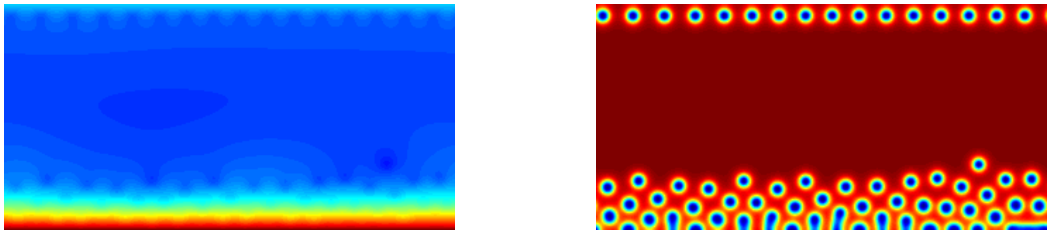

(b) $t = 2200$

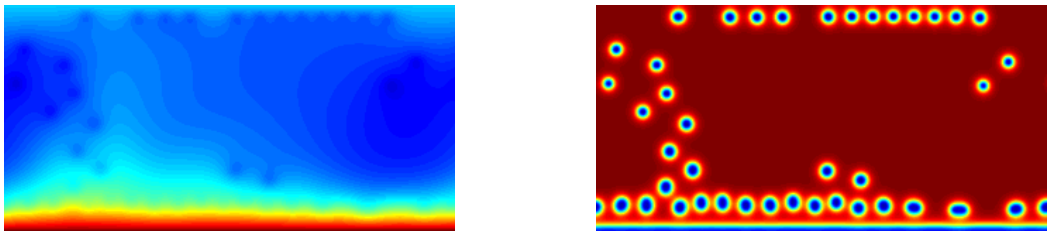

(c) $t = 10600$

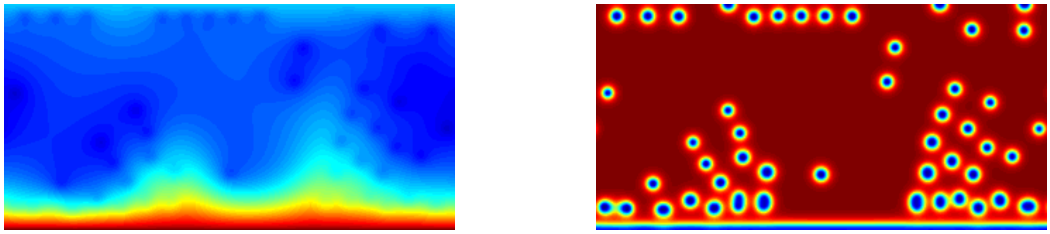

(d) $t = 50000$

Figure 7.15: Temperature and chemical order parameter $(\psi_A - \psi_B)$ fields for an endothermic, convective GS TRD simulation with $\Delta H = 25 \times 10^{-3}$ at several different times through the simulation. The time intervals are logarithmically spaced. See an animation of this simulation in additional digital material.

the average temperature of the bulk of the fluid. This temperature, while being lower than that of the lower boundary, is sufficiently high for a layer of RD spots to persist.

#### 7.3.2.4 Precariousness

In the previous section it was shown that adding a thermal level of description to the kinetics of RD systems produces a whole new branch of behaviours. Broadly speaking, when the reaction is exothermic, it produces a positive feedback effect, and when it is endothermic, it is self-inhibiting. In the spirit of relating the dynamics of RD systems to those of living systems we could then ask: Can RD structures re-pattern their surroundings such that they can expand into regions where they cannot form spontaneously? This notion of creating conditions favourable to your own persistence in hostile areas has been termed precariousness (Virgo, 2010).

Precarious structures are able to outwardly 'colonise' regions where they would not emerge on their own, but they are still vulnerable to perturbations, certain types of which can destroy the organisation which constitutes those structures. Virgo (2010) focusses on precarious dissipative (free energy consuming) structures as analogues for biological organisms. Organisms and precarious dissipative structures so defined, can form spontaneously under certain conditions. Once formed they can then enter regions where they would not form spontaneously, and re-create the conditions under which they emerged, such that they can expand or replicate in the previously hostile environment.

Their persistence is robust to some, but not all, perturbations. For example a human body can withstand an astounding range of disruptions (temperature changes, mechanical stress, immersion in water), but within limits (at extreme temperatures death occurs, very strong impacts can kill and remaining submerged for too long also causes death). Furthermore the human embryo develops in a very special set of conditions. But once fully formed and functioning in the world external to its Mother's womb, it can go on to produce the necessary and sufficient conditions for the emergence of another human. Extremophile bacteria are prime examples of precariousness, seemingly able to reach every last corner of the planet and still make a living even in places that were previously utterly lifeless. Virgo (2010) already characterised the simple self-replicating spots of the GS RD system as precarious structures since a single spot in isolation can replicate to fill its surroundings. This seems like a slightly weaker version of the concept since the environment of a standard GS RD system is not particularly hostile to the formation of further spots.

Keeping this in mind, in this section the objective is to assess the precarious nature of TRD spots. Taking a fluid system in which only half the domain is heated, the emergence of RD structures in that half is expected. Can those structures also expand into non-heated regions where they would not form spontaneously or where the low temperature provides a strong inhibition to their growth? The simulations to follow aimed to answer these questions. For each simulation presented, a control case was performed to ensure that the RD structures could not form spontaneously in the reduced temperature regime (when the whole system was not heated). In all cases, the structures failed to form.

In subsubsection 7.3.2.2 it was found that for $\Delta H \leq -1 \times 10^{-3}$, the system typically undergoes such a strong positive feedback that the majority of the emergent organisation becomes enveloped by a homogenous region of almost pure $B$. This value for the reaction enthalpy is thus a logical starting point in the search for precarious behaviour. The evolution of a partially heated system with this enthalpy change value is shown in Figure 7.16.

After the initial transient the system's steady state consists of a double convection cell and two 'soliton channels' from which RD spots emerge like sprouting spores. However these 'spores' seem unable to seed the growth of further spots elsewhere. The heat that they produce is wholly insufficient to counter the low temperature environment that they get propelled into. Doubling the enthalpy of reaction to $\Delta H = -2 \times 10^{-3}$ allows the spots to survive slightly longer, as shown Figure 7.17.

In this case there is some re-circulation since the spots can persist long enough to be swept into the interior of the convection cell. However, in the steady state the rate of spot production is balanced by the rate at which they disintegrate and so there is no outward proliferation. Decreasing the reaction enthalpy yet further to $\Delta H = -3 \times 10^{-3}$ pushes the dynamics of the system into a rather different mode. Figure 7.18 illustrates the positive feedback effect that is unleashed in this system.

It seems that when the reaction is sufficiently exothermic, a threshold is passed beyond which the expanding reactive zone experiences exponential growth as the system struggles to remove the excess heat produced by the reaction. An extreme example of this occurs when the enthalpy of reaction is decreased further. In Figure 7.19 all traces of structure are wiped out by the prevailing reaction front, which eventually dominates the system.

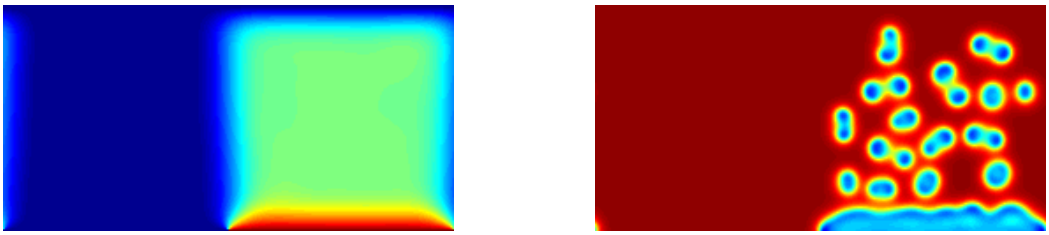

(a) $t = 500$

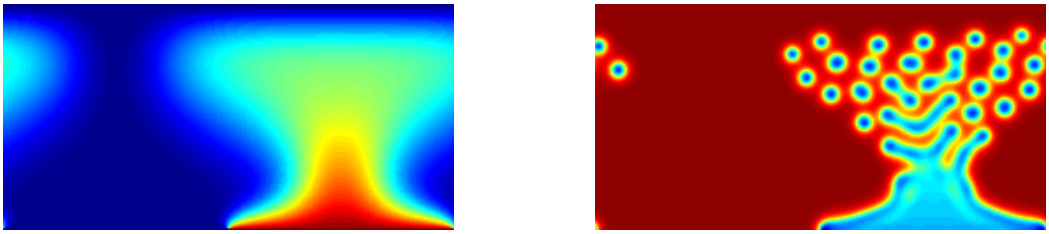

(b) $t = 2300$

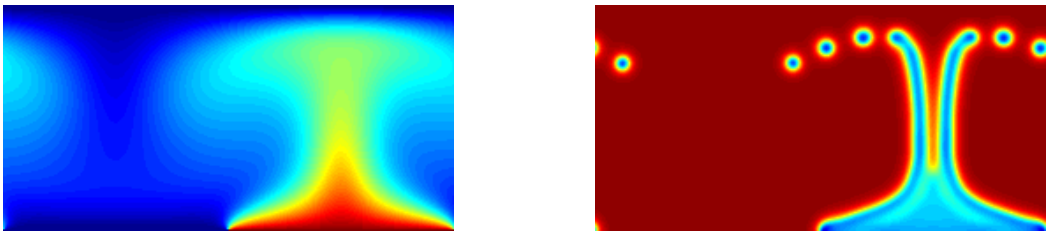

(c) $t = 10800$

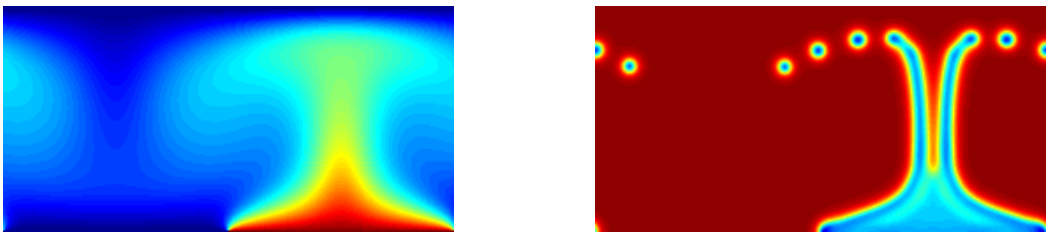

(d) $t = 50000$

Figure 7.16: Temperature and chemical order parameter $(\psi_A - \psi_B)$ fields for an exothermic, convective GS TRD simulation with $\Delta H = -1 \times 10^{-3}$ at several different times through the simulation. The time intervals are logarithmically spaced. See an animation of this simulation in additional digital material.

The enthalpy limits of this exothermic RD system have now been navigated. The question remains as to whether any of these systems can produce RD structures that might deserve the label of precarious. One way to assess this is to simulate a system that reaches a quasi steady state with consistent pattern emergence, and then remove the thermal driving force. This is the most aggressive test for whether the RD structures can persist in foreign environments because the conditions in which they spontaneously

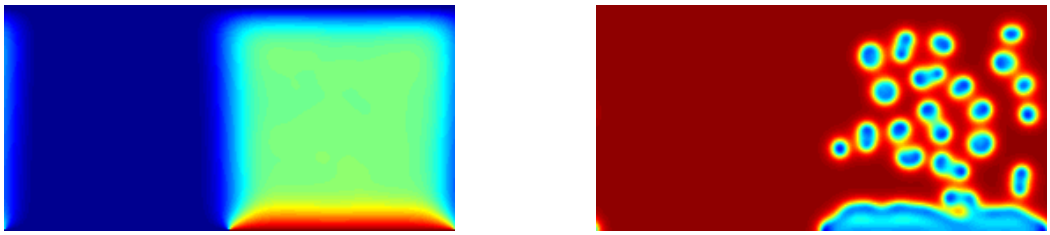

(a) $t = 500$

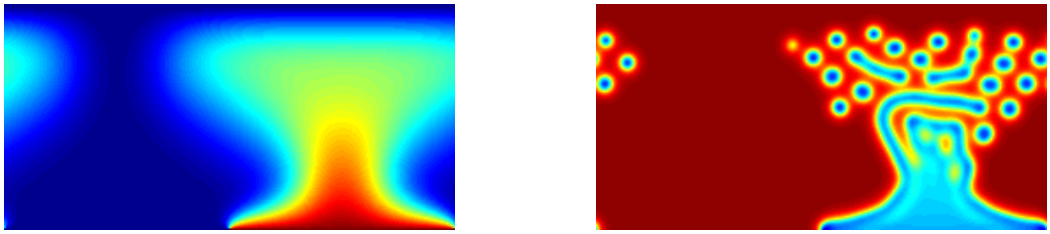

(b) $t = 2300$

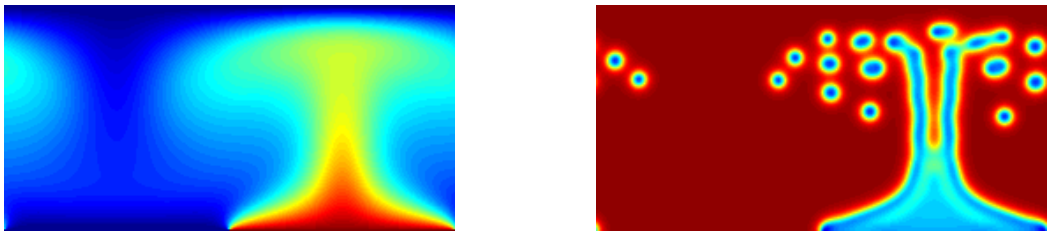

(c) $t = 10800$

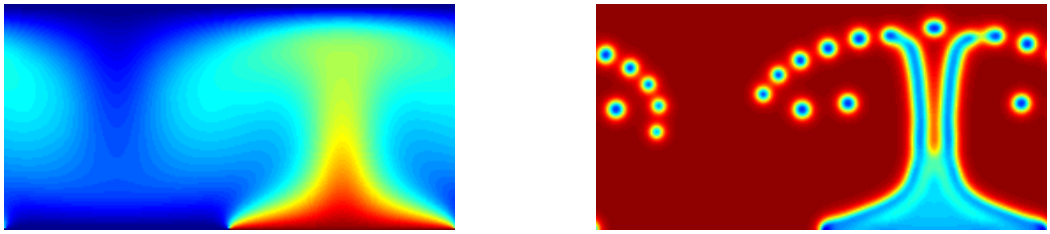

(d) $t = 50000$

Figure 7.17: Temperature and chemical order parameter $(\psi_A - \psi_B)$ fields for an exothermic, convective GS TRD simulation with $\Delta H = -2 \times 10^{-3}$ at several different times through the simulation. The time intervals are logarithmically spaced. See an animation of this simulation in additional digital material.

emerge will be entirely absent from the system once the temperature of the warm boundary section is reduced to that of the other, cooler boundaries.

Thus several systems were simulated that proceeded for twice the duration of the previous simulations. Half way through the simulation at $t = 50000$ time steps, the temperature of the lower right boundary was gradually reduced to match that of the other boundaries. By $t = 70000$ all boundaries were at an equal, low temperature. A temperature at which RD structures cannot form spontaneously. Several system states from

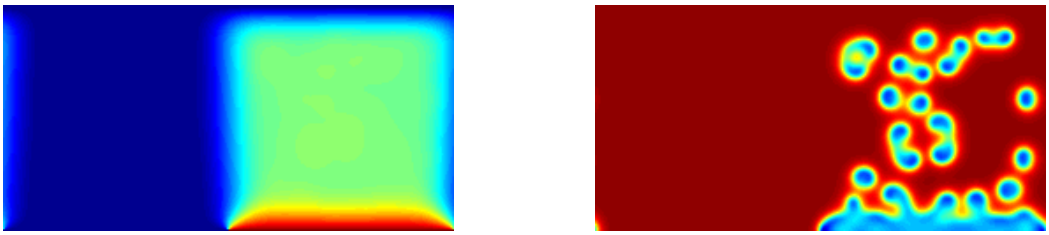

(a) $t = 500$

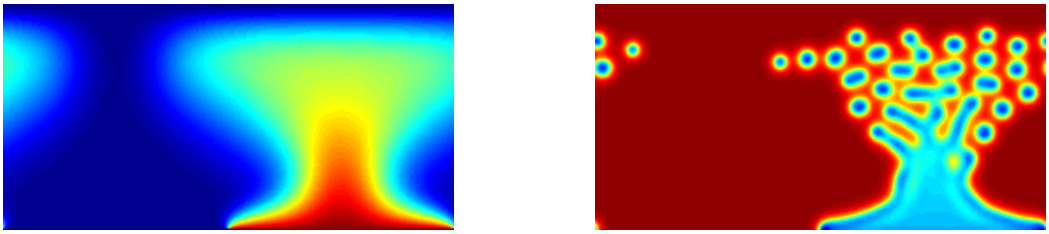

(b) $t = 2300$

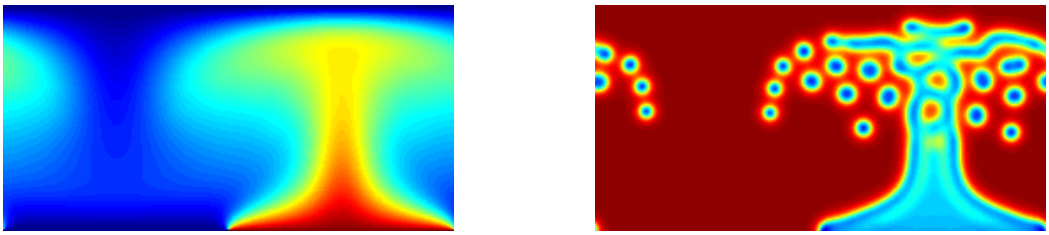

(c) $t = 10800$

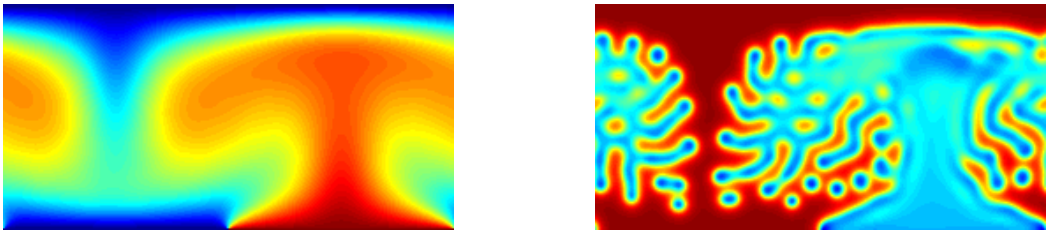

(d) $t = 50000$

Figure 7.18: Temperature and chemical order parameter $(\psi_A - \psi_B)$ fields for an exothermic, convective GS TRD simulation with $\Delta H = -3 \times 10^{-3}$ at several different times through the simulation. The time intervals are logarithmically spaced. See an animation of this simulation in additional digital material.

one such simulation with $\Delta H = -3 \times 10^{-3}$ are displayed in Figure 7.20.

It is clear that while the patterned region does persist beyond the time at which all boundaries reach the reduced temperature, its heat production is not sufficient to withstand the heat removal occurring at the system boundaries. So while the spots are precarious in the sense that they can move into the colder region and survive, they cannot grow and divide and colonise such regions. They cannot persist independently without the support of the spawning heat source.

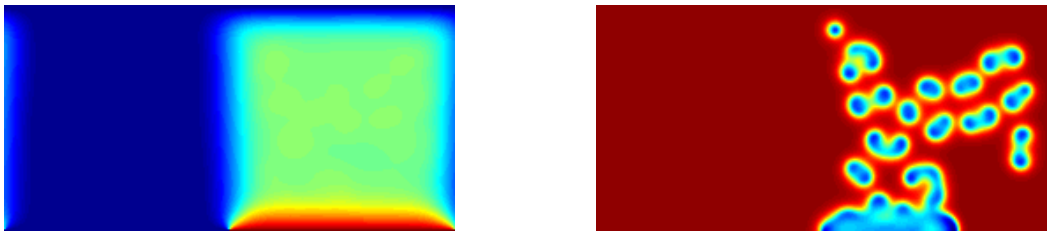

(a) $t = 500$

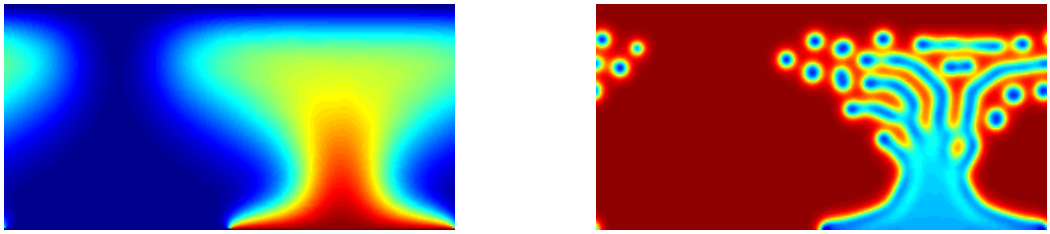

(b) $t = 2300$

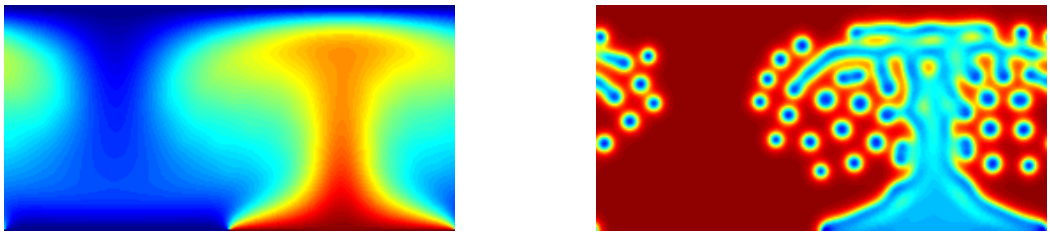

(c) $t = 10800$

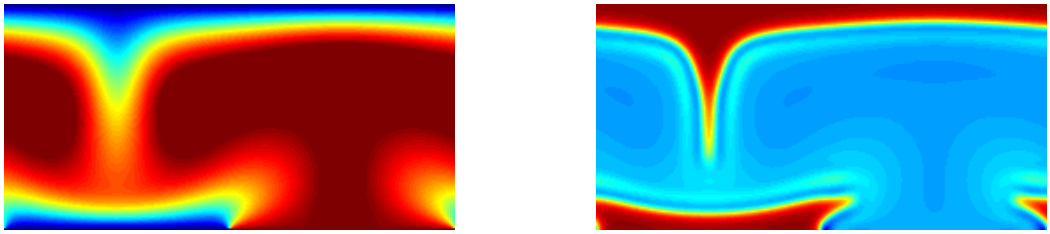

(d) $t = 50000$

Figure 7.19: Temperature and chemical order parameter $(\psi_A - \psi_B)$ fields for an exothermic, convective GS TRD simulation with $\Delta H = -4 \times 10^{-3}$ at several different times through the simulation. The time intervals are logarithmically spaced. See an animation of this simulation in additional digital material.

In fact the enthalpy needs to be as low as $\Delta H = -5 \times 10^{-3}$ for a reacting region to sustain itself through its own heat production against the heat removal pressure of the boundaries. However in such a state there is very little structure, rather just an enclosed region of almost pure $B$, surrounded by a reaction front. Perhaps we could regard this as a super RD spot. Since it does not replicate or undergo any morphological change, it would not appear to qualify as being precarious.

The range of behaviours observable in this exothermic RD system have now been more

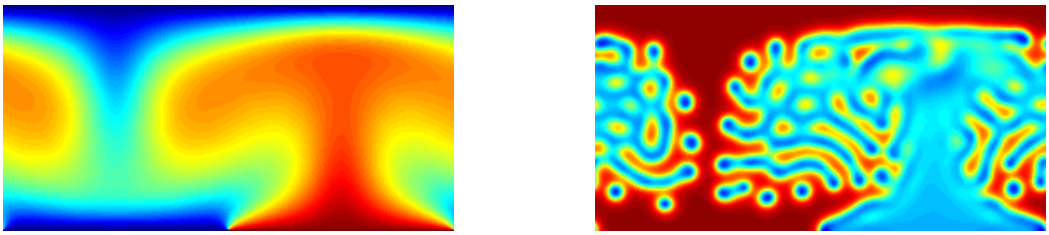

(a) $t = 50000$

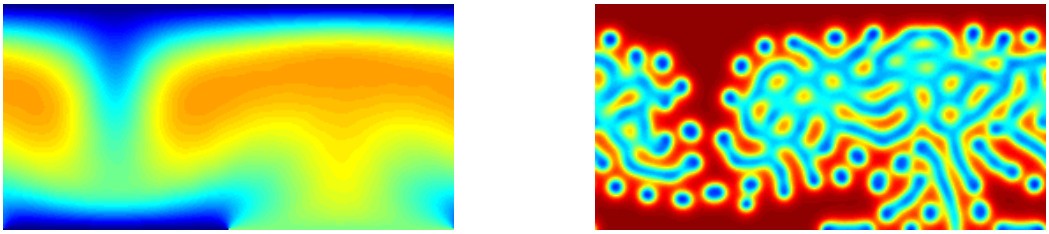

(b) $t = 60000$

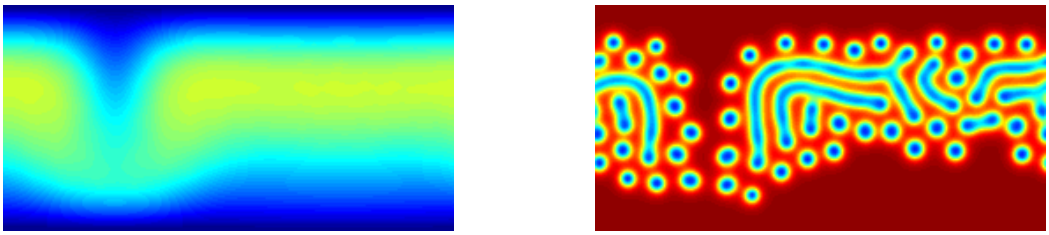

(c) $t = 70000$

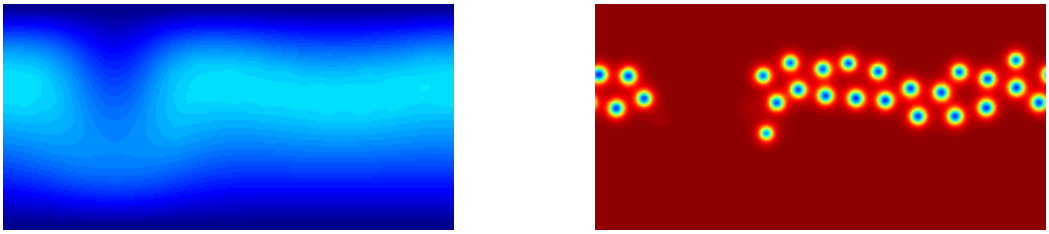

(d) $t = 80000$

Figure 7.20: Temperature and chemical order parameter $(\psi_A - \psi_B)$ fields for an exothermic, convective GS TRD simulation with $\Delta H = -3 \times 10^{-3}$ at several different times through the simulation. The time intervals are linearly spaced and the temperature of the right half of the lower boundary is linearly reduced from $T_{a_r} = 2$ to $T_{a_r} = 1$ between times $t = 50000$ and $t = 70000$. See an animation of this simulation in additional digital material.

or less explored. One parameter that has remained constant throughout is the activation energy $E_f$. If this parameter was to be reduced the reaction rate would gradually become insensitive to temperature. There would then be no requirement for emergent structures to form in warmer regions and heat could no longer be considered as a 'fuel' for such objects. Although interesting dynamics were observed with the endothermic system $(E_f = 0.2, \Delta H = 25 \times 10^{-3})$, it would require an entire dedicated study in itself to

assess the entire $E_f, \Delta H$ parameter space. Such a study would likely reveal even more interesting behaviours.

## 7.4 Thermal Symbiosis: Four-Species Convective

In subsubsection 7.3.2.4 it was shown that an exothermic, partially heated system exhibits either runaway expansion of a reactive zone, enveloping any finer grained structure, or the emitted spots were completely unable to ensure their own survival in hostile environments. However one could envision a system with more than a single spot 'species'. There could be several sets of RD systems existing simultaneously. The purpose of this section is to begin to explore the behaviour of such systems.

In terms of the RTLBM algorithm, it is only required to add an extra two sets of chemical species with identical streaming and collisions steps, and identical equilibria. The same activation energy that has been used previously will be adopted again for the sake of simplicity: $E_{f_1} = E_{f_2} = 1.7$. What can be varied between the two RD systems is their reaction enthalpies: $\Delta H_1$ and $\Delta H_2$. The diffusion constants $D_{A_1}$ and $D_{A_2}$ could also be varied, causing the two spot species to be of different characteristic sizes. This was explored briefly, but not comprehensively. Therefore, only results from equal diffusion rate simulations will be presented here.

To begin with, it would be revealing to establish whether the runaway growth of the reactive zone can be arrested by the presence of a companion, endothermic set of RD structures. Several simulations were carried out with various combinations of enthalpy values. The most important results will be presented.

It was found in subsubsection 7.3.2.4 that $\Delta H = -4\times10^{-3}$ leads to positive feedback and a system-wide takeover by the reactive zone. A logical first assessment would therefore be to set $\Delta H_1 = -4\times10^{-3}$ and $\Delta H_2 = 4\times10^{-3}$ to see whether the second, endothermic RD system can stabilise the first and prevent the encompassing positive feedback effect. Such a system is displayed in Figure 7.21.

Note that the concentration profiles of the two sets of chemical species appear to be identically distributed in space. This phenomenon of phase-locking seemed to occur in all simulations of this type (with one exothermic and one endothermic species of

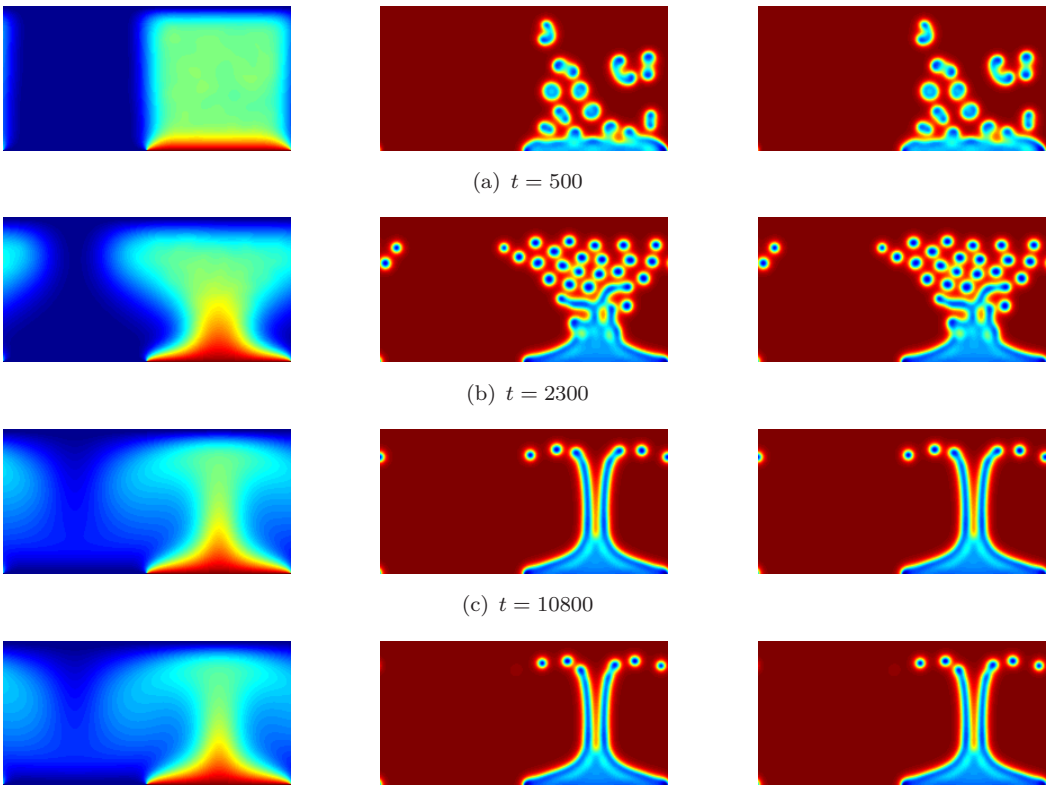

(a) $t = 500$

(b) $t = 2300$

(c) $t = 10800$

(d) $t = 50000$

Figure 7.21: Temperature and chemical order parameter fields $(\psi_{A_1} - \psi_{B_1})$ and $(\psi_{A_2} - \psi_{B_2})$ for a dual spot species, convective GS TRD simulation with $\Delta H_1 = -4 \times 10^{-3}$ and $\Delta H_2 = 4 \times 10^{-3}$ at several different times through the simulation. The time intervals are logarithmically spaced. See an animation of this simulation in additional digital material.

spot). Note that the matching is not perfect, sometimes there are small deviations in concentration profile between the two sets of chemicals. However it seems that in general the endothermic spots have very little chance of sustaining themselves unless they can parasitise the heat given off by an exothermic spot.

This suggests that there might be ways in which a multi-spot system could start forming integrated structures of several components, each serving a particular function. In this case the combined action of the two spots could serve as a temperature homeostasis mechanism. At excessively high temperatures the number of endothermic spots could rise rapidly and act to modulate the temperature and prevent any expansive takeover by a single reactive zone. Conversely at low temperatures the endothermic spots might 'die back', allowing the exothermic species to grow and divide producing excess heat to restore the local temperature to a more amenable value. It would be a valuable study

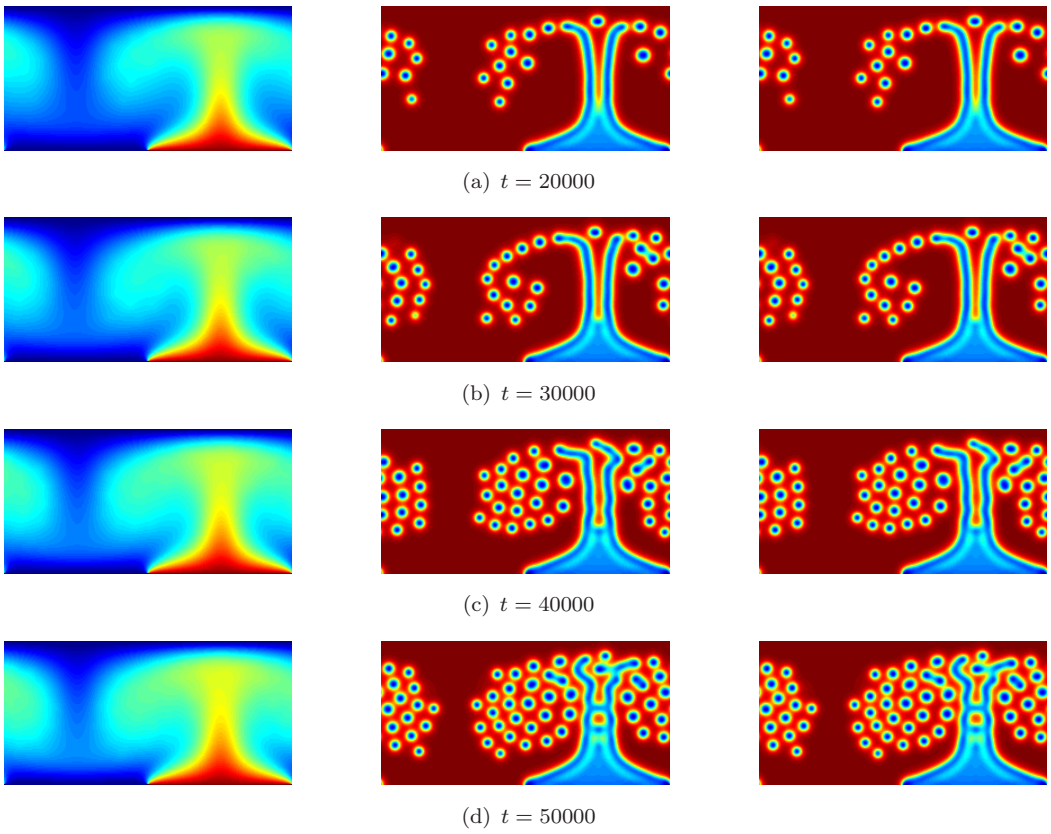

(a) $t = 20000$

(b) $t = 30000$

(c) $t = 40000$

(d) $t = 50000$

Figure 7.22: Temperature and chemical order parameter fields $(\psi_{A_1} - \psi_{B_1})$ and $(\psi_{A_2} - \psi_{B_2})$ for a dual spot species, convective GS TRD simulation with $\Delta H_1 = -4 \times 10^{-3}$ and $\Delta H_2 = 2 \times 10^{-3}$ at several different times through the simulation. The time intervals are linearly spaced. See an animation of this simulation in additional digital material.

to explore this possibility in depth, possibly by setting up systems with a plethora of spot species, each with different kinetic properties, and simply allowing some form of natural selection of stable patterns to filter out the most robust survivors. It would be interesting to see whether complex aggregations, akin to spatially bounded metabolic systems, might emerge spontaneously.

Figure 7.21 reveals that in fact the second spot species is so effective in damping the heat production of the first that both undergo very limited proliferation away from the heated boundary section. To reduce this damping effect, the second species can be made less endothermic with $\Delta H_2 = 2 \times 10^{-3}$. Both species of spots can then occupy a significantly greater area, as illustrated in Figure 7.22.

What is striking about this system is that the mutual action of the two spot species has clearly made their existence more likely. Now, the system sustains a whole region of

spots, circulating with the two convection cells. This configuration appears to be indefinitely stable. There is no runaway feedback and no diminishing of the spot population. A number of spots are existing in the cooled left half of the domain where they cannot form spontaneously, although they do not remain there due to the action of the fluid flow, experiencing circulation instead.

There also appears to be quite a range of spot lifetimes. Some disintegrate after undergoing a single journey within the convection cell if they happen to be advected to a region where the supply of $A$ is locally limited due to overcrowding. Others appear to be robust for much longer periods, perhaps also undergoing division and spawning new spots.

As a stronger test of precariousness, the same system was simulated for twice the duration with a gradual reduction of the lower right boundary temperature from $t = 50000$ to $t = 70000$. System states from this simulation are displayed in Figure 7.23.

Upon reflection, the complete demise of the RD structures in this figure is not wholly surprising. Without a sustained heat supply the endothermic spots soon begin to erode the temperature in excess of the heating provided by the other, exothermic reaction. So while the presence of a second, endothermic spot species can stabilise an exothermic species, the collective configuration of structures, once formed, still cannot sustain itself in a system maintained at a low temperature.

For the final part of this chapter I will see whether the thermal symbiosis uncovered above extends when the reaction enthalpies are increased in magnitude significantly. For example they can be set at $\Delta H_1 = -20 \times 10^{-3}$ and $\Delta H_2 = 25 \times 10^{-3}$. With these values if either RD system exists in isolation, there is no sustained pattern formation. For the exothermic species, there is a rapid assimilation of the whole domain by the B-dominant reaction zone. For the endothermic species, the heat absorbed by the reaction all but damps out any local heat fluxes and the whole system descends to a quiescent, low temperature state with only small fluctuations in temperature at the boundaries. The combined system however, supports the existence of both species by their mutual thermal interactions. Typical examples of system states are shown in Figure 7.24.

The high temperature lower boundary supports larger worm-like structures but in the bulk of the fluid the temperature remains at intermediate values through the combined

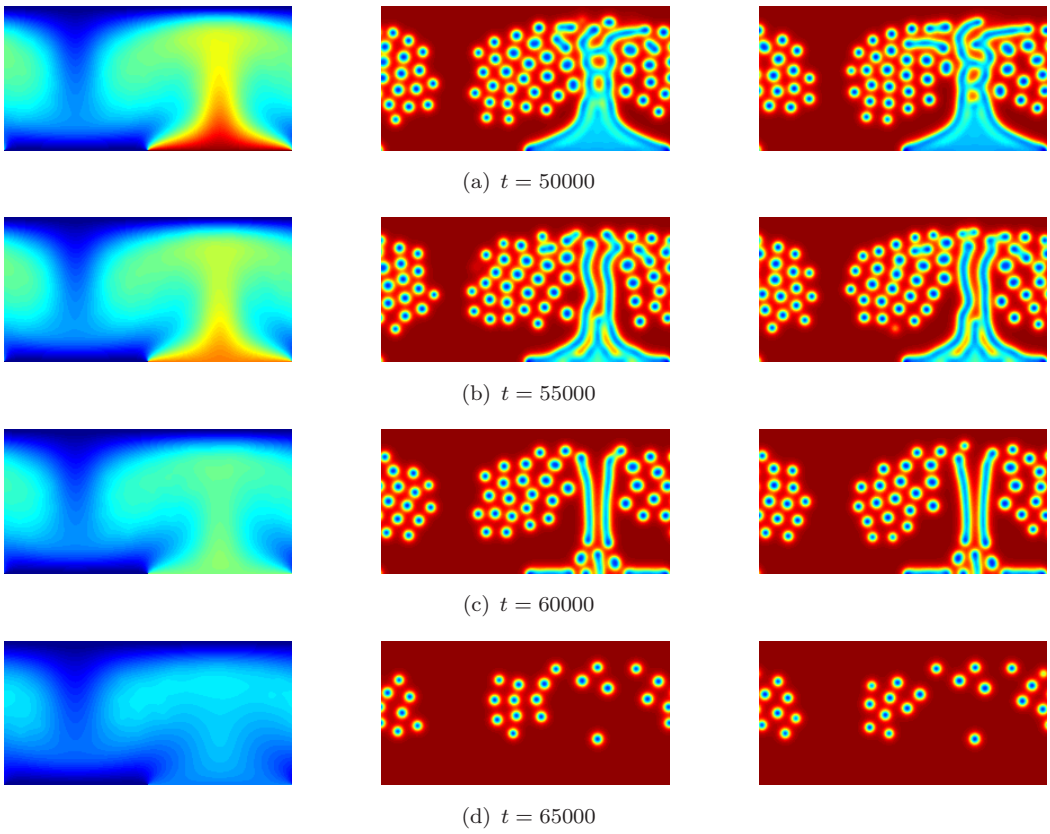

(a) $t = 50000$

(b) $t = 55000$

(c) $t = 60000$

(d) $t = 65000$

Figure 7.23: Temperature and chemical order parameter fields $(\psi_{A_1} - \psi_{B_1})$ and $(\psi_{A_2} - \psi_{B_2})$ for a dual spot species, convective GS TRD simulation with $\Delta H_1 = -4 \times 10^{-3}$ and $\Delta H_2 = 2 \times 10^{-3}$ at several different times through the simulation. The time intervals are linearly spaced and the temperature of the right half of the lower boundary is linearly reduced from $T_{a_r} = 2$ to $T_{a_r} = 1$ between times $t = 50000$ and $t = 70000$. See an animation of this simulation in additional digital material.

heat release and absorption due to the two reactions. Due to the strength of these thermal effects, the setting in of convective motion appears to be prevented.

## 7.5 Conclusions

In this chapter a set of novel systems have been explored: GS TRD systems embedded in a thermal fluid susceptible to convective motion. A range of interesting phenomena has been exhibited, from enhanced heat fluxes in simple linear reaction systems, to the mutual exchange of heat between emergent spot species. The results suggest that adding additional survival requirements for dissipative structures can induce significant new types of phenomena to emerge including competition between very different types

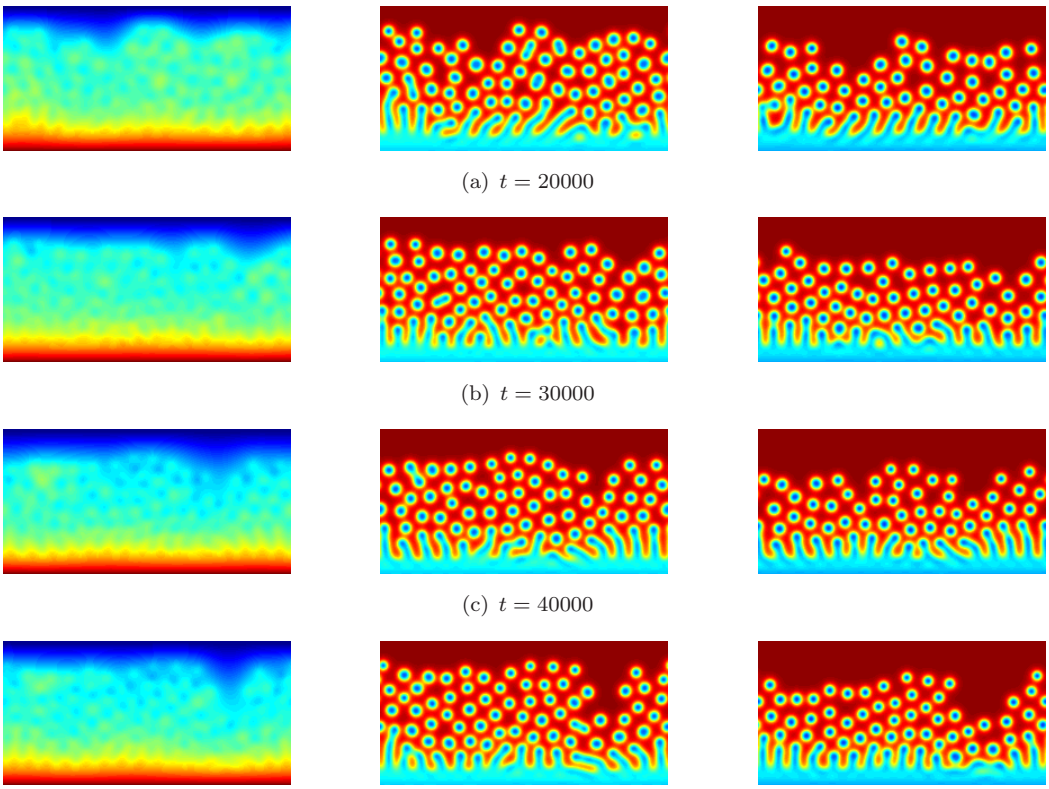

(a) $t = 20000$

(b) $t = 30000$

(c) $t = 40000$

(d) $t = 50000$

Figure 7.24: Temperature and chemical order parameter fields ($\psi_{A_1} - \psi_{B_1}$) and ($\psi_{A_2} - \psi_{B_2}$) for a dual spot species, convective GS TRD simulation with $\Delta H_1 = -20 \times 10^{-3}$ and $\Delta H_2 = 25 \times 10^{-3}$ at several different times through the simulation. The time intervals are linearly spaced. See an animation of this simulation in additional digital material.

of structure (convection cells and RD spots). It was also shown that these extra requirements can force different sets of patterns to form symbioses in order to guarantee their own persistence.

This marks the end of the presentation of results in this thesis. The next chapter will provide an overview of the key findings of my work and the various ways that the foundations of this thesis could be built upon will also be described.

# Chapter 8

# Conclusions and Further Work

In the course of this thesis, we have observed a variety of phenomena, seen long-held assumptions taken apart, and marvelled at the variety of behaviours that emerge from purely physical, non-living systems. When embarking on a study of the thermodynamics of complex pattern-forming systems, it is very difficult to predict where one will end up. Furthermore it is difficult to know how to start. However, "Not all those who wander are lost."(Tolkien, 1954)

My objective was to first establish a numerical framework that was capable of modelling a variety of physical phenomena. I would then simulate a series of non-equilibrium systems with an increasing number of degrees of freedom and observe how the emergent patterns changed, how the thermodynamic variables changed, and whether the systems exhibited any kind of life-like behaviour.

The aspirations were wide and ranged from the testing of conventional wisdom on the role of structure in non-equilibrium systems (primarily that dissipative structures always facilitate increased entropy production), to the generation of new postulates for the connections between chemistry, biology and ecology. My previous work on the emergence of primitive cells from homogeneous mixtures of simple building blocks (Bartlett et al., 2010) had raised the question of whether ecological phenomena may have actually preceded the emergence of biological phenomena. Indeed the intense debate surrounding this idea continues today (Fernando and Rowe, 2007; Meléndez-Hevia et al., 2008; Vasas et al., 2012). It has far-reaching consequences for the field of Astrobiology: chemical

evolution could be ubiquitous in the Universe, while the emergence of life as we know it on Earth is perhaps much more limited.

The results of simulations such as those presented in this thesis might provide guidance for biogenesis research. There is the potential for long held ideas about the emergence of metabolism in prebiotic scenarios to be tested using the modelling framework presented herein. Furthermore such simulations may highlight the action of hitherto unknown emergent phenomena, worthy of further research. The model is also sufficiently versatile that specific scenarios relevant to astrobiology could also be modelled, including hydrothermal vents.

## 8.1 Theories of Maximum Entropy Production

On the journey that was my PhD there ended up being some stopping points. The first was the validity of the Maximum Entropy Production Principle (MEPP). The MEPP had been applied to simple models of the climate system (Paltridge, 1978) and apparently also predicted the steady state properties of natural convection (NC) systems (Ozawa et al., 2001). It struck me that no one had modelled a simple fluid system with the same negative feedback boundary conditions (BCs) of the 2-box model of Paltridge (1978), even though the properties of such a system had been postulated to also follow the MEPP (Kleidon, 2009). There had been numerical studies of atmospheric heat transport using Global Circulation Models (Kleidon et al., 2006; Ozawa et al., 2003) that confirmed a connection to MEPP, but none of a single phase heated fluid. As a result, I carried out the numerical investigations presented in chapter 5. The results of that study, combined with a more meticulous scrutiny of known results for NC systems with fixed BCs, provided evidence that the MEPP is not compatible with simple NC systems, despite the assumption that it is, in the literature (Meysman and Bruers, 2010).

I hope that my work in this area will help change the thinking with regard to the MEPP, that it cannot be simply assumed that non-equilibrium systems obey the principle just because their steady states show increased energy fluxes compared to a simpler, diffusive steady state. The work of chapter 5 has been submitted for publication and is currently under review (Bartlett and Bullock, 2014).

## 8.2 New Avenues for Heat Transfer

Having de-constructed an application of the MEPP, I then moved on to reactive systems. Incorporating space into models of reaction systems is a relatively recent phenomenon due to the limited computational power of decades past. The study of the transport properties of non-equilibrium, reacting fluids also seems to be restricted to specific engineering problems (e.g., Chen et al., 2008). Hence I decided to simulate a differentially heated, closed fluid system with passive scalar species reacting, and releasing and absorbing heat (subsection 7.3.1). The objective was to assess how the system would respond to its additional degrees of freedom (compared to the system with no chemical species). The results showed that the system was able to support a greater heat flux when the boundary temperatures were held constant. When the boundary heat flux was held constant, the boundary temperature difference decreased with the presence of the chemical species and reactions. This suggests that the efficiency of the system's heat transfer abilities was enhanced by the reactive processes.

This makes intuitive sense because the fluid on its own would undergo convective flows. Adding just the passive scalars would cause those scalars to be advected around the system by the flow. If those scalars are then allowed to react in a reversible cycle, where one direction releases heat and one takes it up, this can then play a role in the heat transfer of the whole system. At the hotter boundary, some quantity of thermal energy can be invested in carrying out the endothermic reaction. The products of that reaction can then be transported by the fluid flow towards the colder boundary. As they approach it the exothermic reaction begins to take place, releasing heat. This heat is then funnelled out of the system by diffusion at the cold boundary.

The presence of the extra components thus represents an extra channel for the transport of thermal energy. The results of subsection 7.3.1 showed that as the concentration of chemical species was increased, the system began to reduce the fraction of heat transfer carried out by convection alone, and increase the fraction carried out by the advection and reaction of the chemical species. So we saw a change of duty from one mode of heat flow to another. Such an elementary study of the effects of thermal reactions on the transport properties of a fluid system doesn't appear to have been carried out before. Again, most similar studies always had a specific application in mind (Andres and Cardoso, 2012; Rongy et al., 2007).

## 8.3 The Ecology of Spots

In subsection 7.3.2 the focus switched to the Gray-Scott (GS) reaction diffusion (RD) system. This classic example of non-linear dynamics has something of a history (the first study of RD systems was the seminal work of Turing, 1952), but was only brought into the 2D realm approximately 20 years ago (Pearson, 1993). Since then its entire phenomenological repertoire has been thoroughly investigated (Awazu and Kaneko, 2004; Mahara et al., 2004; Pearson, 1993). It has long been shown to exhibit self-replicating spots, a surprising observation given how simple the system is in terms of its constituents and interactions. Since the isothermal form of the model is well documented, I chose to investigate the influence of thermal kinetics and fluid convection on the pattern-forming processes of this system.

The results of subsubsection 7.3.2.2 showed that when the reaction is exothermic, it produces a positive feedback effect. The heat of reaction has the effect of increasing its own rate. This then causes the release of more heat and the two effects feed back on one another. Such a system can enter a steady state if the boundaries are able to remove heat at a sufficient rate. This depends on the thermal diffusivity of the fluid, since heat must move out of the system by diffusion.

I then simulated an endothermic system in subsubsection 7.3.2.3. As one might expect, the effect of the reaction was opposite to that of the exothermic system: the reaction and emergent structures were self-inhibiting. They reduced their local temperature and thus diminished the conditions for their own existence. The only way for the reaction to proceed at any significant rate was near the heated lower boundary of the domain. This boundary adjusted its heat flux (its temperature was fixed) such that the heat absorption by the reaction was compensated for.

The aim of subsubsection 7.3.2.4 was to test the precariousness of the spot patterns simulated in previous sections. Being able to heat their surroundings, it was expected that the RD spots might be able to move into foreign realms in which they would not form spontaneously (due to the low temperature) and colonise them. I simulated systems where only half of the lower boundary was heated, to allow the exothermic spots to expand into the cold region adjacent to the heated area.

The emergent configuration consisted of a double tubular vertical structure from which spots were emitted like spores from a plant. These spots were able to penetrate into the cold, dead region, but for only a limited time. Their own heating effect was not sufficient to sustain their existence far into the inhospitable zone. If the enthalpy of reaction was decreased, eventually the system exhibited a completely different evolution. With a sufficiently exothermic reaction, the reactive 'zone' underwent an exponential expansion that spread to every corner of the domain. This swamping effect destroyed any hint of fine-grained structure.

Given the two different types of behaviour found in the exothermic model, it was natural to ask whether the presence of additional species and reactions could modulate the phenomena of the two-species system. Therefore in section 7.4 I introduced a second pair of chemical species and non-linear reaction between them. One reaction was set to be exothermic and the other endothermic. It was found that indeed the endothermic structures were able to prevent the runaway feedback that would overcome the system when only the exothermic species was present. However this did not enable the now symbiotic spot patterns to survive when the heat flow into the system was removed.

The final system to be simulated consisted of a very strongly exothermic spot species, sharing the domain with a very strongly endothermic species. The entire system was differentially heated. If left in isolation, the exothermic species underwent catastrophic positive feedback, and the endothermic species cooled the system so much that spots could not persist in any significant quantity. However when both were present, the two sets of spots could persist indefinitely.

This thermal symbiosis is interesting because it is possible to imagine a scenario where it might provide some form of thermal homeostasis. If the temperature were to rise there would be a risk of the structures expanding and undergoing destructive exponential growth. But the extra growth of the endothermic species would provide an extra cooling effect that could eliminate the temperature rise. Conversely in a situation of low temperature, the endothermic spots might recede, allowing the exothermic spots to reproduce, increase their heat production and bring the temperature back into a viable range.

## 8.4 Further Work

In some respects, this thesis represents a starting point. The version of Lattice Boltzmann Model (LBM) presented in chapter 7 could be used to investigate an immense variety of non-equilibrium systems. In this section some of the most interesting avenues that could be explored using this modelling framework will be described.

### 8.4.1 Transport Properties of Closed Systems

In subsection 7.3.1 the transport properties of closed systems consisting of a heated fluid and two dissolved chemical species undergoing the linear reaction $A \rightleftharpoons B$ were analysed. There was a shift of heat transfer duties from convection and diffusion only to convection, diffusion and advection and reaction. A natural question is: how general are these observations? It would be an interesting study to simulate similar systems involving more complicated reaction schemes and more chemical species. For example a simple extension would be the ligation reaction $A + A \rightleftharpoons B$, that has a non-linear rate law.

It would also be informative to experiment with autocatalytic reaction schemes such as the reversible Gray-Scott (GS) reactions: $A + 2B \rightleftharpoons 3B$. Although the reversible GS model has been investigated previously (Mahara et al., 2004), it is not clear whether a closed system is capable of exhibiting the characteristic patterns of the standard system (where there is supply and removal of chemical species due to external reservoirs).

### 8.4.2 Open Reaction Diffusion Systems

In subsection 7.3.2 and section 7.4 we saw what could be described as ecological dynamics in a physico-chemical system. Considering those simulations involved a maximum of four chemical species, it is likely that opening the system up to greater sets of reactions and species would reveal even more levels of emergent phenomena. Very large simulations could be run with a range of different spot species present, each with different thermal properties and characteristic sizes. It might then be possible to observe some form of natural selection where a proportion of the structures fail to persist in any number, but the remainder interact and compete for resources like biological organisms.

With even the simple systems presented in this thesis, it would also be instructive to assess the population dynamics of the RD spots. They may exhibit sigmoidal population growth curves analogous to populations in living systems.

Another interesting option for the four-species system would be to introduce invasive cross reactions. This would allow one spot species to utilise the resources of the other for its growth, adding another level of ecological possibilities to the system dynamics.

### 8.4.3 N-Species Systems

The reactive thermal LBM (RTLBM) presented in chapter 7 can be readily generalised to handle an almost arbitrary range of reactive systems. In this section the additions necessary for such an extension will be briefly described.

Imagine a non-isothermal fluid with $n$ passive scalar species dissolved within it. There are $r$ reactions occurring between the species. One way to represent such a system is through an $n \times r$ stoichiometric matrix $\mathbf{N}$. Each row of the matrix corresponds to a chemical species and each column to a reaction. A vector $\mathbf{v}$ is then required, representing the velocity of each reaction. Multiplying these two objects together gives a new vector giving the rate of change of the concentration of each chemical species. To demonstrate, take the example of the following set of reactions,

$$a \rightarrow 2b \tag{8.1}$$

$$b + c \rightarrow d \tag{8.2}$$

$$d \rightarrow b + c \tag{8.3}$$

$$d + e \rightarrow 2d \tag{8.4}$$

where reverse reactions are included separately to their forward reactions. The stoichiometric matrix reads,

$$\mathbf{N} = \begin{bmatrix} -1 & 0 & 0 & 0 \\ 2 & -1 & 1 & 0 \\ 0 & -1 & 1 & 0 \\ 0 & 1 & -1 & 1 \\ 0 & 0 & 0 & -1 \end{bmatrix} \tag{8.5}$$

and the reaction velocity vector,

$$\mathbf{v} = \begin{bmatrix} A_1[a]e^{-E_{f,1}/T} \\ A_2[b][c]e^{-E_{f,2}/T} \\ A_3[d]e^{-E_{f,3}/T} \\ A_4[d][e]e^{-E_{f,4}/T} \end{bmatrix} \tag{8.6}$$

where it was assumed that all chemical species have unit molar masses (this assumption could be relaxed by first multiplying the matrix $\mathbf{N}$ by a row vector of the molar masses) and the law of mass action and Arrhenius equation have been used to define the kinetic parameters. In the RTLBM, an extra set of distribution functions for each chemical species would be required. Those distribution functions would undergo collision and streaming operations and during the collision operation, the mass changes due to reactions could be calculated using the vector $\mathbf{Nv}$. Then the various reaction enthalpies could be summed and added to the collision operation for the internal energy distribution. The rest of the LBM algorithm remains the same (collision, streaming and forcing of the velocity distribution functions).

One could then experiment with all kinds of chemical reaction network. The kinetic parameters could be adjusted such that oscillations in concentration occurred over a range of time scales. The response of a system driven out of equilibrium by concentration or temperature gradients could then be analysed. Would the system always use its new freedoms to increase its heat transport efficiency, or would some classes of reaction network provide significant inhibition to that process? Indeed in subsubsection 7.3.2.3, the presence of endothermic RD spots prevented the formation of convection cells. Clearly certain reaction schemes would hinder the transport properties of heated fluids, but only a thorough investigation can shed light on the details.

## 8.5 Where are we now?

The process of carrying out and writing this PhD has changed my perspective in all manner of ways. I see the world through a different lens now. Thermodynamics is everywhere and it affects us all. To take an example, the current energy crisis is not an energy crisis at all, but a free energy crisis. As Boltzmann noted, energy is everywhere,

but energy that can be put to use is not. Along with all other living things we are gripped by a struggle for the negative of entropy, information, not energy.

It seems that in fact, life is just a point on a continuous scale of dissipative structures. There is seemingly some kind of natural selection persistence pressure for the ability to acquire greater access to the driving gradients that created you. Life is one class of dissipative structure that is characterised by its unusually innate skills at this process of finding new access to driving gradients (indeed creating new gradients). Like the enveloping 'monsters' of subsection 7.3.2, once life got going there was no stopping it. It spread to every last hole and crevice.

Life may well be common in the Universe, but probably not our kind of life. Given the chemical make up and conditions of other planetary bodies, the universe is likely abundant with simple forms of life, that find isolated niches and evolve rapidly to states of 'complexity saturation'. What I mean by that is they reach an upper limit of complexity, defined by the diversity of chemical constituents in their surroundings, the temperature of their environment, and the chemical (reactive and structural) possibilities available to them given the aforementioned diversity limit. The complexity saturation point of our planet is perhaps not bound from above.

We are surrounded by dissipative structures, most of which are not alive and do not expand and rapidly colonise their environs. On the scale between these simple formations and life as we know it here on Earth, perhaps there is a tipping point, the life-non-life threshold, beyond which the explosion of diversity is permitted. Due to the frustrating (or not) anthropic principle, at the moment, we have no way of shedding light on where we are on this scale. But we can be ever grateful that at least here on Earth, things are on the right side of the line.

# References


Amaya-Ventura, G. and Rodriguez-Romo, S. (2011). 2D lattice Boltzmann simulation of chemical reactions within Rayleigh-Bénard and Poiseuille-Bénard convection systems. *AIP Conference Proceedings*, 1389(1):1798–1801.

Andres, J. T. H. and Cardoso, S. S. S. (2012). Convection and reaction in a diffusive boundary layer in a porous medium: Nonlinear dynamics. *Chaos: An Interdisciplinary Journal of Nonlinear Science*, 22(3):–.

Awazu, A. and Kaneko, K. (2004). Relaxation to equilibrium can be hindered by transient dissipative structures. *Physical Review Letters*, 92:258302.

Ayodele, S. G., Varnik, F., and Raabe, D. (2011). Lattice Boltzmann study of pattern formation in reaction-diffusion systems. *Physical Review E*, 83:016702.

Bains, W. (2004). Many chemistries could be used to build living systems. *Astrobiology*, 4(2):137–167.

Bartlett, S. (2012). Stretching Prigogine's analogy: Dissipative structures and their relationship to life. Presented at the UK Student Conference on Complexity Science, Gloucester, UK.

Bartlett, S. (2013). Closing the loop: Entropy accounting for a sustainable world. Presented at TEDx Southampton University, Southampton, UK.

Bartlett, S., Attard, G., and Bullock, S. (2010). Challenging the robustness of simulated protocells. Poster presented at Artificial Life XII: Twelfth International Conference on the Synthesis and Simulation of Living Systems, Odense, Denmark, 19 - 23.

Bartlett, S. and Bullock, S. (2014). Natural convection of a 2D Boussinesq fluid does not maximise entropy production. *Physical Review E*. Submitted.

Bhatnagar, P. L., Gross, E. P., and Krook, M. (1954). A model for collision processes in gases. i. small amplitude processes in charged and neutral one-component systems. *Physical Review*, 94:511–525.

Boltzmann, L. (1974). *The second law of thermodynamics*. Springer-Verlag New York.

Branscomb, E. and Russell, M. J. (2013). Turnstiles and bifurcators: The disequilibrium converting engines that put metabolism on the road. *Biochimica et Biophysica Acta (BBA) - Bioenergetics*, 1827(2):62 – 78. The evolutionary aspects of bioenergetic systems.

Carnot, S. (1824). *Réflexions sur la puissance motrice du feu et sur les machines propres à développer cette puissance*. Bachelier Libraire.

Chaisson, E. J. (2011a). Energy rate density as a complexity metric and evolutionary driver. *Complexity*, 16(3):27–40.

Chaisson, E. J. (2011b). Energy rate density. II. probing further a new complexity metric. *Complexity*, 17(1):44–63.

Chen, H., Chen, S., and Matthaeus, W. H. (1992). Recovery of the navier-stokes equations using a lattice-gas Boltzmann method. *Physical Review A*, 45:R5339–R5342.

Chen, S. and Doolen, G. D. (1998). Lattice Boltzmann method for fluid flows. *Annual Review of Fluid Mechanics*, 30(1):329–364.

Chen, S., Liu, Z., Tian, Z., Shi, B., and Zheng, C. (2008). A simple lattice Boltzmann scheme for combustion simulation. *Computers & Mathematics with Applications*, 55(7):1424 – 1432.

Chen, S., Martinez, D., and Mei, R. (1996). On boundary conditions in lattice Boltzmann methods. *Physics of Fluids*, 8(9):2527–2536.

Clever, R. M. and Busse, F. H. (1974). Transition to time-dependent convection(in fluid layer heated from below). *Journal of Fluid Mechanics*, 65:625–645.

Cottrell, A. (1979). The natural philosophy of engines. *Contemporary Physics*, 20(1):1–10.

Crooks, G. E. (1999). Entropy production fluctuation theorem and the nonequilibrium work relation for free energy differences. *Physical Review E*, 60:2721–2726.

De Vahl Davis, G. (1983). Natural convection of air in a square cavity: A bench mark numerical solution. *International Journal for Numerical Methods in Fluids*, 3(3):249–264.

Dewar, R. C. (2003). Information theory explanation of the fluctuation theorem, maximum entropy production and self-organized criticality in non-equilibrium stationary states. *Journal of Physics A: Mathematical and General*, 36(3):631–641.

Dewar, R. C. (2009). Maximum entropy production as an inference algorithm that translates physical assumptions into macroscopic predictions: Don't shoot the messenger. *Entropy*, 11:931–944.

Dewar, R. C. (2010). Maximum entropy production and plant optimization theories. *Philosophical Transactions of the Royal Society of London, Series B: Biological Sciences*, 365(1545):1429–1435.

Di Rienzo, A., Asinari, P., Chiavazzo, E., Prasianakis, N., and Mantzaras, J. (2012). Lattice Boltzmann model for reactive flow simulations. *EPL (Europhysics Letters)*, 98(3):34001.

Dixit, H. and Babu, V. (2006). Simulation of high rayleigh number natural convection in a square cavity using the lattice Boltzmann method. *International Journal of Heat and Mass Transfer*, 49(34):727 – 739.

Doering, C. R. and Constantin, P. (1996). Variational bounds on energy dissipation in incompressible flows. iii. convection. *Physical Review E*, 53:5957–5981.

D'Orazio, A., Corcione, M., and Celata, G. P. (2004). Application to natural convection enclosed flows of a lattice Boltzmann BGK model coupled with a general purpose thermal boundary condition. *International Journal of Thermal Sciences*, 43:575–586.

Dyke, J. and Kleidon, A. (2010). The maximum entropy production principle: Its theoretical foundations and applications to the earth system. *Entropy*, 12(3):613–630.

Fernando, C. and Rowe, J. (2007). Natural selection in chemical evolution. *Journal of theoretical biology*, 247(1):152–67.

Frisch, U., Hasslacher, B., and Pomeau, Y. (1986). Lattice-gas automata for the navier-stokes equation. *Physical Review Letters*, 56(14):1505–1508.

Gray, P. and Scott, S. K. (1985). Sustained oscillations and other exotic patterns of behavior in isothermal reactions. *The Journal of Physical Chemistry*, 89(1):22–32.

Grossmann, S. and Lohse, D. (2000). Scaling in thermal convection: a unifying theory. *Journal of Fluid Mechanics*, 407:27–56.

Guo, Z., Zheng, C., and Shi, B. (2002). An extrapolation method for boundary conditions in lattice Boltzmann method. *Physics of Fluids*, 14(6):2007–2010.

He, X., Chen, S., and Doolen, G. D. (1998). A novel thermal model for the lattice Boltzmann method in incompressible limit. *Journal of Computational Physics*, 146(1):282–300.

He, X. and Luo, L.-S. (1997a). A priori derivation of the lattice Boltzmann equation. *Physical Review E*, 55:R6333–R6336.

He, X. and Luo, L.-S. (1997b). Theory of the lattice Boltzmann method: From the Boltzmann equation to the lattice Boltzmann equation. *Physical Review E*, 56:6811–6817.

He, X., Zou, Q., Luo, L.-S., and Dembo, M. (1997). Analytic solutions of simple flows and analysis of nonslip boundary conditions for the lattice Boltzmann bgk model. *Journal of Statistical Physics*, 87(1-2):115–136.

Hill, A. (1990). Entropy production as the selection rule between different growth morphologies. *Nature*, 348:426–428.

Howard, L. N. (1963). Heat transport by turbulent convection. *Journal of Fluid Mechanics*, 17:405–432.

Inamuro, T., Yoshino, M., and Ogino, F. (1995). A non-slip boundary condition for lattice Boltzmann simulations. *Physics of Fluids*, 7(12):2928–2930.

Jaynes, E. T. (1957). Information theory and statistical mechanics. *Physical Review*, 106:620–630.

Johnston, H. and Doering, C. R. (2009). Comparison of turbulent thermal convection between conditions of constant temperature and constant flux. *Physical Review Letters*, 102:064501.

Kauffman, S. A. (1996). *At Home in the Universe*. Penguin Books Ltd.

Kleidon, A. (2009). Nonequilibrium thermodynamics and maximum entropy production in the earth system. *Naturwissenschaften*, 96:653–677.

Kleidon, A. (2010a). A basic introduction to the thermodynamics of the earth system far from equilibrium and maximum entropy production. *Philosophical Transactions of the Royal Society of London, Series B: Biological Sciences*, 365(1545):1303–1315.

Kleidon, A. (2010b). Life, hierarchy, and the thermodynamic machinery of planet earth. *Physics of Life Reviews*, 7(4):424 – 460.

Kleidon, A., Fraedrich, K., Kirk, E., and Lunkeit, F. (2006). Maximum entropy production and the strength of boundary layer exchange in an atmospheric general circulation model. *Geophysical Research Letters*, 33(6).

Kleidon, A., Malhi, Y., and Cox, P. M. (2010). Maximum entropy production in environmental and ecological systems. *Philosophical Transactions of the Royal Society of London, Series B: Biological Sciences*, 365(1545):1297–1302.

Kondepudi, D. and Prigogine, I. (1998). *Modern Thermodynamics: From Heat Engines to Dissipative Structures*. Wiley.

Kraichnan, R. H. (1962). Turbulent thermal convection at arbitrary prandtl number. *Physics of Fluids*, 5(11):1374–1389.

Liu, C.-H., Lin, K.-H., Mai, H.-C., and Lin, C.-A. (2010). Thermal boundary conditions for thermal lattice Boltzmann simulations. *Computers and Mathematics with Applications*, 59(7):2178 – 2193.

Lorenz, R. D. (2010). The two-box model of climate: limitations and applications to planetary habitability and maximum entropy production studies. *Philosophical Transactions of the Boltzmann of London, Series B: Biological Sciences*, 365(1545):1349–1354.

Lotka, A. J. (1922). Natural selection as a physical principle. *Proceedings of the National Academy of Sciences of the United States of America*, 8(6):pp. 151–154.

Mahara, H., Suematsu, N. J., Yamaguchi, T., Ohgane, K., Nishiura, Y., and Shimomura, M. (2004). Three–variable reversible gray–scott model. *The Journal of Chemical Physics*, 121(18):8968–8972.

Maier, R. S., Bernard, R. S., and Grunau, D. W. (1996). Boundary conditions for the lattice Boltzmann method. *Physics of Fluids*, 8(7):1788–1801.

Malkus, W. and Veronis, G. (1958). Finite amplitude cellular convection. *Journal of Fluid Mechanics*, 4(03):225–260.

Malkus, W. V. R. (1954a). Discrete transitions in turbulent convection. *Proceedings of the Royal Society of London, Series A: Mathematical, Physical and Engineering Sciences*, 225:185–195.

Malkus, W. V. R. (1954b). The heat transport and spectrum of thermal turbulence. *Proceedings of the Royal Society of London, Series A: Mathematical, Physical and Engineering Sciences*, 225(1161):pp. 196–212.

Martin, W., Baross, J., Kelley, D., and Russell, M. J. (2008). Hydrothermal vents and the origin of life. *Nature Reviews Microbiology*, 6(11):805–814.

Martin, W. and Russell, M. J. (2003). On the origins of cells: a hypothesis for the evolutionary transitions from abiotic geochemistry to chemoautotrophic prokaryotes, and from prokaryotes to nucleated cells. *Philosophical Transactions of the Royal of London, Series B: Biological Sciences*, 358(1429):59–85.

Martyushev, L. and Axelrod, E. (2003). From dendrites and s-shaped growth curves to the maximum entropy production principle. *Journal of Experimental and Theoretical Physics Letters*, 78(8):476–479.

Martyushev, L. and Seleznev, V. (2006). Maximum entropy production principle in physics, chemistry and biology. *Physics Reports*, 426(1):1 – 45.

McNamara, G., Garcia, A., and Alder, B. (1995). Stabilization of thermal lattice Boltzmann models. *Journal of Statistical Physics*, 81:395–408. 10.1007/BF02179986.

McNamara, G. R. and Zanetti, G. (1988). Use of the Boltzmann equation to simulate lattice-gas automata. *Physical Review Letters*, 61:2332–2335.

Meléndez-Hevia, E., Montero-Gómez, N., and Montero, F. (2008). From prebiotic chemistry to cellular metabolism–the chemical evolution of metabolism before Darwinian natural selection. *Journal of theoretical biology*, 252(3):505–19.

Meysman, F. J. R. and Bruers, S. (2010). Ecosystem functioning and maximum entropy production: a quantitative test of hypotheses. *Philosophical Transactions of the Royal Society of London, Series B: Biological Sciences*, 365(1545):1405–1416.

Niven, R. (2010). Simultaneous extrema in the entropy production for steady-state fluid flow in parallel pipes. *Journal of Non-Equilibrium Thermodynamics*, 35(3):1–13.

O'Brien, D. M. and Stephens, G. L. (1995). Entropy and climate. ii: Simple models. *Quarterly Journal of the Royal Meteorological Society*, 121(527):1773–1796.

Otero, J., Wittenberg, R. W., Worthing, R. A., and Doering, C. R. (2002). Bounds on Rayleigh-Bénard convection with an imposed heat flux. *Journal of Fluid Mechanics*, 473:191–199.

Ozawa, H., Ohmura, A., Lorenz, R. D., and Pujol, T. (2003). The second law of thermodynamics and the global climate system: A review of the maximum entropy production principle. *Reviews of Geophysics*, 41(4):1–24.

Ozawa, H., Shimokawa, S., and Sakuma, H. (2001). Thermodynamics of fluid turbulence: A unified approach to the maximum transport properties. *Physical Review E*, 64:026303.

Paltridge, G. W. (1978). The steady-state format of global climate. *Quarterly Journal of the Royal Meteorological Society*, 104(442):927–945.

Paulus Jr., D. M. and Gaggioli, R. A. (2004). Some observations of entropy extrema in fluid flow. *Energy*, 29(1215):2487 – 2500.

Pearson, J. E. (1993). Complex patterns in a simple system. *Science*, 261(5118):189–192.

Peng, Y., Shu, C., and Chew, Y. T. (2003). Simplified thermal lattice Boltzmann model for incompressible thermal flows. *Physical Review E*, 68:026701.

Rongy, L., Goyal, N., Meiburg, E., and De Wit, a. (2007). Buoyancy-driven convection around chemical fronts traveling in covered horizontal solution layers. *The Journal of chemical physics*, 127(11):114710.

Sagan, C. (1973). Extraterrestrial life. In Sagan, C., editor, *Communication with Extraterrestrial Intelligence (CETI)*. MIT Press.

Schneider, E. D. and Sagan, D. (2005). *Into the Cool: Energy Flow, Thermodynamics, and Life*. The University of Chicago Press.

Schrödinger, E. (1944). *What is life? Mind and Matter*. Cambridge University Press.

Shu, C., Peng, Y., and Chew, Y. T. (2002). Simulation of natural convection in a square cavity by taylor series expansion- and least squares-based lattice Boltzmann method. *International Journal Of Modern Physics C*, 13(10):1399–1414.

Sofonea, V. and Sekerka, R. F. (2005). Diffuse-reflection boundary conditions for a thermal lattice Boltzmann model in two dimensions: Evidence of temperature jump and slip velocity in microchannels. *Physical Review E*, 71:066709.

Tang, G. H., Tao, W. Q., and He, Y. L. (2005). Thermal boundary condition for the thermal lattice Boltzmann equation. *Physical Review E*, 72:016703.

Tolkien, J. R. R. (1954). *The Fellowship of the Ring: The Lord of the Rings, Part 1*. George Allen & Unwin.

Turing, A. M. (1952). The chemical basis of morphogenesis. *Philosophical Transactions of the Royal Society of London, Series B: Biological Sciences*, 237(641):37–72.

Vallino, J. J. (2010). Ecosystem biogeochemistry considered as a distributed metabolic network ordered by maximum entropy production. *Philosophical Transactions of the Royal Society of London, Series B: Biological Sciences*, 365(1545):1417–1427.

Vasas, V., Fernando, C., Santos, M., Kauffman, S., and Szathmary, E. (2012). Evolution before genes. *Biology Direct*, 7(1):1.

Verzicco, R. and Sreenivasan, K. (2008). A comparison of turbulent thermal convection between conditions of constant temperature and constant heat flux. *Journal of fluid mechanics*, 595(1):203–219.

Virgo, N. (2010). *Thermodynamics and the Structure of Living Systems*. PhD thesis, University of Sussex.

Wang, G. M., Sevick, E. M., Mittag, E., Searles, D. J., and Evans, D. J. (2002). Experimental demonstration of violations of the second law of thermodynamics for small systems and short time scales. *Physical Review Letters*, 89:050601.

Wolf-Gladrow, D. A. (2000). *Lattice-Gas Cellular Automata and Lattice Boltzmann Models*. Springer-Verlag, Berlin.

Zhang, J. and Yan, G. (2012). A lattice Boltzmann model for the reaction-diffusion equations with higher-order accuracy. *Journal of Scientific Computing*, 52(1):1–16.

Zou, Q. and He, X. (1997). On pressure and velocity boundary conditions for the lattice Boltzmann BGK model. *Physics of Fluids*, 9:1591.

Zupanović, P. and Juretić, D. (2004). Kirchhoffs loop law and the maximum entropy production principle. *Physical Review E*, 70:056108.